Midrapidity emissions, can they be thermal? First results of the INDRA@GSI Campaign

J. Łukasik and A.S. Botvina for the INDRA-ALADIN Collaboration

High quality experimental data obtained with the 4π multi-detector system INDRA set up on the beam delivered by SIS offer now an unique opportunity to perform a detailed study, including the isospin degree of freedom, of the collisions of both symmetric (Au+Au, Xe+Sn) and asymmetric (C+Au, C+Sn) systems in a broad energy range. It covers the interesting transition region from around the Fermi energy up to relativistic energies, approaching the participant-spectator domain.

Non-central collisions of symmetric heavy systems turn out to be essentially of binary character with pronounced projectile and target like sources. Nevertheless, a sizable amount of detected particles and fragments have parallel velocities intermediate between those of the projectile and of the target [1]-[3] and their importance increases with the increasing centrality of the collision. They are often referred to as midrapidity (-velocity) emissions.

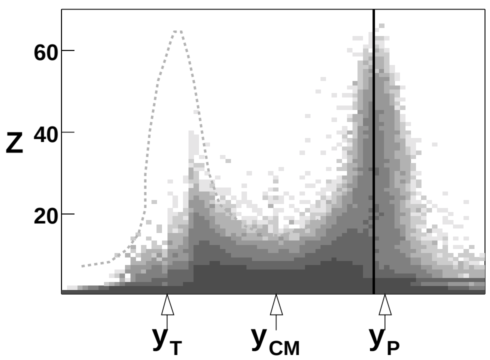

Figure 1: Z vs rapidity distribution of fragments from peripheral collisions Au+Au at 80 MeV/n. The dashed line marks the target-side region which is affected by detection thresholds. The arrows denote the target, CM and projectile rapidities, respectively.

These emissions seem to be strongly influenced by dynamical effects and are thought to proceed on a relatively short time scale. One can imagine various scenarios of formation of those midrapidity fragments following the predictions of various dynamical or hydrodynamical models. These scenarios include fast pre-equilibrium particles, neck emitted particles and fragments, as well as light fission fragments preferentially aligned in between the two main reaction partners. The importance of these midrapidity emissions can be viewed from Fig. 1, which presents the rapidity distribution of fragments emitted from the reaction Au+Au at 80 MeV/n at large impact parameters. The vertical line corresponding to the projectile-like source rapidity is drawn to emphasize a strong forward-backward asymmetry with respect to it.

Numerous analyses assume the existence of a well defined statistically equilibrated source. Can midrapidity emissions be regarded as those originating from such a source? Certainly not all of them, however at least a fraction of these emissions, in the vicinity of the Coulomb ring, can be interpreted in the framework of the statistical multifragmentation model (SMM) [4] provided, the Coulomb influence of the heavy partner on the (multi)fragmenting excited nucleus is taken into account. Inclusion of, preferentially elliptical, flow and angular momentum effects also seems to be important.

Fig. 2 presents the predictions of the SMM (left panels) and of a hybrid, the molecular dynamics model CHIMERA [5] plus the statistical sequential decay model GEMINI [6] used as an afterburner (right panels). These predictions are compared with the experimentally measured (middle panels) invariant cross sections of lithium ions emitted in peripheral Au+Au reaction at 80 MeV/n.

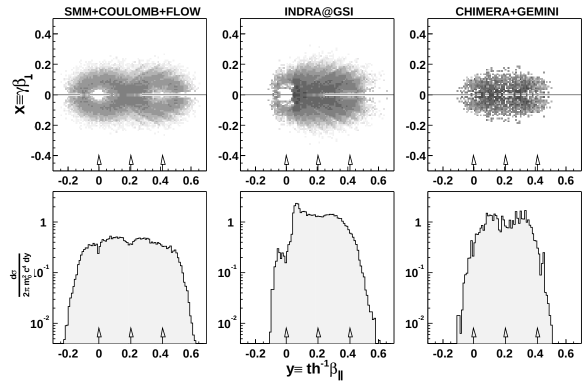

Figure 2: Invariant cross sections of lithium fragments emitted in peripheral reaction of Au+Au @ 80 MeV/n (upper row) and their projections (lower row). The central column gives the experimental results.

The above figure shows that, at least qualitatively, both models: statistical and dynamical, can account for midrapidity emissions. For a clear separation of the equilibrated and the dynamical components further studies are required, including consistent statistical treatment and careful adjustment of flow, and possibly inclusion of angular momentum and deformation effects in SMM, for a range of impact parameters and energies. Dynamical models should be traced more carefully in terms of emission and equilibration times.

References

[1] J.F. Dempsey *et al.* Phys. Rev. C **54**, 1710 (1996).
[2] J. Łukasik *et al.* Phys. Rev. C **55**, 1906 (1997).
[3] E. Plagnol *et al.* Phys. Rev. C **61**, 014606 (2000).
[4] J.P. Bondorf *et al.* Phys. Rep. **257**, 133 (1995), A.S. Botvina *et al.* GSI Preprint 2000-50.
[5] J. Łukasik *et al.* Acta Phys. Pol. B **24**, 1959 (1993).
[6] R.J. Charity *et al.*, Nuc. Phys. **A483**, 371 (1988).

SPECTATOR FRAGMENTATION INDUCED BY RELATIVISTIC ^{12}C PROJECTILES

Ketel TURZÓ for the INDRA-ALADIN Collaboration

In 1998 and 1999, a series of experiments[1] was conducted at the GSI with the INDRA multidetector [2], using high-energy beams from the heavy-ion synchrotron SIS. A part of them was devoted to asymmetric systems like ^{12}C+^{197}Au and ^{12}C+^{112,124}Sn at bombarding energies ranging from 95 to 1800 AMeV. High resolution at backward angles, dominated by emissions from the target spectator, was achieved with the Si-Si-CsI(Tl) calibration telescopes of INDRA. The physics goals in this study of spectator fragmentation are the principal question of thermal and/or dynamical breakup of the source, and, with the isotopically pure tin targets, the role of the isospin degree of freedom in the fragmentation process.

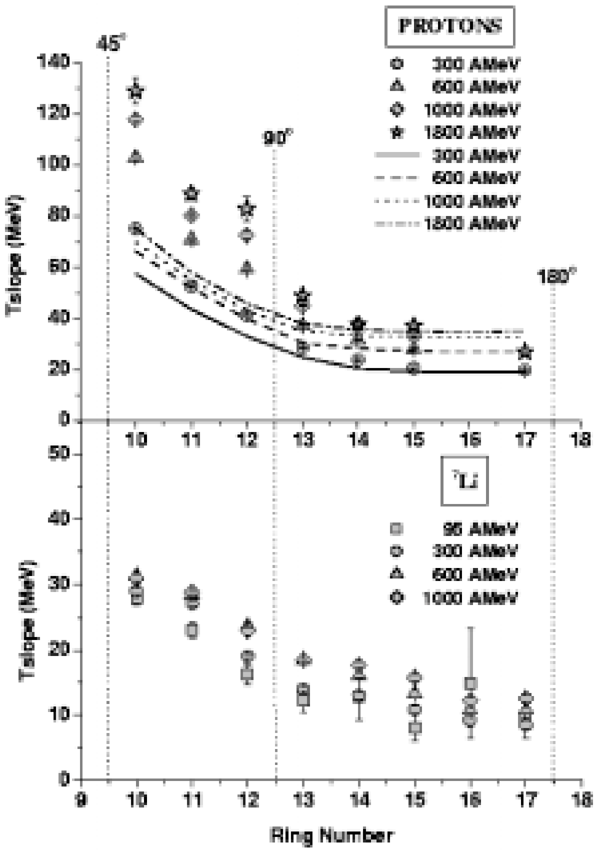

Figure 1: Slope temperatures $T_{\rm slope}$ of protons (top) and ^{7}Li (bottom) as a function of the ring number for ^{12}C+^{197}Au at the indicated bombarding energies. For the protons, the high-temperature values are given and compared with the results of the Gudima-Toneev cascade model (lines).

Inclusive energy spectra measured with the calibration telescopes were fitted, as a first approach, with two-parameter Maxwell-Boltzmann functions. A superposition of two such sources was required for the proton spectra which exhibit a low-energy component, probably containing the contributions of evaporation, and breakup at different time scales, superimposed on the hard component that extends to rather high energies. The temperatures given by the slopes of these Maxwellians show different behaviors. For the low-temperature component of protons and for the ^{7}Li ions, they increase very slowly with the incident energy. The lithium temperatures even seem to reach some saturation near 600 AMeV, consistent with the invariance of the fragment kinetic energies, observed for $3 \leq Z \leq 20$ in the ^{12}C+^{197}Au reaction for 600 to 1000 AMeV [3]. The evolution of the slope temperatures with the polar angle is shown in Fig. 1. A forward peaking is observed for the high-temperature component of protons and for the ^{7}Li ions. But, while the lithium spectra are only weakly dependent on the beam energy, pointing to a source equilibration, the high-temperature component of the protons is much more sensitive to the beam energy, in particular at forward angles. This is consistent with its presumable origin in the initial cascading stages of the reaction.

A comparison with the results obtained with the Gudima-Toneev intra-nuclear cascade model [4] is also shown in the figure. The calculated proton yields were sorted into spectra according to the ring structure of the INDRA geometry and fitted with one-source maxwellians. Between 90° and 180°, the experimental and theoretical slope temperatures are in good agreement, confirming that the primary nucleon yields extend into the spectator rapidity regime. However, the model fails to describe quantitatively the rise of the slope temperatures at polar angles smaller than 90°. Whether this discrepancy is due to the particular model used or a more general feature of the approximations made in the intra-nuclear cascade is not clear at present.

With the calibration part of the data analysis mostly completed, the physics analysis of the INDRA@GSI experiments has started. First results, so far derived from inclusive particle and fragment yields, demonstrate the usefulness of this detector for fragmentation studies up to the relativistic energy regime. The preliminary data for light particles and fragments from the ^{12}C+^{197}Au reaction show a gross behavior in agreement with previous ALADIN [3] and EOS [5] results. From the continuing analysis exclusive data are to be expected, complementing the existing data on this asymmetric collision system obtained in inverse kinematics.

References

[1] INDRA-ALADIN collaboration, Scientific Report 1999, report GSI-2000-1, p. 39 (2000)
[2] J. Pouthas et al., Nucl. Inst. and Meth. A 357(1995)418
[3] A. Schüttauf et al., Nucl. Phys. A 607(1996)457
[4] V.D. Toneev and K.K. Gudima, Nucl. Phys. A 400(1983)173c
[5] J.A. Hauger et al., Phys. Rev. C 62(2000) 024616

Source Shape Parameters in Central Ru + Ru Collisions at 400 AMeV

N. Bastid, J.P. Alard, V. Barret, A. Bendarag, P. Crochet, P. Dupieux, FOPI Collaboration
LPC Clermont-Ferrand, France

Collective flow effects in heavy ion collisions are of interest since they are expected to provide insight into the properties of hot and dense nuclear matter and its Equation of State (EoS). They are not uniquely sensitive to the stiffness of the EoS but also to other effects such as the momentum dependent interaction (MDI) and the in-medium modification of the nucleon-nucleon cross section ($\sigma_{\rm nn}$).

In this context a complete study of the nuclear collective flow has been performed with a method which can be used in a restricted region of momentum space where the spectator contribution is believed to be negligible. In this procedure, applied successfully to DIOGENE data [1], the two-dimensional momentum distributions ($\rm p_z^{cm}/m,\ p_x/m$), ($\rm p_z^{cm}/m,\ p_y/m$) are fitted with anisotropic Gaussian distributions in and out of the reaction plane, respectively. The emission pattern is then approximated by an ellipsoid whose orientation and shape are defined by the flow angle, $\theta_{\rm F}$, and the in-plane and out-of-plane aspect ratios, $\lambda_{31} = \sigma_3/\sigma_1$ and $\lambda_{21} = \sigma_2/\sigma_1$, respectively. $\sigma_{\rm i}$ are the standard deviations, σ_3 is oriented along the flow axis.

Studied were Ru + Ru collisions at 400 AMeV measured with the FOPI detector. We focus on central events ($< \rm b_{geo} > = 1.1$ fm) selected by means of the energy ratio criterion Erat [2]. The reaction plane is reconstructed according to the transverse momentum analysis method [3]. The observables are corrected for autocorrelation and momentum conservation effects [4] and for reaction plane fluctuations as described in [5, 1]. The shape parameters are determined with the data measured in the central part of FOPI and they are shown for proton-like fragments. We emphasise on the possibility to constrain $\sigma_{\rm nn}$ on the basis of the present data. In this purpose the shape parameters are compared in fig.1 to the predictions of the Isospin Quantum Molecular (IQMD) model [7] for a hard EoS including MDI (HM parametrisation) and different values of $\sigma_{\rm nn}$. The shape parameters exhibit important sensitivities to this quantity. Both the flow angle and the aspect ratios rise strongly as $\sigma_{\rm nn}$ increases from $0.5\sigma_{\rm nn}^{\rm free}$ to $2\sigma_{\rm nn}^{\rm free}$ and a saturation of the shape parameters seems to be reached for $\sigma_{\rm nn} > 2\sigma_{\rm nn}^{\rm free}$. It is obvious that the data cannot be reproduced by the IQMD model for $\sigma_{\rm nn} \geq 2\sigma_{\rm nn}^{\rm free}$. A significant reduction of $\sigma_{\rm nn}$ seems to be excluded as well. This is consistent with results on the nuclear stopping obtained from isospin tracer observables [6].

The present work shows that the source shape parameters extracted from gaussian fits to double differential momentum distributions offer the possibility to constrain the range of the nucleon-nucleon cross section in the nuclear medium. This constitutes an important step towards the determination of the Equation of State.

References

[1] J. Gosset et al., Phys. Lett. B 247 (1990) 233 and references therein
[2] W. Reisdorf et al., Nucl. Phys. A 612 (1997) 493
[3] P. Danielewicz and G. Odyniec, Phys. Lett. B157 (1985) 146
[4] C.A. Ogilvie et al., Phys. Rev. C40 (1989) 2592
[5] J.Y. Ollitrault, Nucl-ex/9711003 (1997)
[6] F. Rami et al., Phys. Rev. Lett. 84 (2000) 1120
[7] C. Hartnack et al., Eur. Phys. J. A 1 (1998) 151

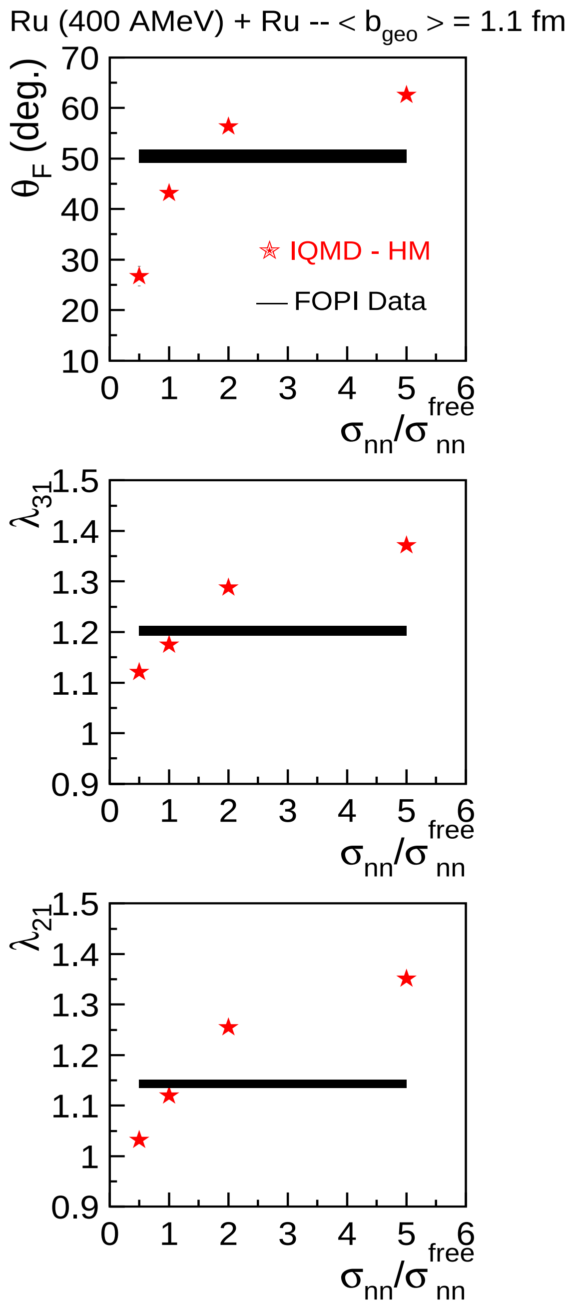

Figure 1: Flow angle and aspect ratios of proton-likes measured in central Ru + Ru reactions at 400 AMeV. The data are compared to the IQMD predictions (HM version) for different values of $\sigma_{\rm nn}$. The stars correspond to the model calculations. The solid line represents the experimental data and includes the statistical uncertainties.

The Isospin Influence on Squeeze-out Phenomena in Heavy Ion Collisions

M. Petrovici[1,2], G. Stoicea[1,2], Y. Leifels[3,2], A. Andronic[1], N. Herrmann[3], K. Hildenbrand[2], and the FOPI Collaboration

[1]NIPNE-Bucharest, [2]GSI-Darmstadt, [3]Univ. of Heidelberg

Equilibration of the isospin degree of freedom, the isospin dependence of the sidewards flow, balance energy, preequilibrium nucleon emission and subthreshold pion production are phenomena proven to be sensitive to the isospin-dependent nuclear equation of state and in-medium nucleon-nucleon cross section [1]. In this contribution we will report on preliminary experimental evidence on the influence of the N/Z content of the spectator matter on the azimuthal distributions. We used the experimental data obtained with the Phase II of the FOPI detector at GSI - Darmstadt for Ru + Zr and Zr + Ru collisions at 400 A·MeV [2]. The charge multiplicity in the central drift chamber was used in order to select the collision geometry. The impact parameter value was extracted from a standard geometrical sharp cut-off approximation for the reaction cross section. The reaction plane reconstruction is based on the transverse momentum method. For an impact parameter of 5 fm, a geometrical estimate based on straight trajectory approximation gives for the fireball three times lower left-right N/Z asymmetry relative to 1.18 : 1.4 corresponding to the spectators for Ru + Zr combination. In such a situation, even if the chemical equilibrium of the fireball is not completely reached the remaining asymmetry can be neglected in a first approximation and we have to do with an expanding object in the presence of spectator matter asymmetric in N/Z.

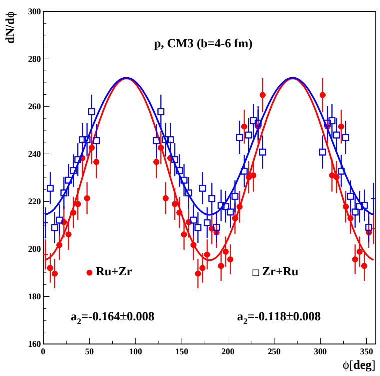

Figure 1: Azimuthal proton distributions for Ru + Zr (dots) and Zr + Ru (squares) measured between 0^o-60^o and 300^o-360^o and reflected relative to 90^o and 270^o, respectively

In the nuclear medium isospin dependent nucleon-nucleon interaction will influence the azimuthal distribution of different particles emitted by the fireball and interacting with the spectator matter. The left - right asymmetry being small, the effect on the azimuthal distributions cannot be expected to be very large. For this reason, our studies are performed in a system of coordinates rotated by the sidewards flow angle [3]. Breaking in this way the azimuthal symmetry of the experimental device we have to symmetrise the experimental distributions obtained in the azimuthal range 0^o-60^o and 300^o-360^o relative to 90^o and 270^o respectively in order to obtain the complete azimuthal distribution. Although, the azimuthal distributions obtained using this recipe do not correspond to the real situation (they correspond to a situation where the fireball has on both sides Ru-like spectators in the case of Ru + Zr or Zr-like spectators for the Zr on Ru combination, respectively) we prefer such representations in order to show also the results of the fits with a standard-second order Fourier expansion in azimuth.

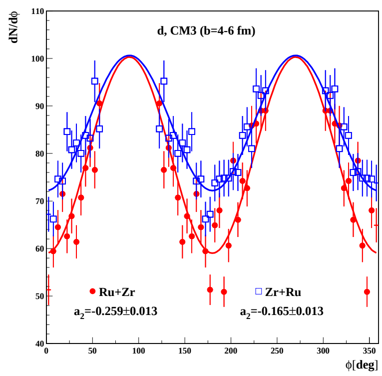

Figure 2: The same as Fig.1 but for deuterons

The results for impact parameters between 4 and 6 fm and a range in the scaled transverse momentum $p_t^{(0)} = (p_t/A)/(p_P^{cm}/A_P)$ of 0.8-1.2 are presented in Fig. 1 for protons and Fig. 2 for deuterons. The distributions are normalised at 90^o. Although quite preliminary, the result seem to indicate an influence of the N/Z value of the spectator matter on the observed azimuthal distributions of the order of 30% for p and about 45 % for deuterons in a_2 coefficients. Detailed analysis will confirm in which extend they are sensitive probes for studying the isospin dependence of the in-medium nucleon-nucleon interaction used in microscopic transport codes.

References

[1] Bao-An Li *et al.*, Int. J. Mod. Phys. **E7**, 147 (1998) and references therein

[2] F. Rami *et al.*, Phys. Rev. Lett. **84**, 1120 (2000)

[3] A. Andronic *et al.*, Nucl. Phys. **A679**, 765 (2001)

$^3H/^3He$ Squeeze-Out - A Signature of the Fireball's Isospin Distribution?

M. Petrovici[1,2], G. Stoicea[1,2], Y. Leifels[3,2], A. Andronic[1,2], N. Herrmann[3], K. Hildenbrand[2], and the FOPI Collaboration
[1]NIPNE-Bucharest, [2]GSI-Darmstadt, [3]Univ. of Heidelberg

The Phase I FOPI data evidence for highly central Au + Au collisions at 100, 150 and 250 A·MeV systematically larger mean kinetic energies for ^3He fragments relative to the ^3H values [1]. The EOS Collaboration find the same trend with somewhat larger size [2]. Microscopic transport models [3] and hybrid hydrodynamical models, including pure Coulomb repulsion at the freeze-out moment [4] do not succeed to explain quantitatively this difference. Similar findings are recently reported by the INDRA Collaboration [5] for ^{129}Xe + ^{119}Sn at 50 A·MeV. At a higher incident energy 1.15 A·GeV it seems that this difference disappears. Both types of fragments have the same mean kinetic energy, following a trend as a function of the fragment mass only, which is specific for the emission from an expanding source.

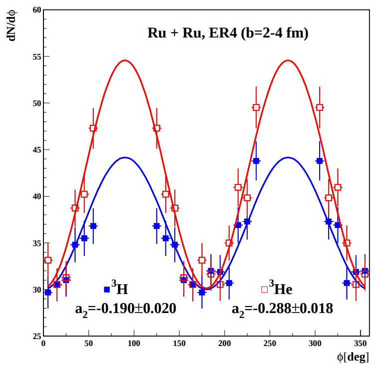

Figure 1: ^3He and ^3H azimuthal distributions for Ru + Ru collision at b=2-4 fm and $p_t^{(0)} = (p_t/A)/(p_P^{cm}/A_P)$ range of 0.8-1.2

Corroborating these facts, based on the dynamics of the expansion suggested by hydrodynamical models, one could imagine that due to the Coulomb repulsion, the outer layers of the initial fireball are to some extend more proton rich than the inner zones. If this is the case, then one expects ^3He fragments originating with higher probability from these regions of the fireball and consequently having larger expansion velocities as far as the expansion has an almost linear dependence as a function of the distance from the the center of the fireball [3, 4]. Within such a scenario, the ^3He fragments are supposed to be emitted preferentially in earlier phases of the expansion than the ^3H fragments, and feel a larger shadowing from the spectators passing by. For mid-central collisions this may lead to a difference in the squeeze-out signal. In order to check this, we analysed data of Ru + Ru collision at 400 A·MeV obtained with the Phase II - FOPI experimental configuration.

The mass and charge identification of A=3 fragments is achieved using the combined information from the central drift chamber (CDC) and the time-of-flight Barrel surrounding the CDC. The low momentum range cannot be used due to the geometrical gap between the CDC and HELITRON. However, the kinetic energy distribution of ^3He and ^3H, for highly central collisions (1% cross section), show similar trends as those observed in Au + Au collision [1]. The selection of the collision geometry and reaction plane determination are explained in a different contribution to this report. The azimuthal distributions are obtained in the reference frame rotated by the sideward flow angle relative to the collision axis. Due to geometrical cuts the experimental data are analysed in the angular range 0^o-60^o and 300^o-360^o. The angular distributions presented in Fig.1 are obtained by symmetrising these results relative to 90^o and 270^o, respectively. For an impact parameter range of b = 2-4 fm one observes a much larger squeeze-out signal for ^3He relative to ^3H. The two azimuthal distributions are normalised at 0^o. A second order Fourier expansion ($f(\Phi) = a_o(1 + a_2 cos(2\Phi))$) is used to fit the azimuthal distributions. The resulting a_2 coefficients for all fragments from A=1 to A=4 are presented in Fig.2. While p,d and ^4He show the well known enhancement of the squeeze-out signal as a function of mass, larger a_2 values for ^3He relative to ^3H can be observed. Different cross-checks and comparisons with microscopic model predictions are in progress. However, this preliminary result seem to indicate that the relative value of the squeeze-out signal of ^3H and ^3He could be related to the isospin distribution in the fireball at the freeze-out moment. Obviously, other contributions (like Coulomb focusing) to the observed effect are not excluded.

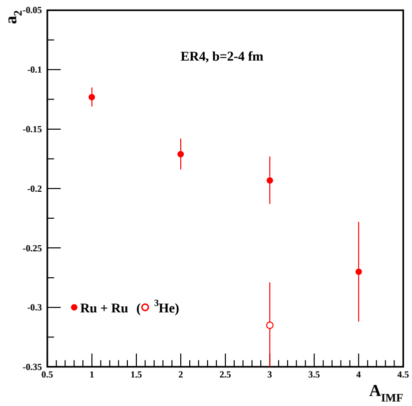

Figure 2: a_2 values as a function of mass of the reaction products for Ru + Ru collision for the same geometry and $p_t^{(0)}$ values as for Fig. 1

References

[1] G. Poggi et al., Nucl. Phys. **A586**, 755 (1995)
[2] M. Lisa et al., Phys. Rev. Lett. 7526621995
[3] P. Danielewicz, et al., Phys. Rep. 517161995
[4] M. Petrovici, FOPI Collaboration, "Heavy Ion Physics at Low Intermediate and Relativistic Energies",World Scientific, 1997, p. 216
[5] D. Gorio et al., Eur. Phys. J. A7,245(2000)
[6] A. Andronic et al., Nucl. Phys. **A679**, 765 (2001)

Incident Energy and A_{part} Dependence of the Fireball Expansion in Au+Au Collisions

G. Stoicea[1,2], M. Petrovici[1,2], A. Andronic[1,2], A. Gobbi[2], N. Herrmann[3], K. Hildenbrand[2], Y. Leifels[3,2], W. Reisdorf[2], and the FOPI Collaboration
[1]NIPNE-Bucharest, [2]GSI-Darmstadt, [3]Univ. of Heidelberg

A unified representation of the squeeze-out trends can be done in terms of the azimuthal distribution of the kinetic energy [1, 2]. A comprehensive description of the squeeze-out phenomena in the energy range 0.25 - 1.15 A·GeV is based on the parametrisation of the transverse mass spectra with an expression describing a radially symmetric expanding shell [1]. As far as such a situation can hardly be encountered in heavy ion collisions and is not specific at all for mid-central collisions, a presentation of the experimental information free of any model is preferred.

In this contribution we present results on azimuthal distributions of the collective flow β (=v/c) which is extracted from the rise of the experimental mean kinetic energy $< E_{kin}^{cm} >$ with the mass of the reaction products. We use the full coverage of the FOPI experimental device in order to extract as precise as possible this experimental information. Therefore, we have to combine the information from the forward plastic wall detector where the reaction products are identified only by their charge with the one from the central drift chamber (CDC) where the reaction products are identified by their mass. This is achieved by using the information obtained during earlier Phase I experiments when Si-CsI telescopes delivered a very good mass and charge separation of the light products within the acceptance of the plastic wall [3]. The collision geometry definition is based on CDC charged particle multiplicity and the ratio of transversal to longitudinal energies [4]. The analysis is performed in a reference frame with the z axis along the sidewards flow direction and within $80^o \leq \Theta_{cm} \leq 100^o$ polar angular range. The azimuthal distributions are symmetric with respect to 90^o and 270^o, hence, we overlap 0^o-90^o and 270^o-360^o azimuthal ranges to decrease the statistical errors, make five bins in azimuth and reflect the results in order to cover the full angular range 0^o-360^o. The average flow value, β_o, and the out-of-plane - in-plane difference, $\Delta\beta$, are taken from a fit to the flow (β=v/c) azimuthal distributions using the following expression:

$$\beta(\Phi)=\beta_o - \Delta\beta \cdot cos2\Phi$$

The elliptic flow characterised by the major axis perpendicular to the reaction plane rises continuously from 90 to 400 A·MeV for mid-central collisions (Fig. 1). At 90 A·MeV the in-plane and out-of-plane flow values are very similar, specific for the E_{tran} region [4]. At all energies the flow β_o increases with the centrality, namely with increasing the baryonic content of the fireball (A_{part}), while $\Delta\beta$, the difference between out-of-plane and in-plane flow, decreases showing the shadowing effect of the spectator matter. At lower centralities, i.e. larger impact parameters, the spectator matter being more compact, the bulk of products detected in the reaction plane emitted by the fireball and not hindered by the spectators correspond to the late phase of the expansion when the flow is weaker and the spectators moved apart from the collision zone.

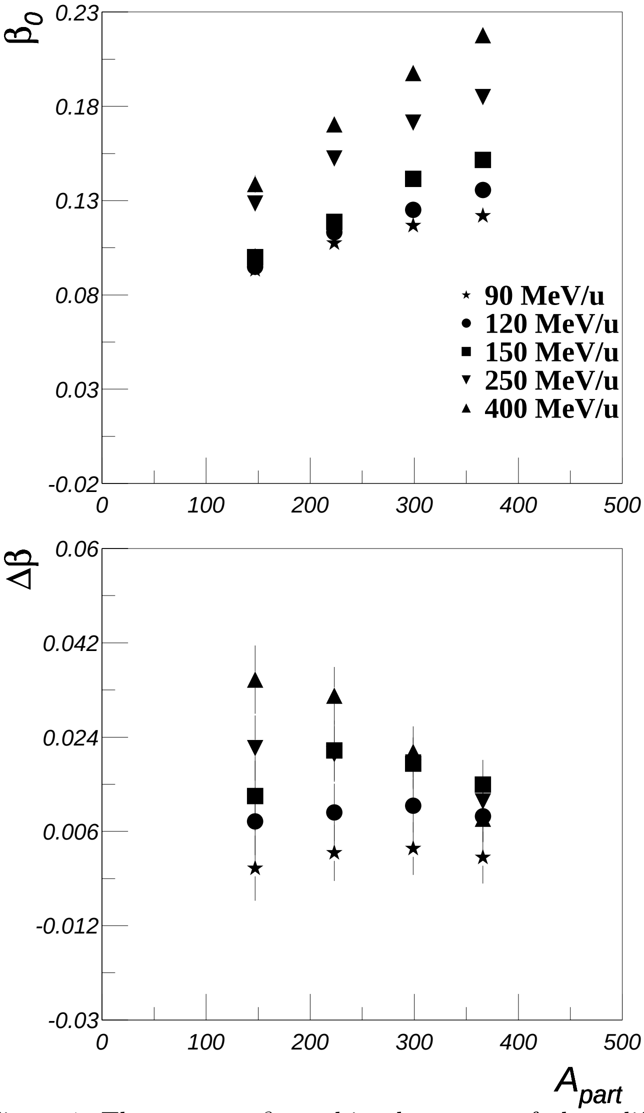

Figure 1: The average, β_o, and in-plane - out-of-plane difference, $\Delta\beta$, of the flow value as a function of centrality, for 90, 120, 150, 250, 400 A·MeV

These experimental trends can be followed in Fig.1. The continuation of these studies at higher energies and detailed comparisons with microscopic transport model predictions are in progress.

References

[1] S. Wang et al., Phys. Rev. Lett. 76 (1996) 3911

[2] M. Petrovici, FOPI Collaboration, Proc. of International Research Workshop on Heavy Ion Physics at Low, Intermediate and Relativistic Energies using 4π Detectors, ed. M. Petrovici et al., World Scientific, 1997, p. 216

[3] G. Poggi et al., Nucl. Phys. **A586**, 755 (1955)

[4] A. Andronic et al., Nucl. Phys. **A679**, 765 (2001)

Kaon and Antikaon Production in Proton-Nucleus Collisions^{B,C}

W. Scheinast (FZ Rossendorf) and the KaoS Collaboration

Recent experiments on K-meson production in nucleus-nucleus at SIS energies found that the K^-/K^+ ratio is enhanced by about 2 orders of magnitude as compared to proton-proton collisions at proton beam energies close to threshold [1]. Within transport calculations, this enhancement is explained by (i) a reduced in-medium mass of K^- mesons and (ii) multiple step processes like strangeness exchange reactions $\pi Y \rightarrow K^-$N with Y = Λ, Σ [2]. The investigation of K^- mesons in proton-nucleus collisions will help to disentangle these two effects because (i) the effective K^- mass is expected to be reduced by about 25% in nuclear matter at saturation density whereas (ii) strangeness exchange reactions are negligible.

Using the Kaon Spectrometer at SIS/GSI we have performed the first measurements of K^- production yields in proton-nucleus collisions at proton energies below 4 GeV. The heavy ion synchrotron delivered protons beam with energies of 1.6, 2.5 and 3.5 GeV with intensities up to 10^{10} protons/sec impinging on C and Au targets of 7 and 2 mm thickness, respectively. A trigger based on the kaon time-on-flight and tracking reduced the data rates to about 5 kHz. The K meson momentum distributions were measured at laboratory angles between Θ_{lab}=32-64 degrees.

Figure 1 presents preliminary double differential production cross sections of K^+ and K^- mesons measured in p+C and p+Au collisions at 2.5 and 3.5 GeV at $\Theta_{lab}=40^o$ as function of the laboratory momentum. The data taken at 3.5 GeV beam energy are not yet corrected for the tracking trigger efficiency. This might be the reason for the structure in the spectra around p_{lab}=700 MeV/c. The smooth spectra measured at 2.5 GeV proton energy were taken at reduced beam intensities without tracking trigger.

Figure 2 shows the K^-/K^+ ratio for p+C and p+Au collisions at a beam energy of 3.5 GeV obtained from the spectra as presented in figure 1. The maximum values of the ratio are about 0.04 and 0.03 for p+C and p+Au, respectively. The corresponding value calculated from inclusive cross sections measured in p+p collisions at 3.5 GeV is about 0.033. Before drawing conclusions on in-medium effects from these values, inclusive K meson production yields have to be extracted from the proton-nucleus data by analyzing the measured polar angle distributions. Moreover, in-medium effects should be more visible in the data measured at 2.5 GeV which is the threshold energy for antikaon production in proton-proton collisions.

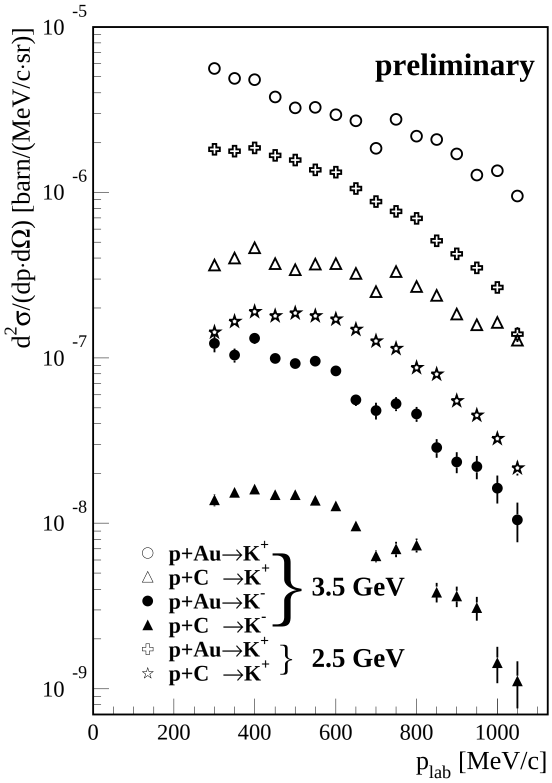

Figure 1: Double differential K^+ and K^- production cross sections measured in p+C and p+Au collisions at 2.5 and 3.5 GeV bombarding energy at a laboratory angle of $\Theta_{lab}=40^o$ as function of laboratory momentum.

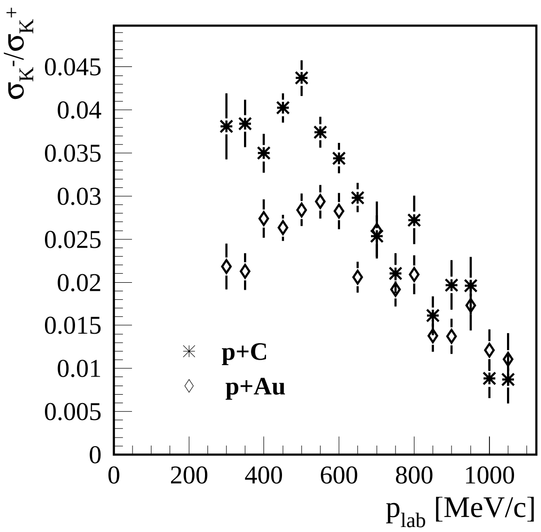

Figure 2: Preliminary K^-/K^+ ratio measured in p+C and p+Au collisions at 3.5 GeV bombarding energy at a laboratory angle of $\Theta_{lab}=40^o$ as function of laboratory momentum.

References

[1] F. Laue, C. Sturm et al., Phys. Rev. Lett. 82 (1999) 1640

[2] W. Cassing and E. Bratkovskaya, Phys. Rep. 308 (1999) 65

Kaon and Pion Production in Nucleus-Nucleus Collisions from 0.6 to 2 AGeV^{B,G}

C.Sturm[2], I.Böttcher[4], M.Dębowski[5], A.Förster[2], E.Grosse[6], P.Koczoń[1], B.Kohlmeyer[4], F.Laue[1], M.Mang[1], M.Menzel[4], L.Naumann[6], H.Oeschler[2], F.Pühlhofer[4], E.Schwab[1], W.Scheinast[6], Y.Shin[3], P.Senger[1], J.Speer[2], H.Ströbele[3], G.Surowka[1,5], F.Uhlig[2], A.Wagner[2,6], W.Waluś[5]
[1]GSI, [2]TU Darmstadt, [3]Univ. Frankfurt, [4]Univ. Marburg, [5] Univ. Cracow (Poland), [6]FZ Rossendorf
KaoS Collaboration

During the past years the KaoS collaboration has provided for various collision systems a rather detailed set of data on meson production at SIS energies from 0.6 to 2 A·GeV. Inclusive spectra of K^+ mesons are published in [1]. A selection of π^+ spectra is shown in Fig. 1 for C+C and Au+Au collisions at various energies around midrapidity. All spectra exhibit the typical concave shapes, interpreted as due to decaying Δ resonances and free pions [2]. The slope parameters of the high-energy parts agree well with those of the K^+ spectra.

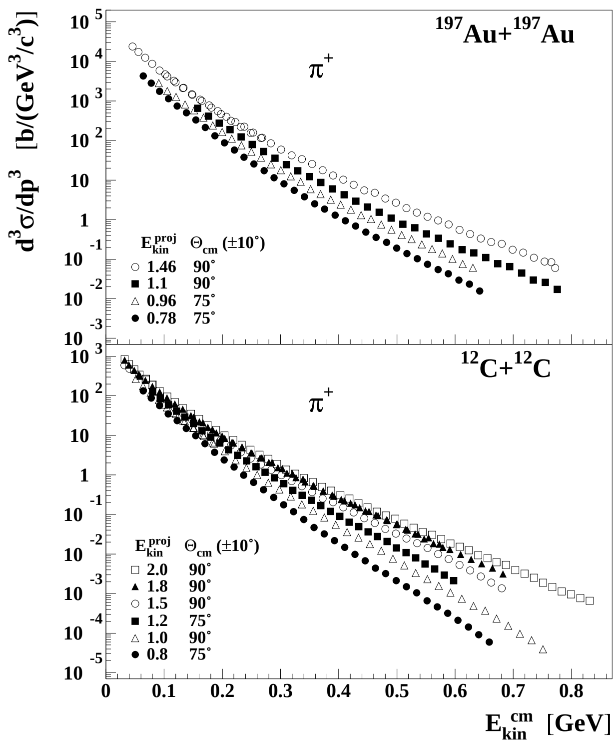

Figure 1: *Spectra of positively charged pions around midrapidity at various incident energies.*

Microscopic transport calculations indicate that the yield of kaons created in collisions between heavy nuclei at subthreshold beam energies (E_{beam} ¡ 1.58 GeV) is sensitive to the compressibility of nuclear matter at high baryon densities [3, 4]. This sensitivity is due to the production mechanism of K^+ mesons at subthreshold beam energies requiring multiple nucleon-nucleon or meson-nucleon collisions. These processes are expected to be enhanced at high baryon densities, and the densities reached in the fireball depend on the nuclear equation of state [5]. Pions are rather insensitive to this parameter of the nuclear equation of state. Their spectra and yields can be used to gauge phase-space effects [1].

Two effects influence the K^+ yield, the compressibility of the nuclear matter as mentioned and possibly a modification of the kaon properties in the dense nuclear medium. Our idea is to disentangle these two competing effects by studying K^+ production in a very light (^{12}C+^{12}C) and a heavy collision system (^{197}Au+^{197}Au) at different beam energies near threshold. The maximum baryonic density reached in Au+Au collisions depends on the nuclear compressibility [4, 6] whereas in the small C+C system this dependence is very weak [7]. The repulsive K^+N potential is assumed to depend nearly (or less than) linearly on the baryonic density [8] and thus reduces the kaon yield accordingly.

Our concept is summarized in Fig. 2. It shows in the upper part the pion and K^+ multiplicity per nucleon for C+C and Au+Au collisions as a function of the beam energy. The pion data points are scaled by a factor of 1/100; they represent the sum of charged and neutral pions as calculated from the measured π^+ multiplicities according to the isobar model [9]. This model explains very well the π^+/π^- ratios measured in Au+Au collisions [10]. The pion multiplicity per nucleon is smaller in Au+Au than in C+C collisions whereas the K^+ multiplicity per nucleon is larger. This observation demonstrates a key difference between pion and kaon emission. In order to illustrate the different behaviour of pions and kaons in nuclear matter we plot the ratio of the pion and kaon excitation functions $(M/A)_{\mathrm{Au+Au}}/(M/A)_{\mathrm{C+C}}$ in the lower panel of Fig. 2. The error bars of the kaon multiplicities include systematic uncertainties due to the extrapolation procedure. The experimental uncertainties due to efficiencies, acceptances and beam normalization, however, cancel in the ratio and therefore have not been taken into account.

The pion ratio $(M/A)_{\mathrm{Au+Au}}/(M/A)_{\mathrm{C+C}}$ (full triangles) is smaller than unity and decreases with decreasing beam energy. A ratio smaller than unity might be caused by the reabsorption of pions which is more effective in the larger system or by decompressional flow of nuclear matter which is expected to be more important in Au+Au than in C+C collisions. In a thermal picture both arguments are equivalent.

In contrast to the pion data, the kaon ratio $(M/A)_{\mathrm{Au+Au}}/(M/A)_{\mathrm{C+C}}$ increases by a factor of almost 3 with decreasing beam energy. An increase of the K^+ yield with decreasing beam energy is found by a transport model calculation in central Au+Au collisions if a soft instead of a hard equation of state is used [4]. The sensitivity

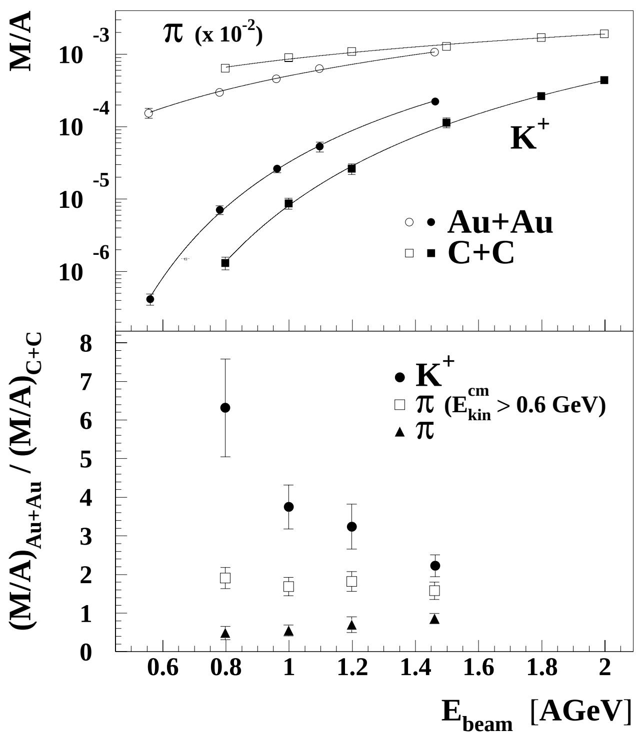

Figure 2: *Upper panel: Pion and K^+ multiplicity per A for the two collision systems as a function of E_{beam}. The pion multiplicities represent all pions species. The lines are to guide the eye. Lower panel: Ratio of the multiplicities per nucleon (Au+Au over C+C collisions) for K^+ mesons (full circles), pions (full triangles) and high-energy pions (E_{kin}^{cm} > 0.6 GeV, open squares) as a function of E_{beam}.*

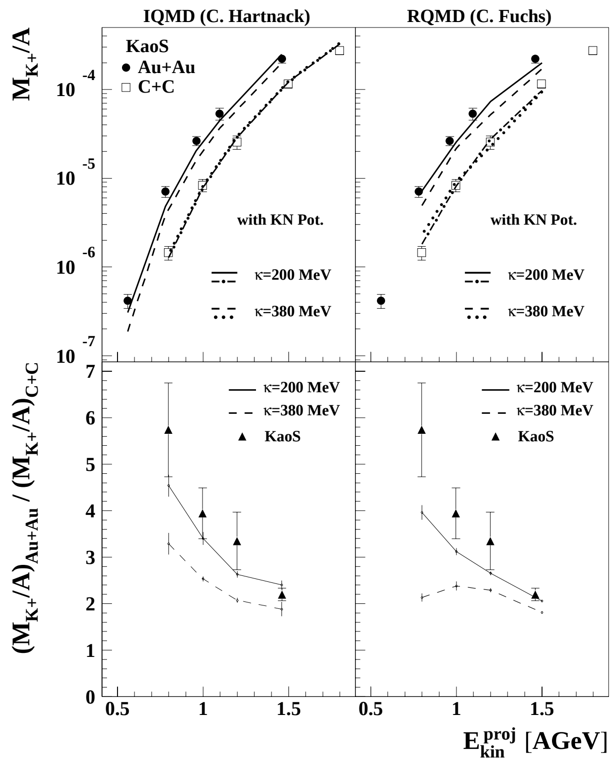

Figure 3: *The upper parts show the inclusive K^+ multiplicities per A together with model calculations for two values of the nuclear compressibility. The lower parts display the ratio $(M/A)_{Au+Au}/(M/A)_{C+C}$ as in fig. 2 together with the model predictions.*

of the kaon multiplicity on the nuclear compressibility is enhanced at beam energies well below the kaon production threshold because the energy required to create a K^+ meson has to be accumulated by multiple collisions of participating nucleons.

In order to exclude trivial phase-space effects as the reason for the observed behaviour we present in the lower panel of Figure 2 the ratio $(M/A)_{\mathrm{Au+Au}}/(M/A)_{\mathrm{C+C}}$ for pions with kinetic energies above $\mathrm{E}_{kin}^{cm} = 0.6$ GeV. The production of these pions is equivalent − in terms of available energy − to the production of K^+ mesons with a kinetic energy above 70 MeV. At this energy the kaon spectra have reached their maximum yields.

Figure 3 shows a comparison of the experimental results with two transport model calculations (lhs: IQMD [11], rhs: RQMD [7]). Both calculations have been performed with KN potential and a compressibilty of 200 MeV and 380 MeV. In the upper part the K^+ multiplicity per A is shown as a function of the beam energy both for Au+Au and C+C collisions. As expected the calculations with $\kappa = 200$ MeV yields higher multiplicities than those with $\kappa = 380$ MeV for Au+Au collisions, while for C+C no sensitivity is seen. The data are best described with $\kappa = 200$ MeV, yet the data are still slightly higher.

The lower part of Fig. 3 shows the ratio of the $(M/A)_{\mathrm{Au+Au}}/(M/A)_{\mathrm{C+C}}$ as measured and as calculated. In both calculations the ratio rises towards lower incident energies using a κ of 200 MeV in agreement with the data. For the stiffer equation of state the two calculation differ somewhat, but clearly deviate strongly from the data. These trends are rather independent whether a KN potential is used or not [7]. This evidences that the used ratio is a very sensitive quantity in extracting the compressibility of nuclear matter and that this ratio does depend little on less known input quantities.

References

[1] C. Sturm et al., Phys. Rev. Lett. **86** (2001) 39

[2] C. Müntz et al., Z. Phys. A **357** (1997) 399.

[3] J. Aichelin and C.M. Ko, Phys. Rev. Lett. **55** (1985) 2661

[4] G.Q. Li and C.M. Ko, Phys.Lett. **B 349** (1995) 405

[5] C. Fuchs et al., Phys. Rev. **C 56** (1997) R606

[6] J. Aichelin, Phys. Rep. **202** (1991) 233

[7] C. Fuchs, et al., Phys. Rev. Lett. (in print)

[8] J. Schaffner-Bielich, J. Bondorf, I. Mishustin, Nucl. Phys. **A 625** (1997) 325

[9] B. J. Ver West and R. A. Arndt, Phys. Rev. **C 25** (1982) 1979

[10] A. Wagner et al., Phys. Lett. **B 420** (1998) 20

[11] C. Hartnack, J. Aichelin, private communication

Centrality Dependence of Kaon and Antikaon Production in Ni+Ni Collisions at SIS Energies ^{B,G}

M. Menzel[4], I.M. Böttcher[4], M. Dębowski[5,6], F. Dohrmann[6], A. Förster[2], E. Grosse[6,7], P. Koczoń[1], B. Kohlmeyer[4], F. Laue[1,*], L. Naumann[6], H. Oeschler[2], F. Pühlhofer[4], W. Scheinast[6], E. Schwab[1], P. Senger[1], Y. Shin[3], H. Ströbele[3], C. Sturm[2], G. Surówka[5], F. Uhlig[2], A. Wagner[6], W. Waluś[5]
[1]GSI Darmstadt, [2]TU Darmstadt, [3]Univ. Frankfurt, [4]Univ. Marburg, [5]Univ. Kraków, [6]FZ Rossendorf, [7]TU Dresden
The KaoS Collaboration

Kaons and antikaons are regarded as a promising probe to study hadron properties in dense nuclear matter. Recent experimental results obtained with the Kaon Spectrometer indicate modifications of the in-medium properties of K^+ and K^-. Remarkable results are that the K^-/K^+ ratio is enhanced compared to pp collisions [1,2,3], the spectral slope for the antikaons is steeper than for the kaons [2] and a preferential out-of-plane emission of K^+ is observed [4].

In order to study the kaon production as a function of the reaction centrality and the beam energy, we have measured K^+ and K^- mesons around midrapidity ($\theta_{lab} = 40^\circ \pm 4^\circ$) in Ni+Ni reactions at beam energies of 1.1 (K^+ only), 1.5 and 1.93 AGeV. The multiplicity of charged particles measured by a target hodoscope is used to determine the centrality. The data set is subdivided in five centrality bins MUL1 to MUL5 for each beam energy. From a measurement under minimum bias conditions the reaction cross section is determined. For all beam energies we find a reaction cross section of $\sigma_R = 2.9 \pm 0.3$ barn, which agrees with the geometric model. The relative reaction cross section for each centrality class $\sigma_{R,MUL}/\sigma_R$ is given in Table 1 for 1.5 and 1.93 AGeV. Errors of about 10 % have to be added to the ratio $\sigma_{R,MUL}/\sigma_R$.

Figure 1 shows the invariant cross sections of K^+ (full circles) and K^- (open circles) for central to peripheral collisions (see middle panel: MUL 5 to MUL 1) as a function of the center-of-mass kinetic energy at beam energies of 1.1, 1.5 and 1.93 AGeV. The K^- mesons are scaled by a factor of 20 (see lower panel) and the yields in the bins are scaled by factors of 10 (see upper panel). The error bars shown are due to statistics only and a systematic error of 10% has to be added, caused by beam normalization, acceptance determination and trigger efficiency. The lines represent Boltzmann distributions $d^3\sigma/dp^3 \propto exp(-E_{CM}/T)$ fitted to the spectra individually for each multiplicity bin. The integrated kaon cross sections $4\pi(d\sigma_K/d\Omega_{CM})$ and the inverse slope parameters T as a function of the centrality are given in Table 1 for 1.5 and 1.93 AGeV. The errors of both quantities include the systematic effects. For all beam energies the spectral slopes decrease (Figure 1) and the inverse slope parameters T increase (Table 1) with increasing centrality of the reaction for both, kaons and antikaons.

We determined the average multiplicity per number of participating nucleons M_K/A_{part} as a function of the number of participating nucleons. M_K is calculated via $M_K =$

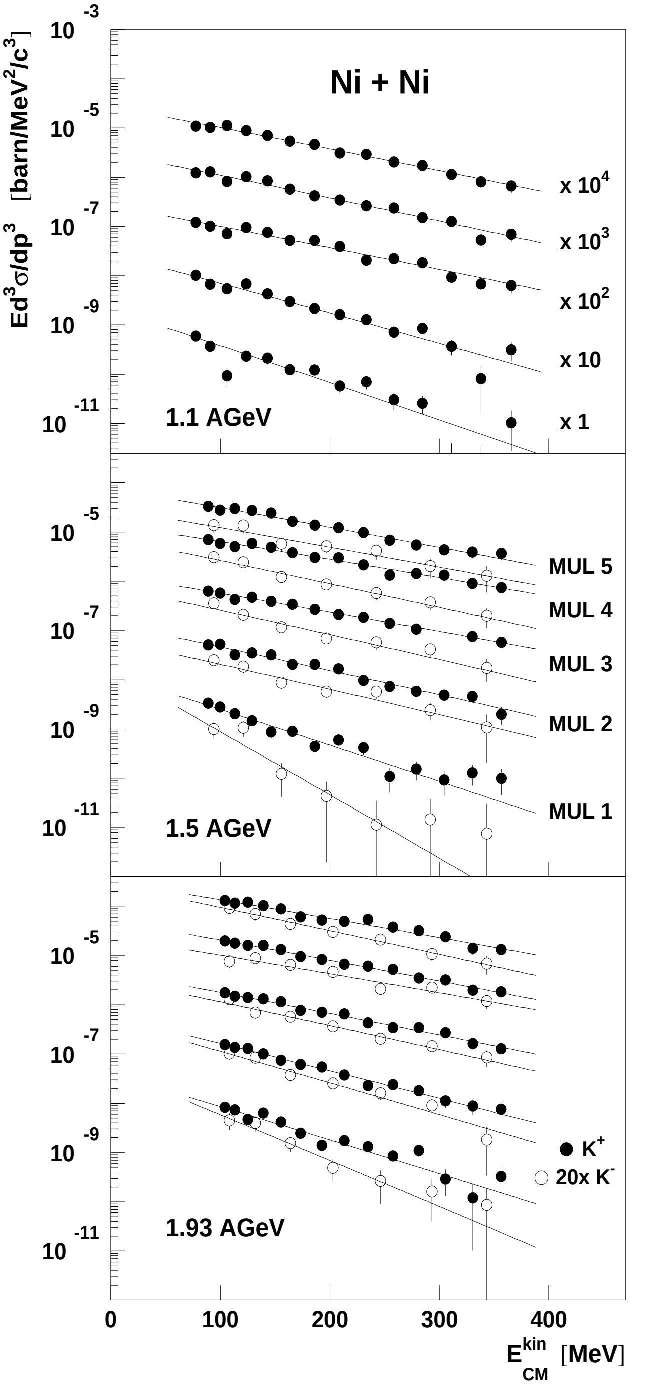

Figure 1: *K^+ and K^- invariant cross sections as a function of the kinetic energy and the centrality of the reaction measured around midrapidity ($\theta_{lab} = 40^\circ \pm 4^\circ$) for Ni+Ni collisions at different beam energies (preliminary).*

Energy	MUL	$\frac{\sigma_{R,MUL}}{\sigma_R}$	$4\pi\frac{d\sigma_K}{d\Omega_{CM}}$ [mb]	T [MeV]
1.5 AGeV K^+	1	0.41	2.2 ± 0.2	55 ± 4
	2	0.23	4.5 ± 0.4	79 ± 6
	3	0.18	6.2 ± 0.5	96 ± 7
	4	0.14	7.2 ± 0.5	101 ± 8
	5	0.05	3.3 ± 0.3	93 ± 7
1.93 AGeV K^+	1	0.44	7.6 ± 0.7	58 ± 5
	2	0.23	14.8 ± 1.2	70 ± 6
	3	0.16	18.1 ± 1.4	88 ± 7
	4	0.11	21.4 ± 1.6	91 ± 7
	5	0.06	14.8 ± 1.2	97 ± 7
1.5 AGeV K^-	1	0.41	0.06 ± 0.011	33 ± 3
	2	0.23	0.10 ± 0.012	74 ± 6
	3	0.18	0.12 ± 0.013	78 ± 7
	4	0.14	0.13 ± 0.014	80 ± 7
	5	0.05	0.07 ± 0.011	90 ± 10
1.93 AGeV K^-	1	0.44	0.30 ± 0.06	43 ± 3
	2	0.23	0.51 ± 0.07	63 ± 7
	3	0.16	0.56 ± 0.06	79 ± 10
	4	0.11	0.57 ± 0.07	96 ± 8
	5	0.06	0.46 ± 0.05	81 ± 7

Table 1: Relative reaction cross sections, K$^+$ and K$^-$ production cross sections and inverse slope parameters as a function of the centrality for Ni+Ni collisions at beam energies of 1.5 and 1.93 AGeV (preliminary).

$\sigma_K/\sigma_{R,MUL}$ with $\sigma_K = 4\pi(d\sigma_K/d\Omega_{CM})$ and with the reaction cross section for each multiplicity class $\sigma_{R,MUL}$. A_{part} is calculated from the number of nucleons in the overlap of the colliding nuclei. The impact parameter b is determined for the center of each multiplicity bin. The kaon and antikaon multiplicity per A_{part} (full circles: K$^+$, open: K$^-$) is shown in Figure 2 (different scaling factors) with a parameterization according to $M_K \propto A_{part}^{\alpha}$ (lines).

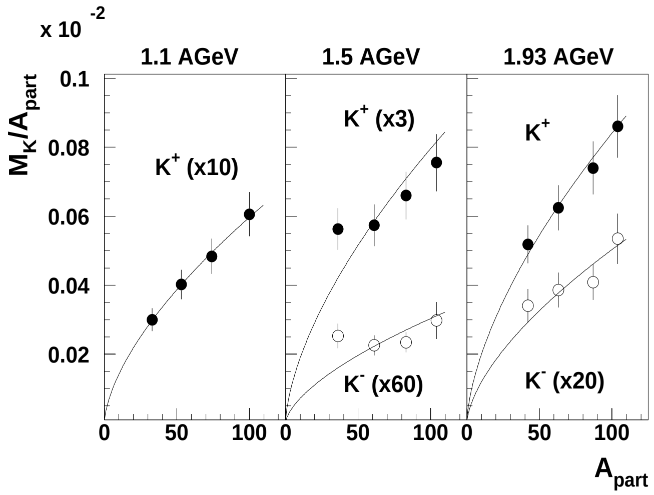

Figure 2: Kaon and antikaon multiplicity per A_{Part} *as a function of* A_{Part} *for Ni+Ni collisions at beam energies of 1.1, 1.5 and 1.93 AGeV (preliminary).*

The multiplicities for MUL 1 are not shown because the errors in integrating the cross sections are larger compared to the other bins. Within the uncertainties of A_{part} we get a common $\alpha = 1.62 \pm 0.21$ for K$^+$ and K$^-$ and for all beam energies. Values of α larger than unity indicate that the nucleons participate more than once in the kaon production.

In Figure 3 we present the K$^-$/K$^+$ ratio as a function of the impact parameter b for the beam energy 1.5 AGeV (full triangles) and 1.93 AGeV (full squares). Within the error bars the values are constant between 1.8 fm and 6 fm and the averaged ratios are 0.020 ± 0.004 for 1.5 AGeV and 0.031 ± 0.004 for 1.93 AGeV. The ratio for 1.93 AGeV

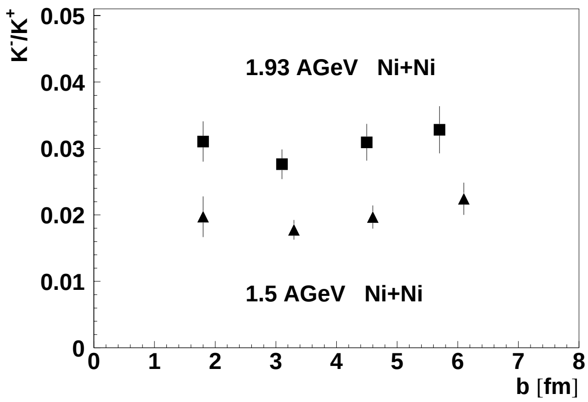

Figure 3: *K^-/K^+ ratio as a function of the impact parameter b for Ni+Ni collisions at beam energies of 1.5 and 1.93 AGeV (preliminary).*

agrees with the value of 0.031 ± 0.005 for non-central and near-central collisions in Ni+Ni measured for the full rapidity range ($\theta_{lab} = 28°$ to $64°$) at the same beam energy [3]. All measured K$^-$/K$^+$ ratios for Ni+Ni can be compared with the smaller system C+C [2] and the corresponding inclusive values of 0.025 ± 0.007 for the beam energy 1.8 AGeV and 0.038 ± 0.013 for 2.0 AGeV.

In conclusion, the K$^-$/K$^+$ ratio at a given bombarding energy is constant as a function of the centrality of the reaction and the size of the collision system. This indicates, that the antikaon yield is coupled to the kaon yield via the strangeness exchange reaction $Y\pi \to K^-N$ (with $Y = \Lambda, \Sigma$).

* now at Ohio State Univ., Columbus, USA

References

[1] R. Barth et al., Phys. Rev. Lett. **78** (1997) 4007
[2] F. Laue et al., Phys. Rev. Lett. **82** (1999) 1640
[3] M. Menzel et al., Phys. Lett. **B 495** (2000) 26
[4] Y. Shin et al., Phys. Rev. Lett. **81** (1998) 1576

Dependence of K^+ Production on the System Size at 1.5 AGeV

A. Devismes[1], N. Herrmann[2], P. Crochet[3], K. Wiśniewski[2], A. Andronic[1], C. Finck[1], A. Gobbi[1], O. Hartmann[1], K.D. Hildenbrand[1], T. Kress[1], Y. Leifels[1] and, W. Reisdorf[1], FOPI Collaboration
GSI Darmstadt[1], University of Heidelberg[2], LPC Clermont-Ferrand[3]

The FOPI collaboration has recently measured K^+ production in Ca+Ca, Ru+Ru and Au+Au collisions at 1.5 AGeV [1] to investigate the dependence on system size and to learn more about modification of kaon properties in dense hadronic matter which is eventually connected to the partial restoration of chiral symmetry. Several theoretical models predict that the K^+ mass increases slightly with baryon density whereas the K^- mass should decrease [2, 3, 4, 5, 6]. These medium modifications of the kaon masses lead to a lower probability for K^+ production since it becomes energetically more difficult to produce them and to a higher probability for K^-.
Previous results from FOPI on kaon flow [7] and K^-/K^+ ratio [8] seem to favor the existence of in-medium potentials for kaons derived from the comparison to transport model calculations [9, 10].

The K^+ mesons are identified in the central part of the FOPI detector by a drift chamber (CDC) surrounded by a barrel of plastic scintillators for the measurement of the time of flight. The TOF subsystem covers the polar angular range between 40° and 130°. For a clean identification of K^+ in the Au+Au system a laboratory momentum cut of $p < 0.4$GeV/c is required. This cut is also applied to the other systems in order to select the same region of the phase space although K^+ can be identified in the lighter collision systems up to p=0.5 GeV/c. A simulation of the FOPI detector response based on the GEANT package is used to estimate the tracking efficiency in each system. The results vary between 87% for the Au system and 99% for the Ca system. The data are further corrected for the matching efficiency between the CDC and the TOF barrel that is estimated from proton tracks and for the kaon lifetime.

Figure 1 shows the number of K^+ per participant as function of the number of participants for Ca+Ca, Ru+Ru and Au+Au at 1.5 AGeV. The charged particle multiplicity measured in the forward plastic wall of the FOPI detector has been used to select central collisions corresponding to 10% of the total cross section. The data are shown by the circles, the error bars include statistical and systematical errors. The experimental results are compared to the predictions of transport models, RBUU [10] (upper panel) and IQMD [11] (lower panel). These calculations are available in two versions: the first one employs the free kaon mass (triangles), the other one includes modified masses (squares), i.e. the K^+ mass depends linearly on density with an increase of 5% at normal nuclear matter density. Within errors the data do not show any dependence on the system size whereas both models consistently predict an increase of the kaon production with the system size. This increase is slightly more pronounced in the absence of medium effects. In both cases, in addition the absolute yields are better described by the versions including the in-medium modification of the K^+ mass.

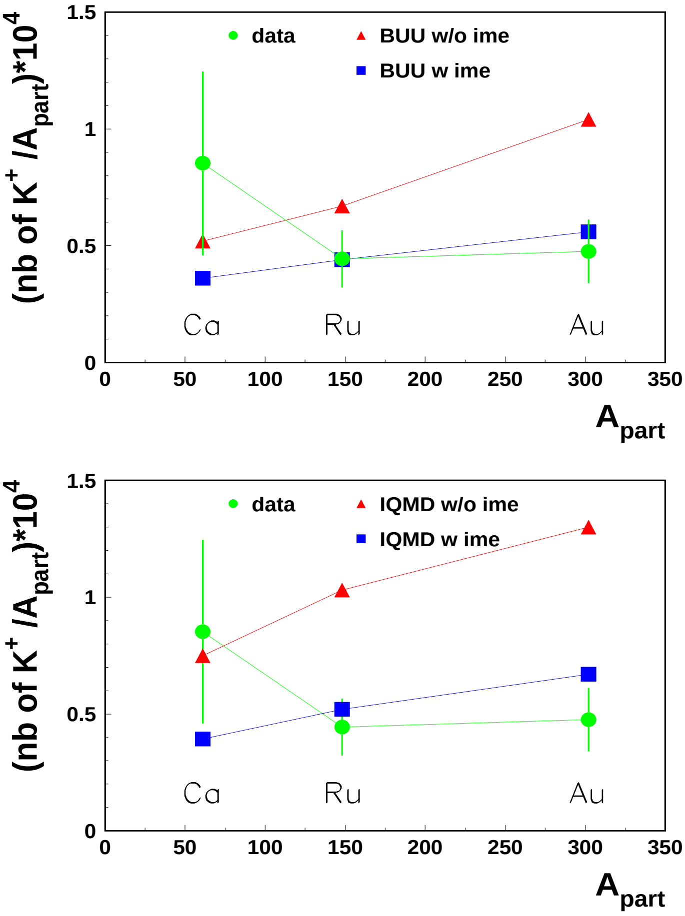

Figure 1: *Number of* K^+ *per participant as function of the number of participant in Ca+Ca, Ru+Ru and Au+Au collisions at 1.5 AGeV. The data (circles) are compared to the predictions of RBUU (upper) panel and IQMD (lower panel) with in-medium modification of kaon mass (squares) and without (triangles).*

References

[1] A. Devismes, PhD. thesis, Univ. Darmstadt, Feb. 2001
[2] G.E. Brown et al., Nucl.Phys. A567 (1994) 937
[3] M.Lutz et al., Nucl.Phys. A574 (1994) 755
[4] G.Q.Li et al., Phys.Rev.Lett. 79 (1997) 5214
[5] J. Schaffner *et al.*, Nucl. Phys. A625 (1997) 325
[6] G. Mao *et al.*, Phys. Rev. C59 (1999) 3381
[7] P. Crochet *et al.*, Phys. Lett. 486 (2000) 6
[8] K. Wiśniewski, Eur. Phys. J. A9 (2001) 515
[9] C.M.Ko, G.Q.Li, J.Phys.G22 (1996) 1673
[10] W. Cassing, E.L. Bratkovskaya, Phys.Rep. 308 (1999) 65 and private communication
[11] C. Hartnack, private communication

Commissioning Results from the Dielectron Spectrometer HADES[B,G,EC]

The HADES Collaboration

Status overview

During the year 2000 most of the detector modules were installed and equipped with readout electronics. All 6 sectors of the Pre-Shower detector, the outer Time-Of-Flight (TOF) wall, the forward Time-of-Flight paddles (Tofino), two complete planes of Multiwire Drift Chambers (MDC, 12 modules) in front of the superconducting magnet as well as the Ring-Imaging-Cherenkov detector (RICH) surrounding the target were installed. Due to the delayed delivery of a few readout modules and since only 4 RICH sectors were equipped with mirrors, common readout was performed for 4 out of the 6 sectors during a commissioning beam-time in November 2000. Since only one out of the altogether 12 outer MDC's was installed, the momentum resolution of the setup was restricted to about 10%. The current setup is shown in Figure 1.
In the following part, first results regarding the performance of this setup are reported.

Figure 1: Upstream view of the Hades setup. Only the support structure and outermost detector layer (Pre-Shower detector, part of TOF) are visible.

Electron Identification in the RICH

The readout electronics of the ring imaging Cherenkov detector (RICH) was completed and extensively tested. The refined gas supply system went into routine operation. In order to allow for commissioning measurements with beam a preliminary RICH mirror was equipped with 4 segments of float glass coated with Al / MgF_2. The photon detector was operated during the beam times under stable conditions with an anode voltage of 2550 V at negligible leakage currents. The VUV transmission of the gas (CH_4 at 1000 hPa) at the detector exhaust was measured to be essentially free of impurities down to the absorption cut-off at λ = 146 nm. This was not yet the case for the standard radiator gas C_4F_{10} due to so far unknown contaminations.
In order to verify the performance of the detector and especially its CsI photon converter a series of measurements were performed with light and medium heavy ions radiating Cherenkov light in a stack of two solid radiator discs (SiO_2 and MgF_2) located close to the regular target station inside the RICH. Since the amount of light can be calculated precisely this configuration is a calibrated and pulsed (τ ~10 ps) light source.
Due to the different refraction indexes two 'super ring' patterns with different radii are generated and the optical dispersion results in a well defined broadening of their radial distributions.
A typical ring pattern accumulated for 600 projectiles and a 600 AMeV C beam is shown in Figure 2 and exhibits the high photon statistics expected for $Z > 1$ particles.

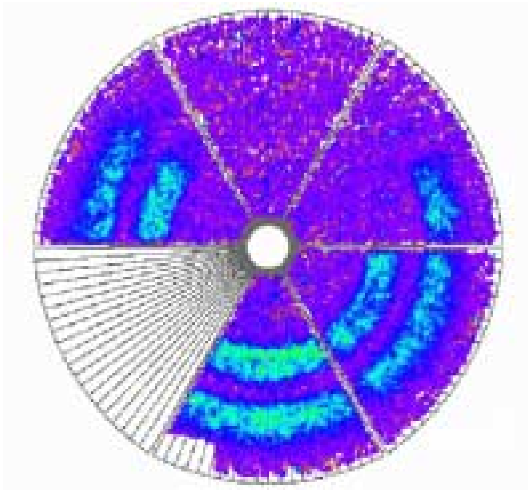

Figure 2: Superposition of ~600 Cherenkov rings from C ions (E = 600 AMeV, β = 0.794) impinging on a MgF_2 and a SiO_2 radiator. The upper sectors are in the shadow of the beam pipe; one lower sector was not equipped with mirrors.

Proper choice of radiator thickness (5mm for SiO_2, 1mm for MgF_2) allowed for a clear spatial separation of single photon hits on the pad plane. The measured shape of the radial distribution of individual photons agrees well with results of a full GEANT simulation using optimum detector parameters. These parameters would translate to a figure of merit N_0 = 110 when the solid radiators are replaced by the C_4F_{10} gas radiator. From a comparison of the amplitudes we deduce for the two lower sectors in Figure 2 values N_0 = 90 and N_0 = 105, the reduction being probably due to a slight deterioration of the CsI quantum efficiency.
Taking pulse height spectra for single photo electrons fitted with a Polya function an effective gas gain of ~$1.5 \cdot 10^5$ slightly above the design value was obtained. With the noise level reduced to about 3500 e^- (3σ) a detection efficiency of ~94% for single photo electrons was extracted.

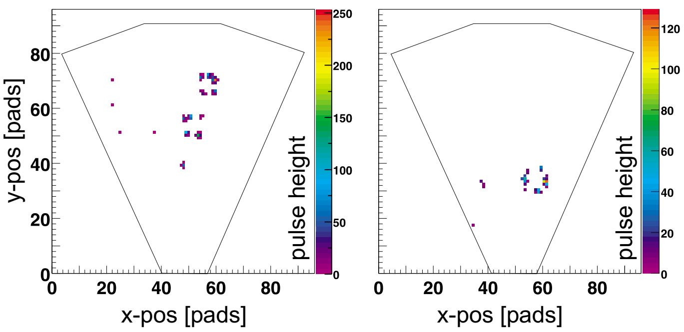

Figure 3: Double and single ring patterns observed in the RICH for electrons from C + C at E = 1.5 AGeV.

From $2 \cdot 10^6$ events recorded for C+C collisions at 1.5 AGeV about 10k events were found showing clear Cherenkov ring patterns as shown in Figure 3. First results from the analysis of the combined detector setup are presented in the following chapters.

Multiwire Drift Chambers

During the past year the inner section of the tracking system was completed and tested in two beam times. It comprises 12 chambers in two different geometries covering an area of 5 m^2. About 13.000 individual drift cells are read out by customised front-end electronics in less than 10 µs. Data is transferred to read-out controllers located close to the detector units. These units were developed in the electronic department of GSI and were used for the first time in the November beam time.

The assembly of the outer tracking system was started with the installation of the first plane III module built at FZ Rossendorf. A second plane III and the first plane IV module (constructed at IPN Orsay) are currently commissioned and will be available in the spring beam time 2001. The completion of the outer tracking system, which will finally cover 28 m^2, is scheduled for 2002. Figure 4 shows the plane IV module being lifted to the service table for commissioning. In particular the size of the plane IV module, with maximum wire length of 280 cm, demanded for customised infrastructure and a thorough construction.

Figure 4: Picture showing the first plane IV module arriving at GSI. For transportation the chamber is mounted on a support structure via surge dampers. It has a height of 3 m and weighs about 200 kg.

During commissioning with beam a stable operation of all chambers was observed. The detectors perform well within the specifications. Operated with a gas mixture of Helium/i-butane (60/40) the chambers reach efficiencies of single cells above 98%. The intrinsic resolution lies around 120 µm. Composed of 6 individual drift cell layers per module, the tracking chambers provide sufficient redundancy to identify tracks even at the highest multiplicities. Due to the optimised wire orientations and multiple measurement of positions, the resolution in the direction of the magnetic kick is about a factor two smaller than the intrinsic resolution. Figure 5 visualises the operation principle of the tracking chamber. The crossing area of the cells being hit by the particle identifies impact positions. The information shown in the Figure 5 is used in the tracking software (version developed by the Dubna group) to search for track candidates.

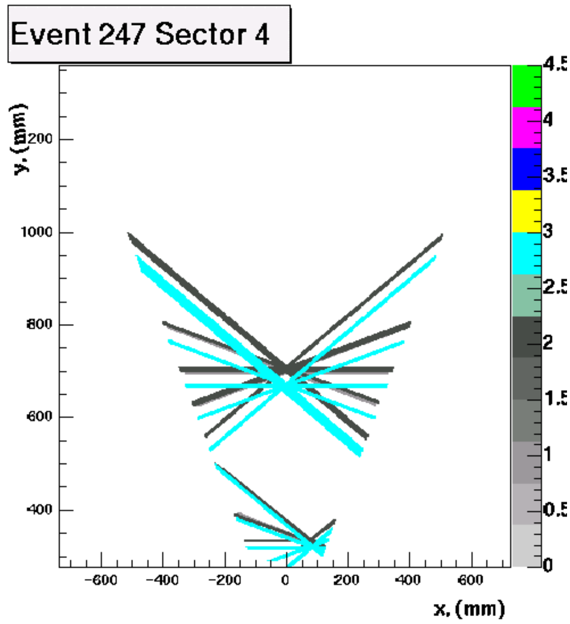

Figure 5: Projection of fired drift cells of three detectors in one sector. Black and dark grey refer to the inner tracking detectors, cyan to the cells of plane III. The shift of the crossing point of plane III with respect to the other two detectors is the result of the momentum kick in the magnetic field.

Start/Veto Detector

A pair of segmented diamond detectors located 75 cm upstream and downstream of the target is used to determine the start time for TOF measurements. The downstream detector vetos ions which were not reacting in the target. For 1 AGeV C+C a veto efficiency of ~90% was obtained. For an optimised beam focussing the veto efficiency should be significantly higher.

Time-Of-Flight Detector

The Time-of-Flight detector consists of an inner part (TOFino, 24 scintillators) in front of the Pre-Shower detector and an outer TOF wall. As of December 2000 both detectors were complete and fully assembled. The 384 scintillating rods of the outer wall, made from BC408 and each one equipped with two photomultipliers, produce fast signals handled by means of 48 constant fraction discriminator modules (16-fold C808 by CAEN). The logical outputs are delayed using 24 32-fold active delay units developed by the collaboration along with the 32-fold TDC units used to digitise the signals. These latter modules, in VME standard, are read-out via the fast Chained Block Transfer (CBT) protocol, allowing to sustain high event rates. The final tests on the amplitude measuring electronics (CAMAC shapers and VME ADCs) have been successful and their mass production is in progress. The forthcoming installation of this electronics, during the first half of 2001, will further improve the TOF performance.

The laser calibration system is complete and allows to evaluate the needed calibration constants for all the detector channels. An extension of this system is already in progress, in order to accommodate for the calibration of the TOFINO as well.

A newly developed slow control software using the EPICS framework allows to initialise and operate the TOF electronics, the high voltage system and the laser calibration system. An online analysis package and a Graphical User Interface (GUI) have been developed within the HYDRA environment that allow a quick and easy monitoring of detector data throughout a beam time. A sample online plot for the TOF detector is shown in Figure 6.

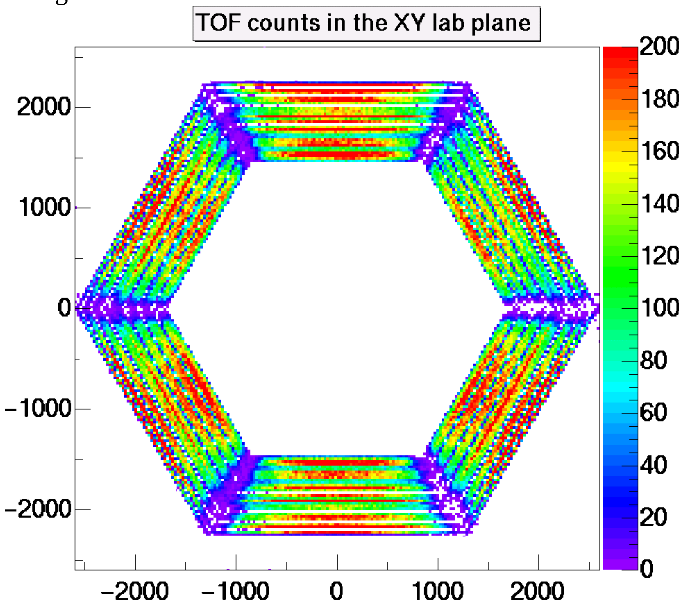

Figure 6: The TOF detector inclusive count distribution in the XY laboratory frame (units are in mm), as seen by means of the online GUI for monitoring.

A preliminary analysis of the collected data shows that the calibration procedure is reliable, and that a few levels of iteration on the related data may further improve the results. Correlated data from TOF and RICH prove that HADES can really identify leptons, as can be seen in Figure 7.

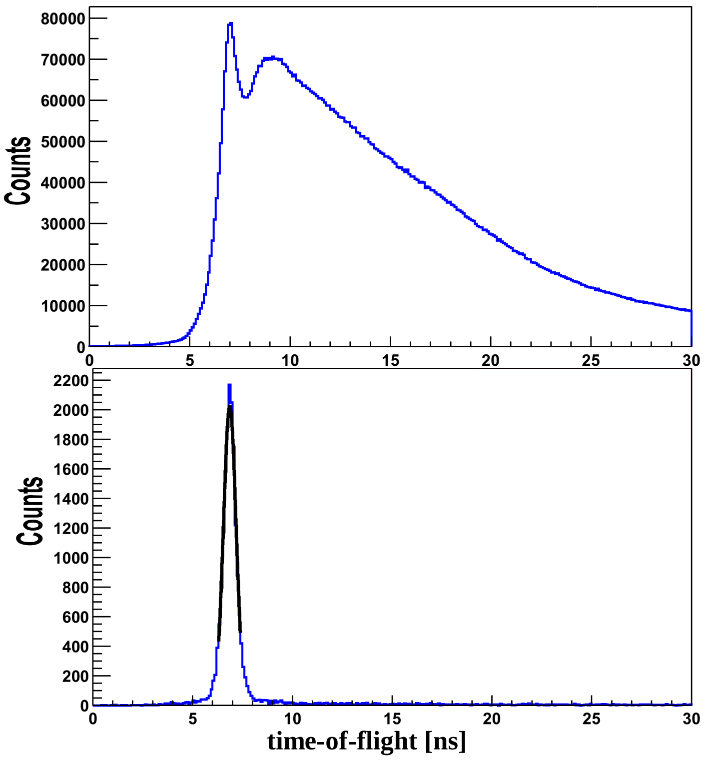

Figure 7: Upper plot: TOF spectrum of all particles detected. Lower plot: TOF spectrum for electron candidates, as selected by means of a position correlation between RICH and TOF hits. Data were taken without magnetic field.

The measured times in the TOF detector have been renormalised to equal flight path (2.1 m). The lepton peak in the upper part of Figure 7 is due to knockon electrons with energies well below the Rich threshold of 10 MeV.

Pre-Shower Detector

The whole Pre-Shower detector has been finally mounted on the HADES spectrometer mainframe. All detector channels are connected to the read-out electronics consisting of 32 channels Front-End cards and fast digital Read-out Boards located directly on the detector. The main goal of this detector is electron identification at forward polar angles (smaller than 45 degree). This should be achieved measuring electromagnetic showering in two lead converters placed between 3 gas chambers with pad readout. As has been shown in simulations, full electron identification can only be achieved when electron candidate hits are matched with rings in the RICH and fast particle hits in the TOFino detector. The Pre-Shower detector can also be used as a tracking device since it provides a hit position of a particle track after bending in the magnetic field and thus allows for a rough momentum determination.
The whole system has been successfully tested in C+C collisions. Charged particle tracks have been reconstructed from Pre-Shower and TOFino hits and from positions in the MDC (plane 2). Figure 8 (upper row) shows the resulting time of flight spectrum and TOF versus momentum correlations. The plots in the lower row present similar distributions with the additional condition on spatially correlated rings found in the RICH and electromagnetic shower candidates found in the Pre-Shower detector. The discrimination of the electron signal in the time of flight spectra is clearly visible. A gaussian fit to the electron peak gives σ=0.67ns, however a TOF correction due to the track length in the magnetic field has not yet been applied. The intrinsic time resolution of TOFino amounts to 0.25-0.3 ns.

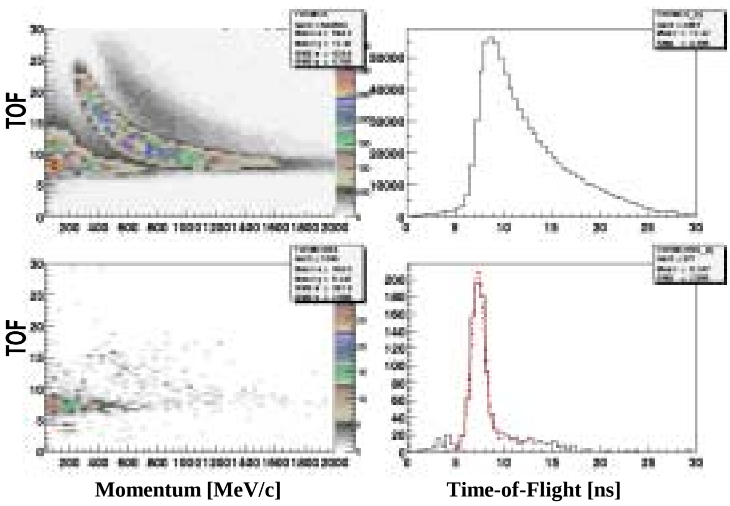

Figure 8: TOF versus Momentum (left) and TOF distributions (right). Upper part: All charged particles. Lower part: Spatial correlation with RICH rings required.

Trigger and Data Acquisition

In order to facilitate the handling of the various detector subsystems during commissioning, the trigger distribution system was enhanced by adding a trigger hub featuring flexible configuration and diagnostics options. In particular, it is now possible under software control to run with any combination of subsystems without recabeling of the trigger bus.

Readout for the Pre-Shower and TOF subsystems

The Pre-Shower readout hardware was completed and integrated into the setup. Zero suppression and calibration were successfully tested.

Readout of the TOF/TOFino-subsystem in Chained Block Transfer Mode (CBLT) was successfully implemented using modified versions of the CAEN TDC/ADC-modules and the new combined TOF readout/trigger modules. Here, a scheme with one SHARC-DSP-based readout/trigger module per VME crate connected to a common concentrator board was used.

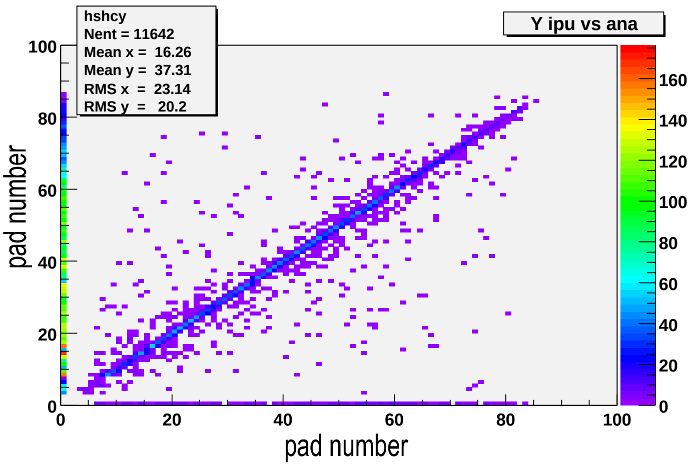

Figure 9: Correlation of x-coordinates of ring candidates found by hardware and by software. Events above and below the diagonal are due to different threshold settings in both algorithms.

RICH Trigger Hardware and Matching Unit

A first successful test of the first/second level trigger/DAQ – scheme with pipelining was conducted during the November commissioning run. Here, the Matching Unit (MU) was connected to the TOF subsystem and to one module of the RICH Image Processor. RICH ring coordinates were transmitted to the MU and recorded event-by-event. Figure 9 shows the result of an off-line analysis showing the correlation of ring center x-coordinates on the RICH padplane found by hardware image processing and by applying the RICH software ring finding algorithm. Additional events, which are non-diagonal are resulting from different thresholds in both algorithms.

Common Event Building

Based on a dedicated ATM network data from the various detector subsystems are transferred asynchronously from 7 VME-CPU's to a common event builder which assembled the full events. A data taping speed of up to 5 MB/s could be achieved, corresponding to up to 2000 events/s for the system C+C.

First Results

The combined analysis of detector signals from one MDC plane and the outer TOF wall allows to identify charged particles. As the outer drift chambers were not yet included, this analysis could be done in a low momentum resolution mode only. The result is shown in Figure 10 for the system C+C at 1.5 AGeV beam energy. Pions, protons and deuterons are clearly separated. The data were taken at 72% of the maximum magnetic field. The calibration of the detector alignment is still in progress and an improved resolution is expected.

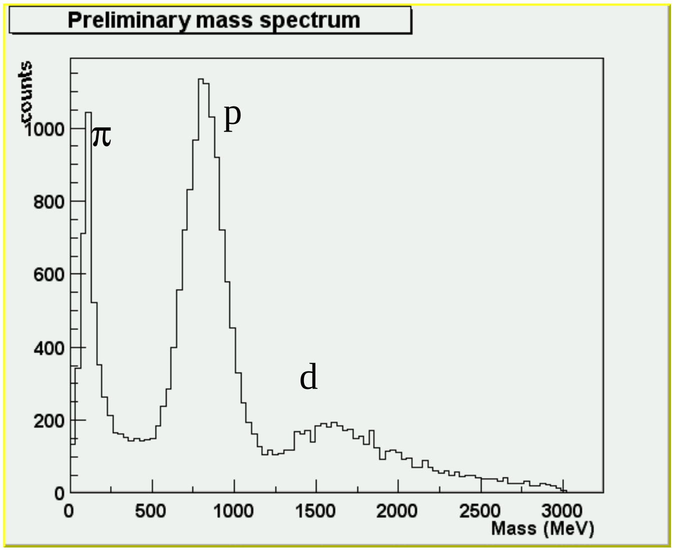

Figure 10: Mass spectrum obtained by analysing the transverse momentum kick within the magnetic field using position and angle information from one inner drift chamber and position measured with the outer TOF wall. Calibration is preliminary.

From a first preliminary analysis of the RICH data an opening angle distribution for lepton pairs was obtained for about 800.000 events C+C at 1.5 AGeV (Figure 11). As expected, the distribution is dominated by small opening angles due to pairs from Dalitz decays of π^0 and conversion of photons in the target and radiator. Besides ring recognition in the Rich no further lepton identification or track matching was required.

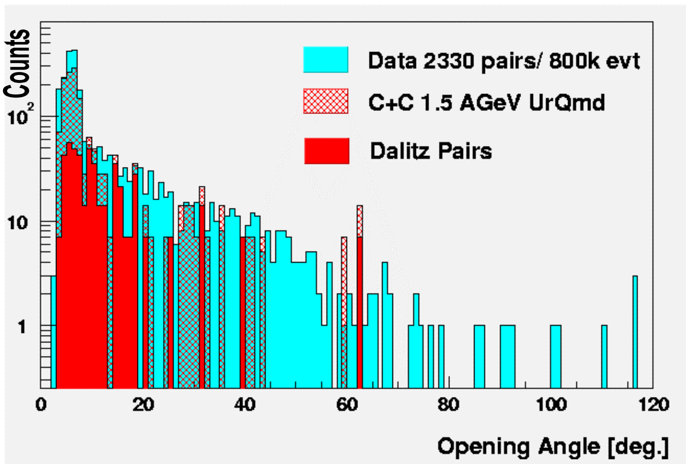

Figure 11: Opening angle distribution of lepton pairs obtained for about 800000 C+C collisions at 1.5 AGeV(blue) as compared to a simulation which includes only Conversion and Dalitz decays of the π^0. Preliminary result.

Summary and Outlook

The setup has proven its capability to measure lepton pairs. With the installation of outer drift chambers during 2001 and spring 2002 the momentum resolution should be significantly improved. Physics runs providing lepton pair spectroscopy with good statistics are expected for this year.

Quenching of resonance production in nuclear collisions around 1 AGeV

A.B. Larionov*, W. Cassing, S. Leupold, U. Mosel
University of Giessen

Pion production in heavy-ion collisions is relatively well studied both theoretically and experimentally. There is still, however, a longstanding open question: Why pion multiplicities produced by transport models like BUU and QMD overestimate the experimental data? The largest discrepancy is observed for central Au+Au collisions at 1 AGeV [1]. In this system pions are mostly produced through the Δ-resonance excitations in a two-step process: $NN \to N\Delta$, $\Delta \to N\pi$. Since this process happens in nuclear matter, in-medium effects (besides evident Pauli blocking of the nucleons in final states) cannot be excluded.

We have studied the effect of possible in-medium modification of the cross sections for the processes $NN \leftrightarrow NR$ on the pion observables. The calculations have been done within the BUU model [2] employing the SM mean field (K=220 MeV). The in-medium spin-averaged matrix element squared for the resonance R production/absorption was parametrized as $\overline{|\mathcal{M}_{NN\leftrightarrow NR}|^2} = \kappa(\rho)\overline{|\mathcal{M}^{vac}_{NN\leftrightarrow NR}|^2}$, where $\overline{|\mathcal{M}^{vac}_{NN\leftrightarrow NR}|^2}$ is the vacuum matrix element squared and $\kappa(\rho)$ is a density-dependent function to be determined from a fit of the experimental data. The function $\kappa(\rho)$ is for simplicity supposed to be the same for all baryon resonances. Fig. 1 shows the π^- multiplicity vs time for a central Au+Au collision at 1.06 AGeV for the three choices of $\kappa(\rho)$: $\kappa(\rho) = 1$ – standard (dashed line), $\kappa(\rho) = 1 + 3\rho/\rho_0$ – amplified (dotted line) and $\kappa(\rho) = \min(1, \max(0, 1 - 2(\rho/\rho_0 - 1)))$ – quenched (solid line). There is a reduction of the pion yield in both cases, but the experimental data are only well fitted for the quenched choice of $\kappa(\rho)$. We checked that a further increase of the amplification factor will not modify the pion multiplicity essentially: it always overpredicts the data at least by 30% [3]. The quenching scenario assumes that at $\rho \leq \rho_0$ the in-medium modifications are absent, at $\rho_0 < \rho \leq 1.5\rho_0$ the resonance production/absorption matrix elements decrease linearly with density and at $\rho \geq 1.5\rho_0$ the matrix elements become zero, i.e. at high density resonances do not experience any elastic or inelastic scatterings with nucleons. They can, however, decay or be produced in processes $R \leftrightarrow N\pi$.

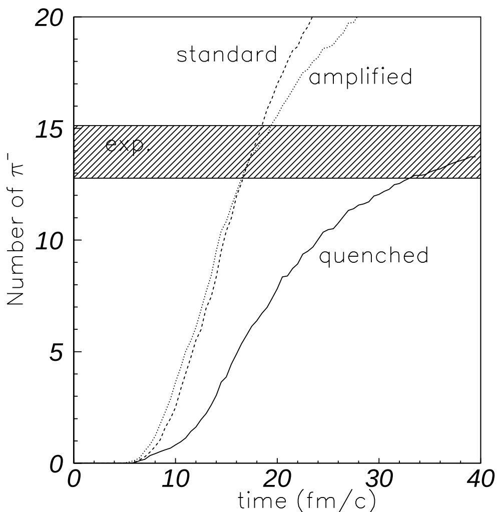

Fig. 1

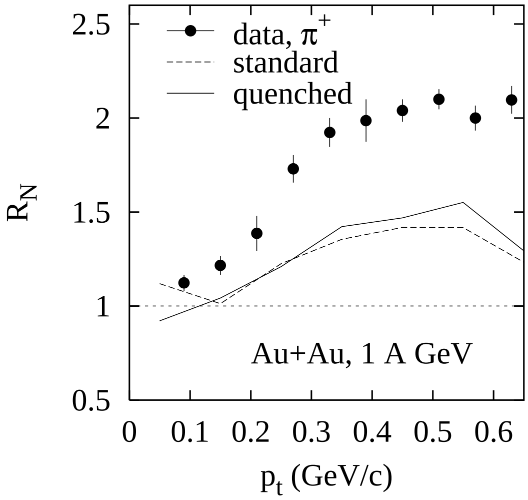

Fig. 2

We show in [3] that for Au+Au at 1 AGeV the quenching results in a vertical downward shift of the pion p_t-spectra, thus improving the agreement with the data [1, 4]. For the light system C+C at 0.8÷2 AGeV, both standard and quenched calculations produce practically the same m_t-spectra of π^o's [3], since in the lighter system medium modifications are weaker.

Both, transverse in-plane and out-of-plane pion flows are weakly influenced by the quenching. There is a good agreement of our calculations with the data on the in-plane $\pi^\pm$ flow [5] (see [3] for details). However, we underpredict the high-p_t π^+ squeeze-out ratio $R_N := (N_{\pi^+}(90^o) + N_{\pi^+}(270^o))/(N_{\pi^+}(0^o) + N_{\pi^+}(180^o))$ [6] as shown in Fig. 2. Therefore, in order to describe the pion squeeze-out some additional effects have to be taken into account. We expect, that the introduction of a momentum-dependent pion potential as well as further modifications of the resonance life time will improve the agreement with data on pion squeeze-out in analogy to the case of nucleon squeeze-out [7].

References

[1] D. Pelte et al., Z. Phys. A **357**, 215 (1997).

[2] M. Effenberger, E.L. Bratkovskaya, and U. Mosel, Phys. Rev. C **60**, 044614 (1999).

[3] A.B. Larionov et al., in preparation.

[4] O. Schwalb et al., Phys. Lett. B **321**, 20 (1994).

[5] J.C. Kintner et al., Phys. Rev. Lett. **78**, 4165 (1997).

[6] Y. Shin et al., Phys. Rev. Lett. **98**, 1576 (1998).

[7] A.B. Larionov et al., Phys. Rev. C **62**, 064611 (2000).

*On leave of absence from RRC "I.V. Kurchatov Institute", 123182 Moscow, Russia

Pion and Kaon Production in central Pb+Pb Collisions at 40 GeV per Nucleon from the NA49 Experiment^{G,B}

A.Billmeier[1], C.Blume[2], R.Bramm[1], P.Buncic[1], P.Dinkelaker[1], M.Gaździcki[1], T.Kollegger[1], I.Kraus[1], C.Markert[2], A.Mischke[2], R.Renfordt[1], A.Sandoval[2], H.Sann[2], R.Stock[1], H.Ströbele[1], M.Wensveen[2], A.Wetzler[1], J.Zaranek[1] for the NA49 Collaboration.
[1]Universität Frankfurt, [2]GSI Darmstadt

The creation of new particles is the most important process in high energy nuclear collisions and its excitation function may allow to detect threshold effects and non-monotonic behavior. The NA49 experiment at the CERN SPS has complemented its 158 GeV per nucleon data by recording 1.8 million Pb+Pb events at 40 GeV per nucleon in fall 1999 and 400.000 central events at 80 GeV per nucleon in fall 2000. Results on pion and kaon production in central (7%) 40 GeV per nucleon events are presented here.

The experiment NA49 was designed for Pb-beams at top SPS energy. The effects of a four times lower Lorentz boost at 40 GeV/nucleon was compensated by lowering the magnetic field strength accordingly. This kept all the essential features of the NA49 detector [1] intact. The identification procedures based on the specific enery loss (dE/dx) were supplemented by time-of-flight identified particles in the TOF acceptance regions. In order to get pion rapidity spectra, one had to identify pions in momentum intervals where their energy loss is the same as for kaons or protons. Therefore we first analysed negatively charged particles [2]. To get the π^- spectrum, we subtracted the kaons and antiprotons as identified by dE/dx (at different laboratory momenta!) and then constructed from the resulting π^- the π^+ spectra using dE/dx determined π^+ to π^- ratios in regions where identification was possible. Those parts of the spectra for which the ratios were not measured have been obtained from extrapolation.

Acceptance losses, tracking inefficiencies and losses due to particle identification procedures were corrected for in bins of rapidity and p_T. The systematic errors on the multiplicity of pions and kaons are estimated to be less then 10%. Since the NA49 acceptance covers only the forward hemisphere, the measured spectra were mirrored at midrapidity to calculate the total multiplicities.

Fig.1 shows the rapidity distribution of negatively charged pions. The rapidity density at mid-rapidity is 110 $\pm$ 5 and the FWHM of the distribution comes out to be 2.45 $\pm$ 0.1. This is to be compared to 3.4 $\pm$ 0.15 at 158 GeV per nucleon. The respective fractions relativ to the full rapidity gap are very similar. The integral over the full rapidity distribution yields an average of 313 $\pm$ 15 π^- per central event. Fig.2 displays the transverse mass distribution of the pions. Its form is obviously not an exponential. We therefore refrain from giving a slope parameter but rather calucte the mean $p_T = 0.36 \pm 0.2$, which is slighly lower than the value found at 158 GeV per nucleon.

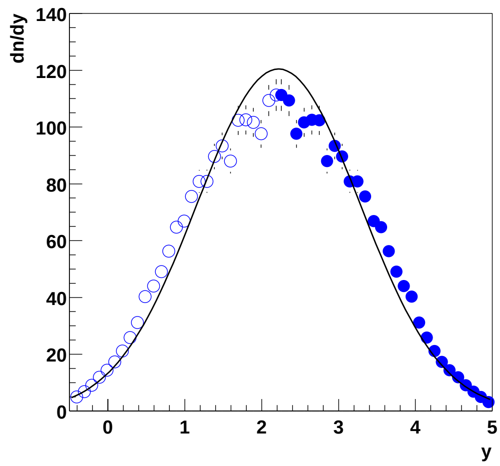

Figure 1: Rapidity distribution of negatively charged pions in central Pb+Pb collisions at 40 GeV per nucleon.

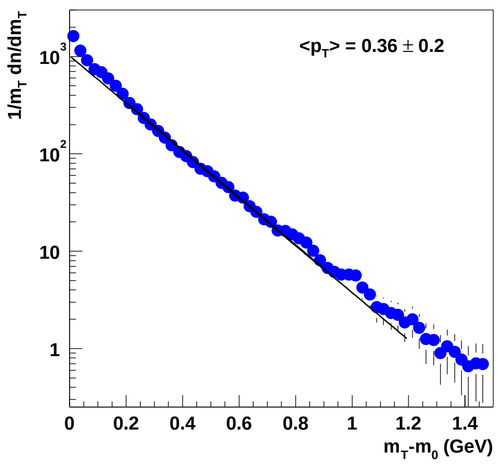

Figure 2: Transverse mass distribution of negatively charged pions in central Pb+Pb collisions at 40 GeV per nucleon.

In Fig.3 we present the rapidity distributions of charged kaons. The integrals over the full rapidity distributions yield 17.8 $\pm$ 0.9 K^- and 56.3 $\pm$ 3 K^+ per central event [3]. The total yields and the multiplicities at midrapidity are summarized in table 1.

	total yield	midrapidity yield
π^-	313 ± 15	110 ± 5
π^+	282 ± 15	99 ± 7
K^-	17.8 ± 0.9	8.18 ± 0.4
K^+	56.3 ± 3	20.52 ± 1

Table 1: Pion and kaon multiplicities in central 40 A·GeV Pb+Pb collisions, the midrapidity yields are calculated for $\left| \frac{y - y_{cm}}{y_{cm}} \right| < 0.125$.

These measurements allow together with previous NA49 measurements at 158 GeV per nucleon [4], measurements at the AGS [5] and RHIC [6] to plot the energy dependence of the $K^+/\pi+$-ratio. It shows a non monotonic behavior in the SPS energy range (figure 4). To further study this structure, the 80 GeV per nucleon data is currently being analysed and NA49 will take additional Pb+Pb data at 20 and 30 GeV per nucleon.

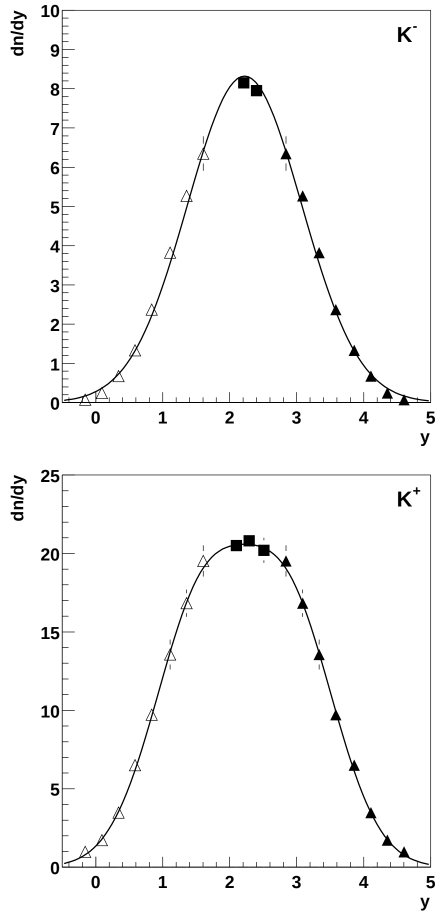

Figure 3: Rapidity distribution of charged kaons in central Pb+Pb collisions at 40 GeV per nucleon. Squares are from TOF-dE/dx analysis, triangels from dE/dx-only analysis. Open symbols are reflected at midrapidity.

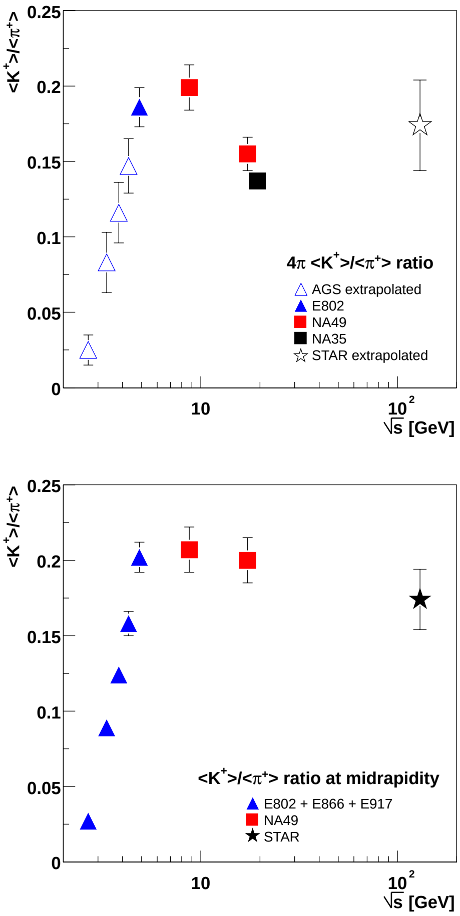

Figure 4: $K^+/\pi+$-ratio as function of collision energy for central Au+Au and Pb+Pb collisions. Figure a) shows the 4π-ratios, b) the midrapidity ratios

References

[1] S. Afanasiev *et al.* [NA49 Collaboration], Nucl. Instrum. Meth. **A430** (1999) 210.

[2] R. Bramm, diploma thesis, Universität Frankfurt, 2001.

[3] T. Kollegger, diploma thesis, Universität Frankfurt, 2001.

[4] J. Bachler *et al.* [NA49 Collaboration], Nucl. Phys. A **661** (1999) 45.

[5] L. Ahle *et al.* [E866 Collaboration and E917 Collaboration], Phys. Lett. **B476** (2000) 1.

[6] H. Caines for the STAR collaboration, QM2001, to appear in the proceedings.

Λ Hyperons Produced in 158 *A* GeV Pb+Pb Collisions^{G,B}

A.Billmeier[1], C.Blume[2], R.Bramm[1], P.Buncic[1], P.Dinkelaker[1], M.Gaździcki[1], T.Kollegger[1], I.Kraus[1], C.Markert[2], A.Mischke[3], R.Renfordt[1], A.Sandoval[2], H.Sann[2], R.Stock[1], H.Ströbele[1], M.Wensveen[2], A.Wetzler[1], J.Zaranek[1] for the NA49 Collaboration.
[1]Universität Frankfurt, [2]GSI Darmstadt

Most of the Λ hyperons observed in the final state of nucleus-nucleus collisions at SPS energies are truly participating baryons and their rapidity distribution is an appropriate measure of baryon stopping. In addition correlations between Λs probe the Λ-Λ interaction which is the decisive parameter for a possible six-quark bound state, the H-Dibaryon. Finally, the relativ yield of Λ resonances may be compared in p+p and Pb+Pb collisions in order to learn about the differences between in-medium effects of baryons and baryonic resonances. In the past, reconstruction of Λ hyperons proved to be difficult in central Pb+Pb collisions due to the high track density and the resulting confusion when searching for the characteristic V^0 decay topology. Similarily the identification of the Λ(1520) excited state by a signal in the (K^-p) invariant mass was hampered by the large combinatorial background. New software improvements in V^0 detection and in particle identification have led to reliable Λ and Λ(1520) signals. In this contribution we present new preliminary results on the Λ rapidity distribution in 1.5< y <4.5, on Λ-Λ correlations and on the comparison of the Λ(1520) signal in p+p and central Pb+Pb collisions.

Fig. 1 shows the rapidity distribution of Λs in the 5% most central Pb+Pb collisions. The data are not corrected for feed down from Ξ and Ω decays. Also shown is the published result from experiment WA97 [1] again not corrected for feed down and derived from the 3% most central collisions. It should be noted that the feed down corrections need not to be the same for the NA49 and WA97 analysis. For a comparison of the data to p+p measurements see [2].

In Fig. 2 the Λ-Λ correlation is plotted as a function of the invariant momentum difference (q_{inv}). At low q_{inv} a significant dip signals the Pauli principle for fermions. The absence of a positive correlation at small q_{inv} suggests that the s-wave interaction is rather weak. A fit to the correlation function yields a radius parameter of approximately 2 fm assuming the absence of final state interactions.

Fig. 3 shows the invariant (K^-p) invariant mass distributions after background subtraction for inelastic p+p (upper) and central Pb+Pb (lower) collisions[3]. The Λ(1520) resonance is clearly visible in both data samples; their positions are within errors the same and agree with the PDG value. It seems that the width of the Λ(1520) from Pb+Pb is slightly broader than from p+p. The yield per participating nucleon pair is slightly lower in the nuclear reaction, although the Λ yield per nucleon pair shows a strong enhancement in A+A over p+p.

References

[1] E. Andersen et al., Phys. Lett B449(99)401
[2] A. Billmeier et al., this GSI Annual Report
[3] C. Markert, PhD Thesis, Universität Frankfurt, 2000

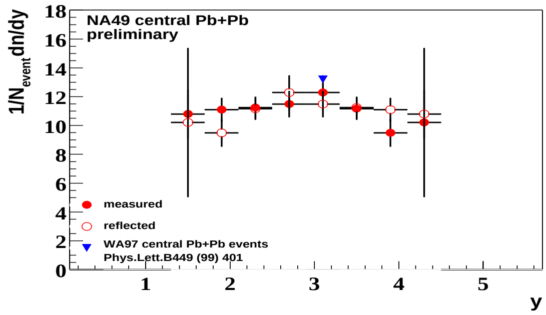

Figure 1: Rapidity distribution of Λ hyperons in central Pb+Pb collisons at 160 GeV per nucleon)

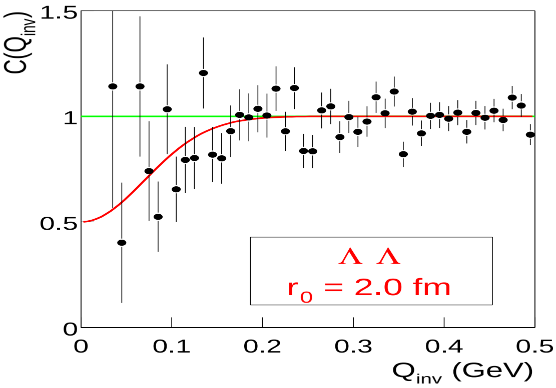

Figure 2: Λ-Λ correlation function from central Pb+Pb collisions.

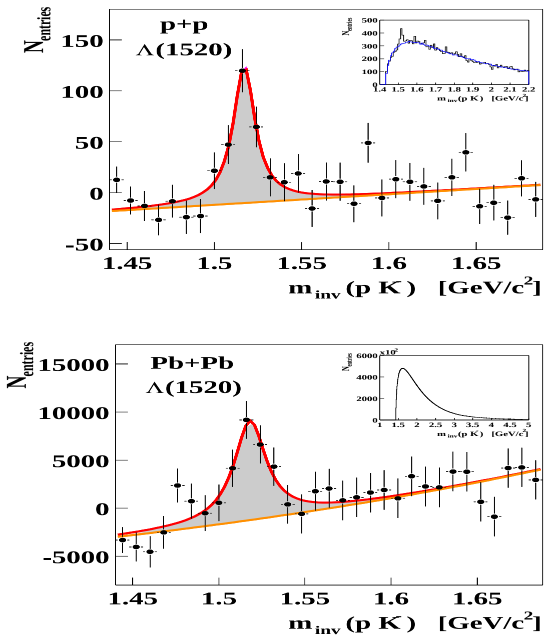

Figure 3: Invariant mass distribution of K^-p pairs in p+p (upper) and central Pb+Pb(lower) collisions at 158 A GeV. The widths of the Λ(1520) signals are 15±4 MeV and 23±6 MeV.

Strangeness Production in ultrarelativistic p+p Collisions at 158 GeV from the NA49 Experiment^{G,B}

A.Billmeier[1], C.Blume[2], R.Bramm[1], P.Bunčić[1], P.Dinkelaker[1], M.Gaździcki[1], T.Kollegger[1], I.Kraus[2], C.Markert[2], A.Mischke[2], R.Renfordt[1], A.Sandoval[2], H.Sann[2], R.Stock[1], H.Ströbele[1], M.Wensveen[2], A.Wetzler[1], J.Zaranek[1] for the NA49 Collaboration

[1]Universität Frankfurt, [2]GSI Darmstadt

The interpretation of results from high energy nuclear collision experiments requires accurate knowledge about the corresponding reaction characteristics in elementary hadron-hadron interactions. This information is not always available with the wanted precision, as early particle physics experiments either did not cover full phase space or suffered from low statistics. The SPS experiment NA49 [1] has therefore started a program to study hadron production in p+p interactions at 158 GeV/c beam momentum. An important part of this program is the measurement of strangeness production in full phase space [2].

The NA49 experiment has recorded a total of 2.26 million p+p interactions at 158 GeV. After event selection cuts, which ensure that the interaction occurs in the liquid hydrogen target, 83 % of the total inelastic cross section remain for the analysis. The detection of the measured strange hadrons is based on the recognition of the characteristic V^0 topology, which arises from the decay of long lived neutral particles into two charged decay products. Λ and K_S^0 decays are searched for by intersecting tracks from oppositely charged particles and by studying the resulting invariant mass distribution of those pairs which have a valid secondary vertex. Cuts on its position, the distance of the daughter particles in the target plane as well as the cm-decay angles are used to maximise the signal to noise ratio in these distributions. The double strange hyperon Ξ^- and its antiparticle $\overline{\Xi}^+$ were identified by combining the trajectories of all Λ and $\overline{\Lambda}$ candidates with those of negatively (Ξ^-) and positively ($\overline{\Xi}^+$) charged particles. The whole procedure is applied to equal-sized, non-overlapping intervals in rapidity and transverse momentum, which have been chosen according to signal statistics in these two variables. Detection efficiencies and acceptance corrections were determined in the same $y-p_T$ bins by processing simulated strange particle decay topologies using the complete analysis chain.

Figs. 1a,b and 2 show the rapidity distributions of K_S^0, Λ, and Ξ-hyperons in inelastic p+p interactions. Also shown for the neutral strange hadrons are previously measured data [3] at similar energies. The transverse momentum distributions (not shown) follow within experimental errors an exponential function with slope parameters of $\simeq$ 138, 142, 174 MeV for K_S^0, Λ, and Ξ hyperons respectively.

The scaling of the p+p spectra by the number of participants in Pb+Pb collisions at the same energy allows a direct comparison of both systems. Fig. 3 shows the rapidity distributions of K_S^0 for both – central Pb+Pb data as well as the scaled p+p results together with a fit to the identified charged kaons [4]. A strangeness enhancement of a factor ≈ 2 in the Pb+Pb compared to p+p reactions is clearly visible.

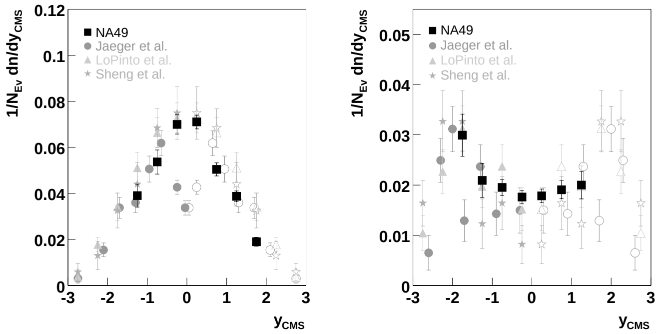

Figure 1: Rapidity distributions for K_S^0 (left) and Λ (right) compared to reference data at similar energies [3]. The shape of the distributions is reproduced, the dip around midrapidity in the K_S^0 spectra cannot be verified.

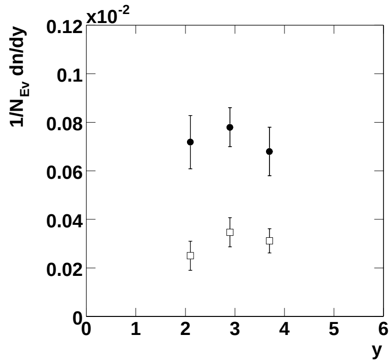

Figure 2: Rapidity distributions for Ξ^- ($\bullet$) and $\overline{\Xi}^+$ ($\square$).

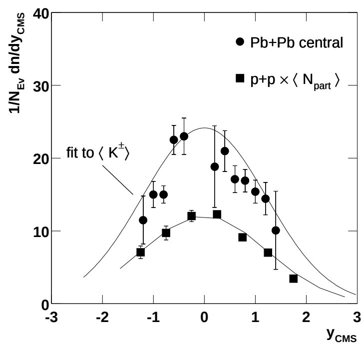

Figure 3: Comparison of the rapidity distribution for K_S^0 in central Pb+Pb collisions with the scaled p+p results.

References

[1] S. Afanasiev *et al.*, NIM A430 (1999), 210–244.

[2] A. Billmeier, Ph.D. Thesis, Universität Frankfurt (2001).

[3] Data compiled in: M. Gaździcki, O. Hansen, Nuclear Physics **A528** (1991) 754–770.

[4] J. Bächler *et al.*, Nucl. Phys. **A661** (1999) 45–54.

^{G,B} supported by GSI and BMBF

Stability and instability of a hot and dilute nuclear droplet: adiabatic isoscalar modes

W. Nörenberg, G. Papp*and P. Rozmej†

The diabatic approach to dissipative large-amplitude collective motion [1] is reformulated in a local energy-density approximation. We consider a general displacement field, which is defined by an expansion of the displacement potential in terms of multipoles, and include Coulomb interactions. This expansion allows the analytical evaluation of collective mass and stiffness tensors within a consistent harmonic approximation. The set of eigenvalue equations couple modes with different number of nodes in the radial function of the displacement field. The orthogonal eigenmodes of the droplet are determined as function of the relaxation time τ for the decay of deformations of the local Fermi sphere, *i.e.* continuously from the adiabatic to the diabatic limit. Furthermore we consider also pure surface modes and compare the instability properties for soft and stiff equations of state.

In a first application the adiabatic ($\tau = 0$) isoscalar modes are studied and results for the eigenvalues of compressional (bulk) and pure surface modes are presented as function of density and temperature inside the droplet, as well as for different mass numbers and for soft and stiff equations of state [2]. We have studied these adiabatic isoscalar modes in detail, because they are related to thermodynamics and to many studies performed in the past.

The results on adiabatic isoscalar bulk instabilities are summarized as follows.

- As compared to infinite nuclear matter the spinodal region for compressional (bulk) instabilities shrinks to smaller densities and temperatures with $T_{\rm crit} = 6$ MeV (8 MeV) for a soft (stiff) EOS. The observed fragmentation temperatures of about 5 MeV are consistent with spinodal decomposition after expansion. Typical values for the growth rates are $\gamma \approx 5$ MeV (10 MeV for a stiff EOS) corresponding to growth times $\hbar/\gamma \approx 40$ fm/c (20 fm/c).
- Effects from Coulomb interactions on the bulk instabilities are negligible.
- With decreasing density and temperature the modes with the lowest multipolarities and no radial node become unstable first.
- At densities below $0.3\varrho_0$ (with $\varrho_0 = 0.16$ fm^{-3}) the instability growth rates for different multipolarities ($l = 2, 3, 4, 5$) and number of nodes ($n = 0, 1, 2, 3$) are practically equal. This property can yield a power-law behavior $A^{-\sigma}$ with $\sigma \approx 2.0$ of the fragment-mass distribution in agreement with experimental observations and is not related to the critical point.

* *Permanent address:* HAS Research Group for Theoretical Physics, Eötvös University, Budapest, Pázmány P. s. 1/A, H-1117 Budapest, Hungary

† *Permanent address:* Institute of Mathematics, Technical University of Zielona Góra, ul. Podgórna 50, Pl-65246 Zielona Góra, Poland

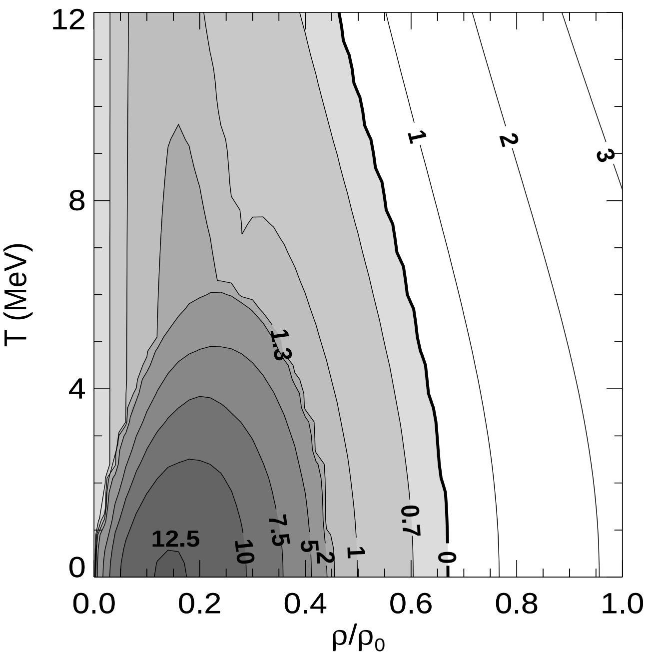

Figure 1: Combined bulk (below $T_{crit} = 6$ MeV) and surface instabilities for a gold-like droplet and a soft EOS. Shown are the largest growth rates (shaded areas) and the lowest vibrational energies (surface modes).

For finite nuclear droplets surface modes are important in addition to the compressional modes. Indeed, pure surface modes show some interesting features.

- The instability region of pure surface modes extends to larger densities up to about the spinodal line of infinite nuclear matter and to large temperatures.
- In general the growth times are smaller by half an order of magnitude as compared to the typical values for bulk instabilities.
- In the stable region surface modes are slow, such that deformations initiated in the excitation process will persist during expansion and clustering.
- The surface instability is dominated by quadrupole deformation.

References

[1] W. Nörenberg, *New Vistas in Nuclear Dynamics*, ed. P.J. Brussard and J.H. Koch (Plenum Press, New York 1986) p. 91; W. Nörenberg, *Heavy Ion Reaction Theory*, ed. by W.Q. Shen, J.Y. Liu and L.X. Ge (World Scientific, Singapore 1989) p. 1.

[2] P. Rozmej, W. Nörenberg and G. Papp, Eur.Phys.J. A **9**, 327 (2000)

Statistical evolution of fragment isospin in nuclear multifragmentation.

A.S. Botvina, *GSI Darmstadt and INR Moscow.*

The knowledge of the isotope composition of fragments produced in nuclear multifragmentation can help in resolving important problems: Do the fragments keep the memory of the initial dynamical stage or are they produced statistically? How does the isospin influence the disintegration of finite nuclei and what is the difference to the case of nuclear matter? What is the isospin dependence of the nuclear equation of state? Generally, this study addresses an intriguing interdisciplinary problem of the phase transition in a finite-size two-component system (i.e. in a nucleus consisting of neutrons and protons), that is instructive for all fields dealing with finite systems. The problem was investigated within the statistical multifragmentation model (SMM) [1], which is successfully used for explanation of experimental data. A new Markov chain method of partition generation was incorporated in the model [2], that allows for considering the multifragmentation process on a solid microcanonical basis. The reported results reflect statistical properties of the fragment production and can be used for identification of the phenomenon.

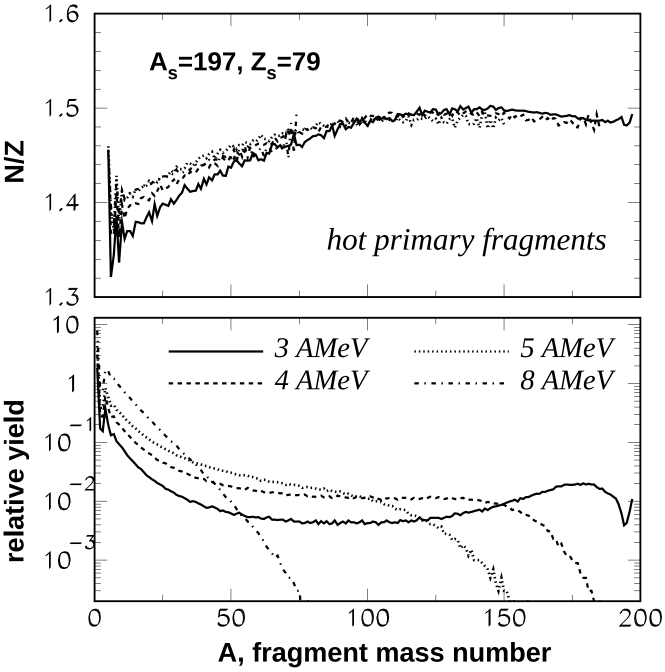

Figure 1: The neutron-to-proton ratio N/Z (top) and relative yield (bottom) of hot primary fragments produced after break-up of Au nuclei at different excitation energies: 3 (solid lines), 4 (dashed lines), 5 (dotted lines) and 8 (dot-dashed lines) MeV per nucleon.

The mass distributions and neutron-to-proton ratios (N/Z) of hot primary fragments produced after multifragmentation of a Au source (mass number A_s=197, charge Z_s=79) are shown in Fig. 1. One can see a general statistical trend: the N/Z ratio of the fragments increases with their mass numbers. This is a consequence of the interplay between the Coulomb and symmetry energy contributions to the binding energy of fragments [1]. This trend persists up to $A \leq A_s/2$, while at larger A the finite-size effects due to the mass and charge conservation prevail. In Fig. 1 one can also see the evolution of the N/Z ratio in the excitation energy range E_s^*=3–8 MeV/nucleon, where the fragment mass distribution evolves from the U–shape, at the multifragmentation threshold $E_s^* \sim 3$ MeV/nucleon, to an exponential fall at the highest energy. This energy range is usually associated with a liquid-gas type phase transition in finite nuclei: During this evolution the temperature reaches a "plateau" and is nearly constant [1, 3]. As the energy increases the N/Z ratio of primary intermediate mass fragments (IMF, charges Z=3–20) increases, too. The reason is that the heaviest neutron-rich fragments are destroyed at increasing excitation energy, and some of their neutrons are bound in the IMFs, since the number of free neutrons is still small at this stage. Simultaneously, the N/Z ratio of the heaviest fragments decreases slightly. At very high excitation energy ($E_s^* > 8$ MeV/nucleon) the N/Z ratio of IMFs does not rise anymore but drops because no heavier fragments are left and the number of free neutrons increases rapidly, together with the temperature. This isospin evolution shows how the isospin fractionation phenomenon predicted for nuclear matter [4] actually shows up in finite nuclear systems. Such a mechanism is consistent with recent experimental data [5]. New experiments for studying mass and isospin effects in multifragmentation are planned at GSI [6].

Interesting phenomena are also predicted for peripheral nucleus–nucleus collisions [2]: 1) The neutron content of IMF increases if a considerable angular momentum is transfered to the source, because of an interplay of the rotational and Coulomb energy. 2) There is a break of the symmetry of the phase space population, including the space isospin distribution, because of the external Coulomb field of the partner nucleus. The space asymmetry leads to predominant population of the midrapidity kinematic region by neutron-rich IMFs, that should be considered as purely statistical alternative to a dynamical explanation of the midrapidity emission [7]. Such processes are examples of a new kind of statistical emission influenced by an inhomogeneous long–range field.

References

[1] J.P.Bondorf et al., *Phys. Rep.* **257**, 133 (1995).
[2] A.S.Botvina and I.N.Mishustin. GSI preprint 2000-50, Darmstadt, 2000; nucl-th/0011072, 2000.
[3] J. Pochodzalla et al., *Phys.Rev.Lett.* **75**, 1040 (1995).
[4] H.Müller and B.D.Serot, *Phys.Rev.* **C52**, 2072 (1995).
[5] P.M.Milazzo et al., *Phys.Rev.* **C62**, 041602(R) (2000).
[6] K.Kezzar et al., Proposal-S254, GSI, 2000.
[7] J.Lukasik et al., Contrib. to this Scientific Report.

Thermal Boson Expansion

Z. Aouissat and J. Wambach
Institut für Kernphysik, Technische Universität Darmstadt.

Based on recent progress in the application of thermo field dynamics (TFD) [1] to thermal many-body systems, several authors [2, 3, 4] have considered a consistent thermal boson expansion (TBE). In this regard two points of view have been taken [2]. The first (path I) consists of a bosonization of the original degrees of freedom of the system, substituting for these ideal boson images. The thermalization is then achieved by doubling those newly introduced bosons as according to TDF prescription. The second possibility (path II) proceeds on the other hand via a thermalization of the system by doubling the original degrees of freedom and a subsequent bosonization of the entire new system. The two paths do not lead to the same results. Moreover, when applied to the Lipkin model, a closer look shows that the choice of path I implies that the thermal density of states are of bosonic type although the original system is purely fermionic.

To circumvent this problem one may choose path II where the thermal density of states is of fermionic type, since the thermalization is performed on the original fermions. However, inconsistencies related to the quasi-particle energies defining the thermal density of states, emerge. The latter are usually taken as solutions of a Hartree-Fock-Bogoliubov (HFB) approximation which, in most cases, leads to a dynamical mass generation. For massless modes, such as Goldstone modes, this gives the wrong solution. On the other hand, a mean-field description that is compliant with the symmetry requirements, is the Hartree-Bogoliubov (HB) approximation which can be obtained after a bosonization à la Holstein-Primakoff (HP). Therefore, when considering the symmetry constraints, it is rather path I that is favored. Amendments are, however, needed in order to reconcile it with the requirements of the statistics as explained earlier.

It was shown in [5] that a Boson expansion approach that treats on equal footing pair- as well as single-particle mapping offers a simple solution to the problems outlined above. For that matter the extended form of the bosonic HP mapping has been proposed in [6] which accommodates single-boson and boson-pair mappings:

$$\begin{aligned} (\vec{a}\vec{a})_I &= \mathcal{G}_N(n,m)A \; , \qquad (\vec{a}^+\vec{a})_I = 2n+m \; , \\ (a_i)_I &= \mathcal{G}_N(n,m)\Gamma_N(m)\alpha_i + 2\alpha_i^+ A\Gamma_N(m) \; , \\ (\vec{a}^+\vec{a}^+)_I &= (\vec{a}\vec{a})_I^+ \; , \qquad (a_i^+)_I = (a_i)_I^+ \; , \end{aligned} \tag{1}$$

where N is an integer, $n = A^+A$, $m = \sum_i \alpha_i^+\alpha_i$, and Γ_N is given by

$$\begin{aligned} \mathcal{G}_N(n,m) &= \sqrt{2N+4(n+m)} \; , & (2) \\ \Gamma_N(m) &= \left[\frac{m+N-2}{2(2m+N)(2m+N-2)}\right]^{\frac{1}{2}} \; . & (3) \end{aligned}$$

Thus, instead of the original bosons a_i, one has an ideal boson α_i which, as was shown in ref. [6], can accommodate the symmetry requirements. This is at the expense of introducing a power series in an auxiliary boson A. The thermalization of the system is then undertaken in a consistent way by using the TFD formalism. The time-translation operator, $\mathcal{H} = H - \tilde{H}$, of the system is obtained as usual by considering the tilde conjugate of all operators such as A and α_i among others. However, the independent thermal quasiparticle representation is obtained by rotating only the ideal bosons α_i, α_i^+ and their tilde conjugate (t.c.), via a unitary thermal Bogoliubov transformation

$$\alpha_i^+ \;=\; u(T)\gamma_i^+ + v(T)\tilde{\gamma}_i \; , \tag{4}$$

into the thermal quasiboson operators γ_i, γ_i^+, and their t.c. We insist here on the fact that the bosons $A, \tilde{A}$ need not be transformed since they are only auxiliary modes. This point of view is different from those adopted in all earlier works [2, 3, 4].

For fermionic systems, the situation is rather similar to the bosonic case. The extended form for the fermionic HP mapping proposed by Marshalek [7] is given by

$$\begin{aligned} (J_z)_I &= \frac{1}{2}n_f + B^+B \; , \\ (J_+)_I &= B^+\sqrt{N-(B^+B+n_f)} \; ; \quad (J_-)_I = (J_+)_I^+ \\ (c_{2p})_I &= N^{-1}\left(\sqrt{N-(B^+B)}\, a_{2p} + B\, a_{1p}\right) \\ (c_{1p})_I &= N^{-1}\left(\sqrt{N-(B^+B)}\, a_{1p} - B\, a_{2p}\right) \\ n_f &= \sum_{p=1}^{N}(a_{2p}^+a_{2p} - a_{1p}^+a_{1p}) \, . \end{aligned} \tag{5}$$

where B^+ and a_{ip}^+ are ideal boson and fermion operators, respectively. It allows a consistent mapping of pairs and single-fermion states. The thermalization is again obtained following the amended path I. Thus one introduces as previously the thermal Bogoliubov transformation which rotates only the ideal fermions and their tilde transform, such that

$$a_{ip}^+ = x_i\beta_{ip}^+ + y_i\tilde{\beta}_{ip} \; , \tag{6}$$

while the auxiliary bosons B are left unaltered. Obviously our procedure cures the problems of path I that were encountered in ref. [2] regarding the fermion statistics [5].

References

[1] Y. Takahasi, H. Umezawa, Coll. Pheno., 2 (1975) 55.
[2] T. Hatsuda, Nucl. Phys. A492 (1989) 187.
[3] N. R. Walet, A. Klein, Nucl. Phys. A510 (1990) 261.
[4] O. Civitarese et al., Phys. Rev. C60 (1999) 34302.
[5] Z. Aouissat, A. Storozhenko, A. Vdovin, J. Wambach, Submitted to Phys. Rev. C.
[6] Z. Aouissat, Phys. Rev. C62 (2000) 012201(R)
[7] E.R. Marshalek, Nucl. Phys. A224 (1974) 221.

Chiral Phase Transition in the scaled $O(4)$-Model

O. Bohr, B.-J. Schaefer, J. Wambach
Institut für Kernphysik, Technische Universität Darmstadt.

Due to the non-Abelian character of QCD gluons self-interact and form bound states, so-called glueballs. Such glueballs have been seen in recent lattice simulations and are actively searched for in experiment. Glueballs can be used to construct effective models of QCD which respect the symmetries and anomaly structure of the theory.
At the classical level and in the limit of vanishing quark masses QCD for n flavors exhibits a global chiral $U(n)_L \times U(n)_R$ symmetry and is in addition invariant under scale transformations. Due to anomalies not all of the associated currents are conserved and the symmetry is broken down to $SU(n)_L \times SU(n)_R$ which, in the case of two flavors, is isomorphic to $O(4)$. This symmetry is spontaneously broken to $SU(n)_{L+R}$. The divergence of the anomalous scale current is given by the trace of the energy-momentum tensor which, in the limit of massless quarks, is given by

$$\langle \theta^\mu_\mu \rangle = \langle \frac{\beta(g)}{2g} G^a_{\mu\nu}(x) G^{a\mu\nu}(x) \rangle \ , \tag{1}$$

where $G^a_{\mu\nu}(x)$ denotes the gluonic field-strength tensor and $\beta(g)$ is the usual QCD beta function. An effective realization of the scale anomaly can be achieved by adding to the classical Lagrangian a scalar color singlet dilaton field χ with an interaction potential of the form

$$V(\chi) = h \left(\frac{\chi}{\chi_0}\right)^4 \left(\ln \frac{\chi}{\chi_0} - \frac{1}{4}\right) \ , \tag{2}$$

where h is a constant that is related to the vacuum energy density ε_{vac} via $h = -4\varepsilon_{vac}$, when there are no quarks. The potential has a minimum at $\chi = \chi_0$.
In a previous work [?] we have tested a novel renormalization group approach to investigate chiral symmetry restoration at finite temperature and could analyze the critical behavior at the chiral phase transition of the $O(N)$-model. In this work we investigate the influence of the additional dilaton field on the chiral phase transition and the critical behavior. Therefore we couple a massive scalar dilaton field, which breaks the scale invariance, to the $O(4)$-model. Here we follow here the work in [?] and consider the following Lagrangian

$$\begin{aligned} \mathcal{L} \;\; = \;\; & \frac{1}{2}\partial_\mu\sigma\partial^\mu\sigma + \frac{1}{2}\partial_\mu\vec{\pi}\partial^\mu\vec{\pi} + \frac{1}{2}\partial_\mu\chi\partial^\mu\chi \\ & - \frac{\lambda}{4}\left(\sigma^2 + \vec{\pi}^2 - \frac{\chi^2}{\zeta^2}\right)^2 - V(\chi) \ , \end{aligned} \tag{3}$$

where σ, $\vec{\pi}$ denote the sigma- and the pion fields respectively.
Lattice calculations hint that the lightest glueball has a mass of 1.3 - 1.6 GeV. We use this mass as a constraint to fix the parameters of the model at $T = 0$. We then perform a finite-temperature calculation, where we calculate the vacuum expectation value (VEV) of the meson fields and the critical exponents of the chiral phase transition. From a comparison with the $O(4)$-model calculation without the dilaton field we can then estimate the influence of the dilaton field on the chiral phase transition.

The temperature dependence of the scalar mesonic VEV $\langle\phi\rangle$ (cf. Fig. 1) is very similar to the temperature dependence in the pure $O(4)$-model calculation without the dilaton field. Around T_c we again obtain a scaling behavior of the VEV $\langle\phi\rangle$ and of the mesonic coupling constant λ with critical exponents $\beta = 0.39$ and $\nu = 0.79$.

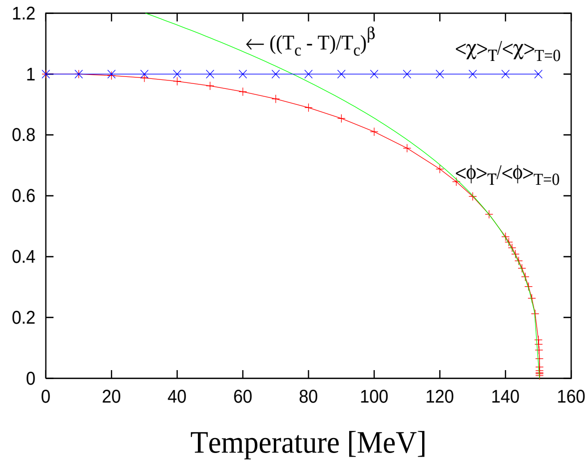

Figure 1: The temperature evolution of the vacuum expectation values of the dilaton field $\langle\chi\rangle$ and the scalar meson field $\langle\phi\rangle$ in the chiral limit.

These values of the exponents coincide within the estimated numerical error bars with the pure $O(4)$-model values.
On the other hand the glueballs themselves change very little in the temperature region up to the chiral phase transition. The change of the mass as well as of the VEV of the dilaton field (cf. Fig. 1) is less then 0.1% in this region. Calculations within the framework of a pure dilaton model show that the glueballs begin to be modified considerably at temperatures around 250 MeV.

In summary we can conclude that the glueballs, due to their high mass of ≈ 1.5 GeV, have very little influence on the temperature evolution in the mesonic sector where we still find a second order chiral phase transition with $O(4)$ critical exponents.

References

[1] O. Bohr, B.-J. Schaefer and J. Wambach, eprint: hep-ph/0007098

[2] H. Gomm, J. Schechter, Phys. Lett **B158** (1985) 449; E. K. Heide, S. Rudaz, P. J. Ellis, Phys. Lett. **B293** (1992) 259.

Chiral Fluctuations in Nuclei

Z. Aouissat, C. Isselhorst and J. Wambach
Institut für Kernphysik, Technische Universität Darmstadt.

The near-threshold enhancement in the $\pi^+\pi^-$ invariant mass distribution in nuclei, observed by CHAOS collaboration [1] and for $\pi^0\pi^0$ pairs by the Crystal Ball collaboration [2], offers the interesting possibility of directly observing a signal for partial restoration of chiral symmetry in a dense medium. There seems to be theoretical consensus on a strong in-medium reshaping of the s-wave isoscalar pion-pair correlations as a direct consequence of increased fluctuations of the chiral order parameter. This translates into a significant downward shift of the strength in the $\pi\pi$ T-matrix in the scalar-isoscalar channel as seen in Fig. 1.

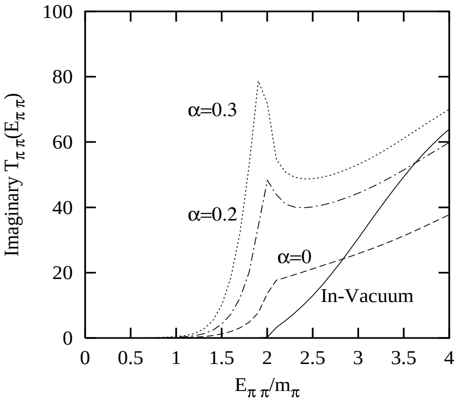

Figure 1: The imaginary part of the in-medium $\pi\pi$ T-matrix at normal nuclear density. The parameter α represents the medium effects on the mean field sigma-mass. See ref. [3] for details.

The reaction theory for the $A(\pi, 2\pi)$ knockout process has been thoroughly studied in the past [4], but only recently has the in-medium $\pi\pi$ final-state interaction (FSI) been seriously considered [5]. Taking into account the elementary $\pi\pi$ production process on the nucleon, the experimental acceptance, the Pauli constrained phase-space, and the nuclear absorption of the incoming and outgoing pions, the total cross-section for the $A(\pi, 2\pi)$ process in local density approximation reads

$$\begin{aligned}\sigma \;=\; & \frac{\pi}{q}\int d^2bdzA_{in}(\rho(\vec{r}))A^+_{out}(\rho(\vec{r}_1))A^-_{out}(\rho(\vec{r}_2)) \\ & \int \frac{d^3k}{(2\pi)^3}\frac{d^3q_1}{(2\pi)^3}\frac{d^3q_2}{(2\pi)^3}n(\vec{k})[1-n(\vec{q}+\vec{q}-\vec{q}_1-\vec{q}_2)] \\ & \delta(q_0+\varepsilon_{\vec{k}}-\omega_{\vec{q}_1}-\omega_{\vec{q}_2}-\varepsilon_{\vec{k}+\vec{q}-\vec{q}_1-\vec{q}_2})\frac{1}{2\omega_{\vec{q}_1}}\frac{1}{2\omega_{\vec{q}_2}} \\ & |T_{(\pi N\to\pi\pi N)}|^2\left|\frac{T_{\pi\pi}}{V_{\pi\pi}}\right|^2_{FSI} \times \mathit{Acceptance}\,. \qquad (1)\end{aligned}$$

To remove both experimental and theoretical uncertainties in the reaction dynamics, the CHAOS collaboration has considered the composite ratio, $C^A_{\pi\pi} = \frac{\sigma^A(M_{\pi\pi})}{\sigma^A_T}/\frac{\sigma^N(M_{\pi\pi})}{\sigma^N_T}$, where $\sigma^A(M_{\pi\pi})$ ($\sigma^N(M_{\pi\pi})$) denotes the invariant mass distribution in the nucleus (nucleon), while σ^A_T (σ^N_T) is the corresponding total cross section for the $A(\pi, 2\pi)$ process [6]. Comparing this ratio for both $\pi^+\pi^-$ and $\pi^+\pi^+$ final states, one can argue that the observed near-threshold enhancement must be an $I = 0$ effect. The theoretical pre-

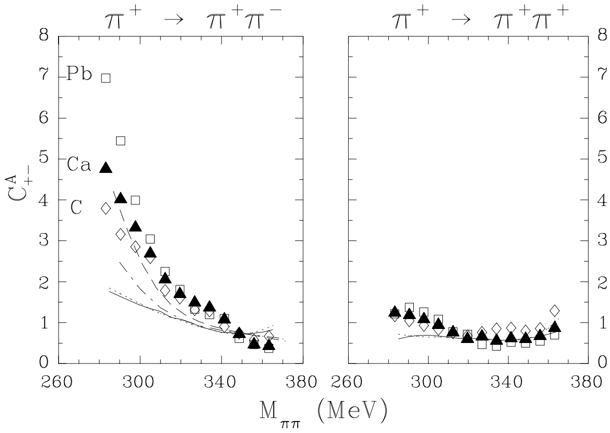

Figure 2: The ratio $C^A_{\pi\pi}$ for various nuclear targets [6].

dictions shown on Fig. 2 assume the effect of the FSI as appearing in Fig. 1. The various curves reflect the current state-of-the-art calculations by different groups (see [7] for details). The dashed curve uses the model in [3].
However, improvements in the reaction calculations are needed. The kinematical analysis of the 3-body final state, for instance, reveals that the average momentum of the pion-pair is about 200 MeV/c. Therefore the back-to-back kinematics assumption used in all previous calculations needs to be revised [8].
On the experimental side, a very exciting possibility which circumvents the strong absorption in the initial state is the photoproduction $A(\gamma, 2\pi^0)$. Such experiments have been conducted at MAMI in Mainz and are currently analyzed [9]. A theoretical description is also in progress [8].

References

[1] F. Bonutti et al., Phys. Rev. Lett. 77 (1996) 603.
[2] A. B. Starostin et al., submitted to Phys. Rev. Lett.
[3] Z. Aouissat, G. Chanfray, P. Schuck, J. Wambach, Phys. Rev. C 61, (2000) 12202
[4] M. J. Vicente Vacas, E. Oset, nucl-th/9907008
[5] P. Schuck, Z. Aouissat, F. Bonutti, G. Chanfray, E. Fragiacomo, N. Grion, J.Wambach, Proceedings of the XXXVI, international Winter Meeting on Nuclear Physics, Ed. I. Iori, Bormio (Italy), January 1998.
[6] F. Bonutti et al., Nucl. Phys. A677 (2000) 213.
[7] J. Wambach, Z. Aouissat, P. Schuck, to appear in Nucl. Phys. A.
[8] Z. Aouissat, C. Isselhorst, J. Wambach, in progress.
[9] V. Metag, to appear in Nucl. Phys. A.

Nonpertubative renormalization flow and infrared physics

J. Meyer, K. Schwenzer, T. Spitzenberg and H.J. Pirner,
Institut für Theoretische Physik der Universität Heidelberg

Renormalization group flow equations have proved to be a good tool to analyze the dynamics of strong interaction in the nonperturbative region. They have been successfully applied to effective mesonic models in a thermal environment and revealed detailed insight into the chiral phase transition [1]. The basic aim of the renormalization group treatment is to systematically integrate out quantum and/or thermal fluctuations with momenta above a certain cutoff scale k and include them into the couplings of an effective action.
We are interested in the low energy theory of strong interaction resulting from the integration of high momentum modes. Assuming a dominant one gluon exchange or a instanton vacuum, gluonic degrees of freedom can be absorbed into an instantaneous four fermion interaction described by the NJL-model. Our analysis shows that the standard solution of the NJL-model and the flow of the linear σ-model, which we are using, coincide in the large N_C-limit, where the dynamics is dominated by fermion loops. In the full solution though, the additional dynamics of the mesonic degrees of freedom becomes important and yields an improved low energy behaviour compared to the NJL-model. The linear σ-model describes a massless two flavour quark field q interacting with chiral fields $\Phi = (\sigma, \vec{\pi})$ and is believed to give a valid description of chiral dynamics at scales $\leq$ 1GeV. It has the action

$$S_{UV} = \int d^4x \left[\bar{q}\left(i\partial\!\!\!/ - g\left(\sigma + i\vec{\tau}\vec{\pi}\gamma_5\right)\right) q + \frac{1}{2}\left(\partial\Phi\right)^2 - U(\Phi^2)\right],$$

with a general O(4) symmetric potential $U(\Phi^2)$. From this, we compute the effective action in a one loop approximation using Schwinger proper time regularization [2]. The resulting expression is truncated to second order derivative in order to include the relevant terms for the flow. This inclusion of higher order terms, results in a splitting in the dynamics of the massive σ-mode and the massless Goldstone-bosons. By a renormalization group improvement the one loop expressions are turned into nonperturbative flow equations. The resulting flow for the most important parameters is plotted below. An interesting feature is, that like the four boson coupling λ also the Yukawa coupling g_σ vanishes in the infrared. Therefore, aside from providing a broken vacuum, the σ decouples from the dynamics and leaves the pions as the only dynamic particles. We obtain the resulting infrared effective action

$$\Gamma_{IR} = \int d^4x \Big[\bar{q}\left(i\partial\!\!\!/ - m_q - ig_\pi\vec{\tau}\vec{\pi}\gamma_5 + \frac{g_\pi}{f_\pi}\pi^2\right) q - \frac{1}{2}\left(\partial\vec{\pi}\right)^2 + \text{derivative couplings}\Big].$$

Our approximation obeys the chiral Ward identities and ensures that the $\pi\pi$-scattering amplitude vanishes at tree level due to a $\bar{q}q\pi^2$-contact term that cancels the 1π-contributions in the IR.

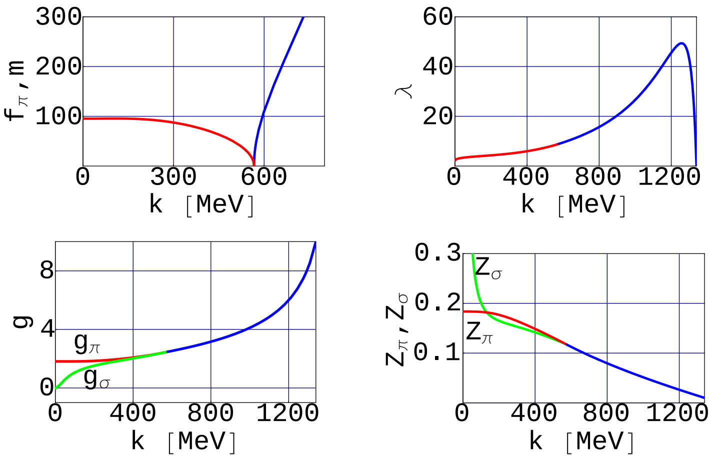

Once the flow equations for the linear σ-model are written down, the chiral order parameter $\langle\bar{q}q\rangle$ can be calculated from the partition function. Using the same cutoff function as for the flow equations one obtains in the local potential approximation

$$\partial_k \langle\bar{q}q\rangle = -\frac{N_c g k^5 \phi_k}{2\pi^2\left(k^2 + g^2\phi_k^2\right)^2}.$$

Starting in the symmetric regime where the order parameter is zero, we find a value of $\langle\bar{q}q\rangle = -(194\text{Mev})^3$, as shown below.

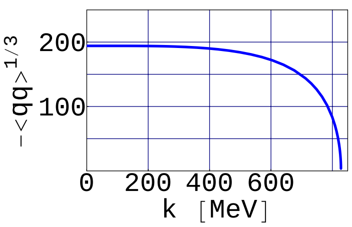

It is now tempting to derive a flow equation for the spectral density $\rho(\lambda)$ of the Dirac operator. This may be done by establishing a relation between $\langle\bar{q}q\rangle(\lambda)$ and $\rho(\lambda)$ similar to the Banks-Casher relation. It would be interesting to compare the results with recent data available from lattice QCD.
Another promising idea is to connect our cutoff parameter to a physical momentum scale and continue our Euklidian flows to the full complex plane. By this, it would be possible to compute spectral functions of mesonic resonances and make a direct connection to low energy hadron phenomenology.

References

[1] J. Berges, N. Tetradis and C. Wetterich, to appear in Phys. Rep., hep-ph/0005122
[2] B.-J. Schaefer and H.-J. Pirner, Nucl. Phys. **A660** (1999) 439, nucl-th/9903003

e^+e^--pair production in π^-p reactions

Matthias Lutz, Bengt Friman (GSI) and Madeleine Soyeur (CE Saclay)

The cross section for the reaction $\pi^- p \to e^+e^-$ is computed, using vector-meson dominance and the amplitudes for the processes $\pi^- p \to \rho^0 n$ and $\pi^- p \to \omega n$, obtained in a coupled channel analysis of meson-nucleon scattering at energies near the threshold for vector-meson production [1]. These amplitudes are sensitive to the coupling of the vector mesons to baryon resonances below the vector meson production threshold. Data that directly reflect these amplitudes would provide very useful constraints on the dynamics of vector mesons propagation in nuclear matter and e^+e^- pair production in heavy-ion collisions. The $\pi^- p \to e^+e^- n$ reaction offers the possibility to experimentally test the pion induced vector meson production amplitudes below threshold. The interference of the two light vector mesons in the e^+e^- channel is sensitive to the magnitudes and the relative phase of the ρ^0 and ω production amplitudes (see Fig. 1). An experimental test of the N*Nρ^0 and N*Nω vertices through the $\pi^- p \to e^+e^- n$ reaction below the vector meson production threshold would be a most valuable constraint on the in-medium propagation of ρ^0- and ω-mesons.

We shall restrict our discussion to e^+e^- pairs of invariant masses ranging from 0.5 to 0.8 GeV. The exclusive measurement of the $e^+e^- n$ outgoing channel ensures that the e^+e^- pairs come from vector meson decays (pseudoscalar mesons decay into an e^+e^- pair and an additional photon). We note however that only s- and d-wave pion-nucleon resonances are at present included in the model of Ref. [1]. To be complete, the description of the $\pi^- p \to e^+e^- n$ reaction in the energy range discussed in this work ($1.2 < \sqrt{s} < 1.8$ GeV) should include also the effect of other partial waves.

The magnitude of the $\rho^0 - \omega$ interference in the $\pi^- p \to e^+e^- n$ is illustrated in Fig. 2, where we show the cross section for this reaction as function of the total center of mass energy. We have selected e^+e^- pairs of invariant mass m=0.55 GeV. This figure elucidates the role of baryon resonances with masses in the range of 1.5 to 1.6 GeV in generating strong interference effects.

Above the vector meson threshold, the $\rho^0 - \omega$ interference in the $\pi^- p \to e^+e^- n$ cross section is particularly interesting for e^+e^- pair invariant masses close to the ω mass. This effect is manifested in the invariant mass spectrum shown in Fig. 3 ($\sqrt{s}$=1.8 GeV). The model of Ref. [1] for the $\mathcal{M}_{\pi^- p\to\rho^0 n}$ and $\mathcal{M}_{\pi^- p\to\omega n}$ amplitudes predicts a constructive interference at this energy. This feature appears to be a very sensitive test of the model.

References

[1] M. Lutz, G. Wolf and B. Friman, Nucl. Phys. **A 661** (1999) 526c and Proc. of Hirschegg 2000.

[2] M. Lutz, B. Friman and M. Soyeur, in preparation.

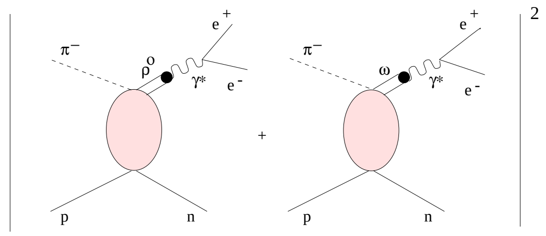

Figure 1: Squared amplitude for the $\pi^- p \to e^+e^- n$ reaction with intermediate ρ^0- and ω-mesons.

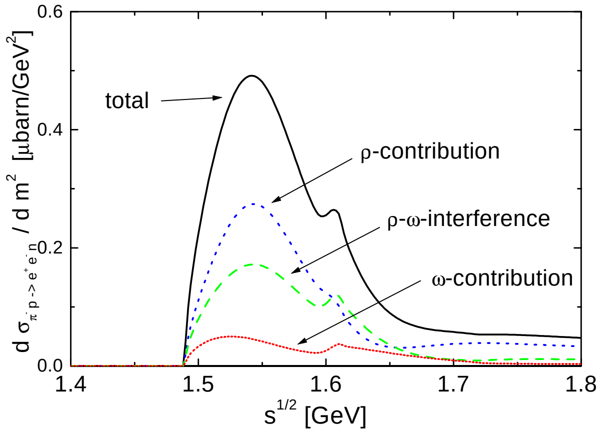

Figure 2: Differential cross section dσ/dm^2 for the $\pi^- p \to e^+e^- n$ reaction as function of $\sqrt{s}$ for a fixed e^+e^- pair invariant mass m=0.55 GeV.

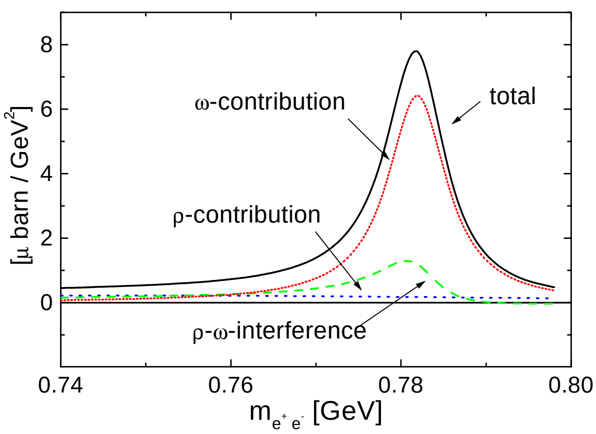

Figure 3: Differential cross section dσ/dm^2 as function of the e^+e^- pair invariant mass for a fixed total center of mass energy $\sqrt{s}$=1.8 GeV.

e^+e^- production in pp, pd and pA reactions at SIS energies

E.L. Bratkovskaya, W. Cassing, and U. Mosel
University of Giessen

The modification of hadron properties in the nuclear matter is of fundamental interest. The dilepton data from heavy-ion experiments at SPS energies have provided first experimental evidence for a change of the vector meson properties, however, the heavy-ion data can be interpreted within different scenarios of in-medium modifications, i.e. by the dropping mass scenario or the collisional broadening approach. Since in heavy-ion experiments the nuclear matter is probed at different densities and temperatures within the complex dynamical evolution, it will be very useful to have independent experimental information from photon-nucleus, pion-nucleus or proton-nucleus reactions, where the properties of vector mesons are probed at normal nuclear density or below. This question becomes very actual with respect to the HADES experiments coming up at GSI soon [1].

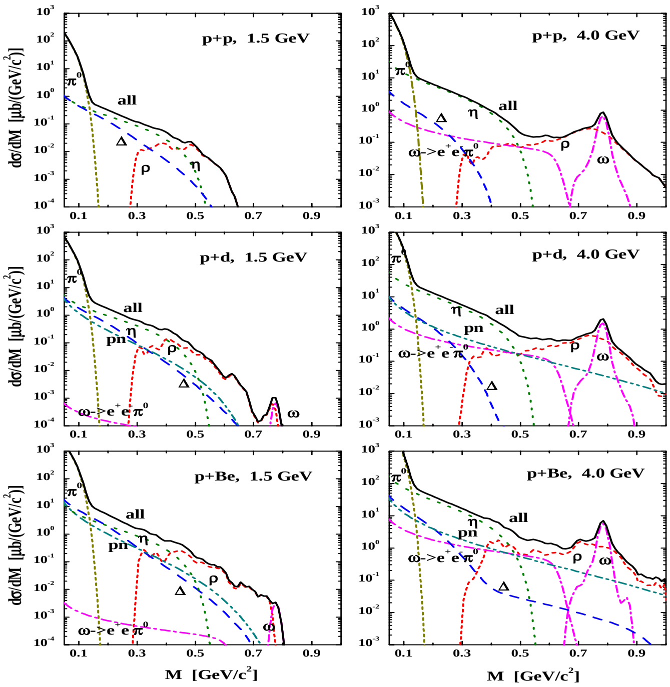

Figure 1: The dilepton invariant mass spectra $d\sigma/dM$ for pp (upper part), pd (middle part) and pBe collisions (lower part) at 1.5 GeV (left panel) and 4.0 GeV (right panel) including a 10 MeV mass resolution [2].

Dilepton production in from pp, pd and pBe collisions from 1 − 5 GeV has been studied in Ref. [2] within the framework of the combined resonance-string approach [3]. here, it has been found that the DLS data for pp and pd collisions can be reasonably well described whereas for pBe systems (especially at 4.9 GeV) our calculations give slightly higher dilepton yield. We have demonstrated, futhermore, the importance to measure dileptons from pp and pd (or even pBe) collisions simultaneously since such data provide constraints on the isospin dependence of pp and pn interactions, which is important for an understanding of heavy-ion data.

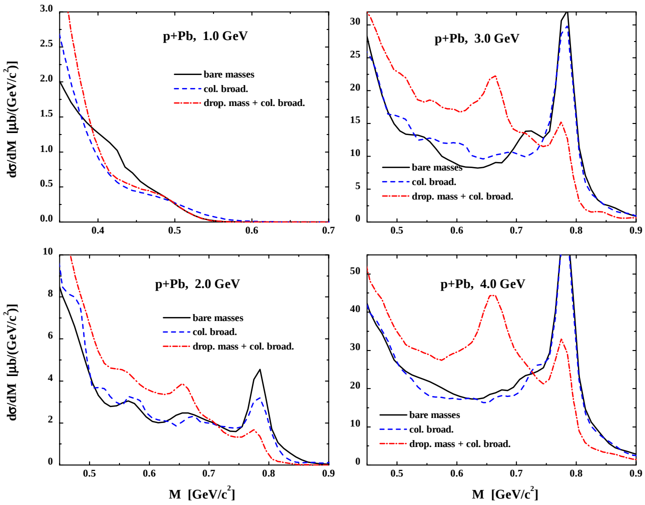

Figure 2: The comparison of different in-medium modification scenarios, i.e. collisional broadening (dashed lines) and collisional broadening + dropping vector meson masses (dash-dotted lines), with respect to the bare mass case (solid lines) for $p + Pb$ from 1–4 GeV [4].

In Fig. 1 we show our detailed predictions for the differential dilepton spectra from pp, pd and pBe collisions at 1.5 and 4.0 GeV energy with a 10 MeV mass resolution that can be controlled experimentally by the HADES Collaboration in near future.

A comparison of the different in-medium modification scenarios is shown in Fig. 2, i.e. collisional broadening (dashed lines) and collisional broadening + dropping vector meson masses (dash-dotted lines), with respect to the bare mass case (solid lines) on a linear scale for $p+Pb$ collisions from 1–4 GeV. The collisional broadening + 'dropping mass' scenario leads to an enhancement of the dilepton yield in the range $0.5 \leq M \leq 0.75$ GeV and to a reduction of the ω-peak, which is more pronounced for heavy systems (up to a factor 2 for $p + Pb$ at 3–4 GeV), since most of the ρ's and ω's now decay in the medium approximately at density ρ_0. This leads to a pronounced peak around $M \approx 0.65$ GeV, which can be attributed to the in-medium ω decay since the ρ spectral strength is distributed over a wide low mass regime. Especially when comparing dilepton spectra from C and Pb targets, it should be experimentally possible to distinguish an in-medium mass shift of the ω meson by taking the ratio of both spectra.

References

[1] The HADES Collaboration, Proposal, GSI 1994.
[2] E.L. Bratkovskaya et al., Nucl. Phys. A 686 (2001) 476.
[3] M. Effenberger et al., Phys. Rev. C 60 (1999) 044614.
[4] E.L. Bratkovskaya, nucl-th/0101067.

Renormalisation of Self-consistent Resummation Schemes^{G}

H. van Hees, J. Knoll (GSI)

For the description of physical systems with strong interactions generally perturbative methods are insufficient. Rather on the basis of effective field theories non-perturbative methods such as partial resummation schemes have to be applied. There are a couple central questions connected with such methods which concern symmetries and conservation laws as well as thermodynamic consistency and detailed balance. While the question of conserving approximations was addressed by Baym's Φ-functional method [1, 2, 3], in field theoretical descriptions a further complication arises, namely that of renormalization. Loop integrals generally diverge and renormalization concepts were developed in perturbation theory. In the context of resummation schemes the question arises under which conditions they are still renormalizable with temperature and density independent counter terms. In the past only a few specific examples were investigated.

Our purpose was to analyze self consistent partial Dyson resummation schemes defined by a set of basic generating self energy diagrams with dressed propagators. In terms of perturbative diagrams this leads to an infinite iterative insertion of all basic diagrams. The sum of all these perturbative diagrams defines the self consistent self energy which determines the dressed propagator, cf. (1). All diagram subpieces with the topology of a single loop which are connected to the rest of the diagram at most via two vertices, are divergent and have to be renormalized. These structures, however, appear in a nested way such that first the most inner ones have to be renormalized through counter-terms given by the reduced diagrams where the divergent sub-pieces are contracted to a point. The so obtained reduced diagrams themselves are to be subjected to the same procedure. This iterative process is formalized as the BPHZ-renormalization scheme. For the self consistent scheme under consideration the key issue is to find a compact iteration scheme that generates all the required counter terms at once.

For an initial study we choose a simple scalar field theory model, the ϕ^4-model. For the Hartree approximation given by the tadpole self-energy diagram the subtraction scheme can be formulated as a gap equation. As a new part we included a genuine two-point contribution, namely the sunset diagram. The latter gives rise to an imaginary part in the self-energy, i.e., a finite width for the particles in the medium. In terms of perturbative diagrams the self consistent scheme then leads to all kinds of "super-daisy", "super-sunset" diagrams and all possible mixtures of them, cf. (1).

It could be shown that also this approximation can be renormalized in a BPHZ-type procedure (for details see [4]). The considerations show that one first has to solve the problem in the vacuum where subtracted dispersion relations can be used to renormalize the self-energy. In the same way one obtains the renormalized vertex functions which are needed to replace the corresponding divergent vacuum sub-diagrams in the finite temperature case. This means that for the renormalization of the finite temperature case one needs only *local temperature independent vacuum counter-terms* in perfect analogy to the well known theorem for perturbative finite-temperature quantum field theory.

We argue that the Φ-functional properties of the self energies indeed enforces the consistency of the counter-terms and symmetry factors for the explicit as well as the hidden nested and overlapping divergences since the divergent sub-diagrams are given by higher derivatives of the Φ-functional with respect to the dressed Green's function.

This substitution of divergent sub-diagrams together with direct subtractions of counter-terms on the level of the integrands provides a scheme where one has to deal only with convergent integrals without any explicite beforehand regularization which opened the possibility to calculate the self–energy and thermodynamic quantities such as the entropy in full self–consistency.

The results are important, e.g., for the description of hadrons in dense matter, e.g. [5] or for an effective description of gauge fields such as QCD in cases where the damping width of the particles is of considerable importance. Supplementary to the renormalization question functional methods have been developed on the basis of the Φ-functional concept, which permit to investigate and cure possible violations of symmetries and conservation laws at the level of higher order correlation functions [4]. This is of particular importance for gauge theories[5].

$\Sigma =$ 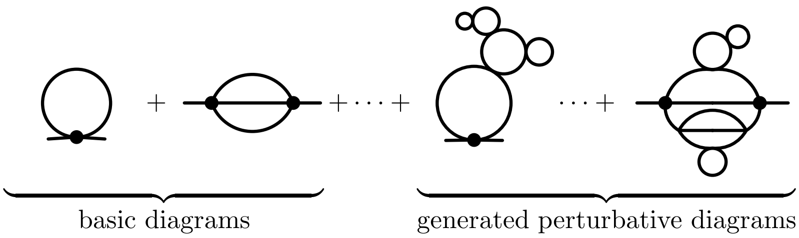 (1)

References

[1] G. Baym, Phys. Rev. **127** 1391 (1962).

[2] Y. B. Ivanov, J. Knoll, D. N. Voskresensky, Nucl. Phys. **A657** 413 (1999), `hep-ph/9807351`.

[3] Y. B. Ivanov, J. Knoll, D. N. Voskresensky, Nucl. Phys. **A672** 313 (2000), `nucl-th/9905028`.

[4] H. van Hees, Renormierung selbstkonsistenter Näherungen in der Quantenfeldtheorie bei endlichen Temperaturen, Ph.D. thesis, TU Darmstadt (2000), `http://elib.tu-darmstadt.de/diss/000082/`.

[5] H. van Hees, J. Knoll, Nucl. Phys. **A683** 369 (2001), `hep-ph/0007070`.

Vector mesons within a conserving self-consistent approximation^{G}

H. van Hees, J. Knoll (GSI)

The experimental results on di-lepton production in heavy ion collisions by the CERES and DLS collaborations has shown an enhancement of the di-lepton production rate in the invariant pair mass region between 300-600 MeV compared to the rate to be expected from proton-proton collisions. Since dileptons are direct signals from the decay of vector mesons within the hot reaction zone this enhancement points towards in-medium modifications of vector-mesons in dense hadronic matter.

From the theoretical point of view a consistent description of such phenomena within effective quantum field theoretical models needs a treatment of particles which considers the finite spectral width. This concerns not only the widths of resonances but also the width due to collisions of the particles within the hot and dense medium. For such questions a perturbative approach is generally insufficient and a self-consistent treatment is at place.

There is a class of self-consistent approximations derived from a generating functional which leads to a closed set of conserving equations of motion for the mean fields and the Dyson resummed dressed propagators [1]. They posses exact conservation laws for the expectation values for conserved Noether-currents (including those from space-time symmetry, i.e., energy, momentum and angular momentum).

A detailed symmetry analysis nevertheless shows that on the level of higher order correlation functions such as propagators the Ward-Takahashi identities (WTI) of the underlying symmetries are not fulfilled [2]. In the case of vector or gauge fields this has serious consequences: The WTI are necessary to ensure the physicality of states. A violation of this symmetry causes the excitation of unphysical degrees of freedom and violates unitarity and causality within the dressed propagators and currents are no longer conserved at the correlator level.

On the other hand corrections which restore current conservation on the correlator level have been studied within a diffusion equation approximation of the according kinetic equation (Fokker-Planck-equation) [3]. The study shows that the space components of the polarization tensor suffer only small corrections, if the scattering of a particle is isotropic on the average. The self consistent time component, however has a completely wrong behavior as it also exponentially decay in time within this approximation, while it should stay constant in time due to charge conservation.

In order to cure this defect we have invented a particular projection method. It discards the wrong time components of the polarization tensor and solely uses the space components. This way a 4-dimensionally transverse polarization tensor for the vector field can be constructed. The two independent components of the thermal polarization tensor, the longitudinal and transverse components, $\Pi_T(q)$ and $\Pi_L(q)$, can be obtained from

$$2\Pi_T + g_{ik}\Pi^{ik} = -\frac{q_i q_k}{\vec{q}^{\,2}}\Pi^{ik} = -\frac{(q^0)^2}{q^2}\Pi_L.$$

Here the indices (i,k) run over the spatial components from 1 to 3. We have numerically solved the coupled self-consistent equations of motion for this projected self-energies. For details see [2, 4].

The results show a significant enhancement of the spectral width in the low energy mass region and all thresholds, present in the perturbative quantities, are gone due to collision broadening of the self-consistently treated pions.

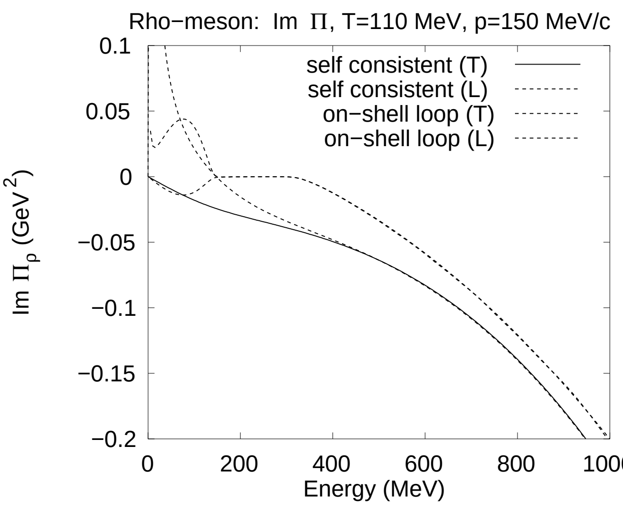

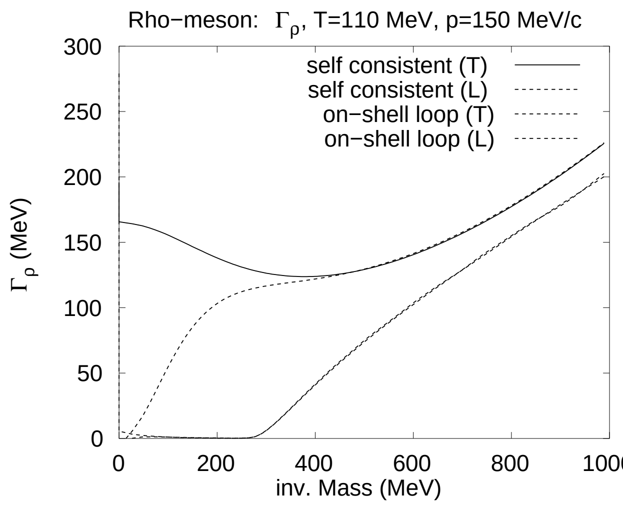

The transverse components of the imaginary part of the self-consistent ρ–meson self-energy (left) and the corresponding spectral width (right).

References

[1] G. Baym, Phys. Rev. **127** 1391 (1962).

[2] H. van Hees, Renormierung selbstkonsistenter Näherungen in der Quantenfeldtheorie bei endlichen Temperaturen, Ph.D. thesis, TU Darmstadt (2000), `http://elib.tu-darmstadt.de/diss/000082/`.

[3] J. Knoll, D. Voskresensky, Annals of Physics **249** 532 (1996).

[4] H. van Hees, J. Knoll, Nucl. Phys. **A683** 369 (2001), `http://de.arXiv.org/abs/hep-ph/0007070`.

Exact Conservation Laws in the Gradient Expanded Kadanoff–Baym Equations^G

Jörn Knoll, Yuri B. Ivanov, and Dmitri N. Voskresensky
GSI Darmstadt

One of the challenging problems in quantum many-body physics is the appropriate inclusion of resonances or particles with broad damping width into a self-consistent non-equilibrium dynamics. Such kind of description can be constructed on the basis of the so called Kadanoff–Baym equations (KBE) derived within the non-equilibrium Green function technique [1]. While the KBE are exact, in actual calculations one has to rely on further approximations. They provide (a) a truncated self-consistent scheme and (b) through the gradient approximation they lead to transport type of equations of motion. Interested in the dynamics of particles with broad mass width one has to avoid the quasi-particle approximation, and solely rests on the first-order gradient approximation of the KBE. This concept was first addressed by Kadanoff and Baym [1] and recently reconsidered in the context of hadronic matter and heavy ion collisions [2–7]. As for any such approximation, however, symmetries and conservation laws as well as detailed balance and thermodynamic consistency may no longer a priori be guaranteed.

In ref. [8] we re-investigated a generalization of the Φ derivable method of Baym [9] to the real-time Green function technique which provides truncated self-consistent approximations which are conserving and thermodynamically consistent at the level of KBE. In particular a conserved energy-momentum tensor could be derived for local field couplings. The subsequent gradient approximation leads to two coupled equations: a quantum transport equation, which governs the four-phase distribution functions $f(\vec{x},t,p)$, and a retarded equation, which determines the time evolution of the spectral function $A(\vec{x},t,p)$. For this approximate set of equations the conservation laws generally are expected to become only *approximate*. Such approximate nature of conservation laws may be well acceptable theoretically as its accuracy precisely corresponds to that of the approximation. Nevertheless, both from a principle perspective and also from a practical point of view this situation is less satisfactory.

In this work [10] we investigated the quantum kinetic equations in the form originally derived by Kadanoff and Baym. The key point is to do a systematic first-order gradient expansion of all gradient terms even those internally present in the self-energies. Through a careful investigation of all gradient terms we could in fact prove that the quantum kinetic equations possess the generic feature of exact conservation laws at the expectation value level.

The conserved currents and the energy-momentum tensor take the original Noether form [8] ($X=(\vec{x},t)$)

$$J^\mu(X) = \int \frac{\mathrm{d}^4p}{(2\pi)^4} p^\mu f(X,p)A(X,p), \tag{1}$$

$$\begin{aligned}\Theta^{\mu\nu}_{\mathrm{loc}}(X) &= \int \frac{\mathrm{d}^4p}{(2\pi)^4} v^\mu p^\nu f(X,p)A(X,p) \\ &\quad + g^{\mu\nu}\left(\mathcal{E}^{\mathrm{int}}_{\mathrm{loc}}(X) - \mathcal{E}^{\mathrm{pot}}_{\mathrm{loc}}(X)\right)\end{aligned} \tag{2}$$

now however in the so called local form, i.e. void of any gradient corrections. For the energy–momentum tensor the first term accounts for the single particle part which by itself overcounts the interaction energy. This is compensated by gradient terms which assemble to the difference between interaction energy density and single-particle potential energy density, $\mathcal{E}^{\mathrm{int}}_{\mathrm{loc}}(X) - \mathcal{E}^{\mathrm{pot}}_{\mathrm{loc}}(X)$, both obtained from the same Φ-functional in the local approximation as the self-energies driving the gradient expanded KBE.

In order to preserve the exact conserving property, a few conditions have to be met. First, the original KBE should be based on a Φ-derivable approximation scheme that guarantees that the KBE themselves are conserving [8, 9]. Second, all possible memory effects due to internal vertices within the self-energy diagrams are also consistently expanded to first-order gradients. Finally it is important that after the gradient expansion no further approximations are applied that violate the balance between different first-order gradient terms.

The presence of exact conservations puts the Kadanoff–Baym formulation of quantum transport on the level of generic phenomenological equations. They offer a phenomenological approach to the dynamical description of particles with broad damping widths, such as resonances, with built-in consistency and exact conservation laws. For practical simulations of complex dynamical systems this approach may even be applied in cases, where the smallness of the gradients can not always be guaranteed.

References

[1] L.P. Kadanoff and G. Baym, *Quantum Statistical Mechanics*, Benjamin, 1962.

[2] Yu.B. Ivanov, J. Knoll, and D.N. Voskresensky, Nucl. Phys. **A672** (2000) 313.

[3] M. Effenberger, U. Mosel, *Phys. Rev. C* **60** (1999), 51901.

[4] W. Cassing and S. Juchem, *Nucl. Phys. A* **665** (2000), 377; **672** (2000), 417.

[5] S. Leupold,*Nucl. Phys. A* **672** (2000), 475.

[6] Yu. B. Ivanov, J. Knoll, H. van Hees and D. N. Voskresensky, e-Print Archive: nucl-th/0005075; *Yad. Fiz.* **64** (2001).

[7] H. van Hees, and J. Knoll, *Nucl. Phys. A* **A683** (2001), 369.

[8] Yu.B. Ivanov, J. Knoll, and D.N. Voskresensky, Nucl. Phys. **A657** (1999) 413.

[9] G. Baym, Phys. Rev. **127** (1962) 1391.

[10] J. Knoll, Yu.B. Ivanov, and D.N. Voskresensky, nucl-th/0102044, submitted to Ann. Phys. (NY)

Production of vector mesons in pion nucleus reactions^{B,G}

W.Schön, R.Schneider, W.Weise
Physik-Department TU-München

Model independent constraints from QCD sum rules connect the vector meson mass with the gap Δ between the nπ continuum and the $< q\bar{q} >$ vacuum state. At normal nuclear density, Δ is expected to be reduced by about 15% as a consequence of the restauration of chiral symmetry [1, 2]. In this work, the spectral functions of the vector mesons calculated in infinite matter are combined with a Monte Carlo simulation of π^- induced production and propagation of vector mesons inside nuclei.

The self-energy of the vector mesons in matter Π_v is based on the low density approximation which connects the vacuum self-energy Π_0 with the meson nucleon scattering matrix T_{vN}: $\Pi_v(\omega, \vec{q}, \rho) = \Pi_0(\omega, \vec{q}) - \rho T_{vN}(\omega, \vec{q})$. The potential (and therefore the mass shift) depends to leading order linearly on the baryon density ρ: $2\omega U = \Pi_v(\omega, \vec{q}, \rho) - \Pi_0 = \rho T_{vN}(\omega, \vec{q})$. The resulting spectral functions for infinite matter at $\rho = \rho_0$ show a different behavior for the ω- and the ρ meson. While the pole mass of the ρ meson is shifted only slightly, its width is heavily influenced by $\rho N \to \pi N$, $\rho N \to \pi\Delta \to \pi\pi N$ and $\rho N \to \omega N \to \pi\pi\pi N$ scattering. Effectively the ρ-meson is dissolved in the nuclear medium. The ω-meson pole mass is shifted by about -80 MeV/c^2 and the width is broadened from 8 to 40 MeV/c^2. However at $\rho = \rho_0$ the ω-meson still keeps its quasi-particle character. The MC-simulation is based on measured cross sections for $\pi^- + p \to \rho, \omega, \phi + n$ reactions. The absorption channels are calculated via detailed balance. The baryon density distribution of the Pb nucleus is based on measured charge distributions. The fermi motion of the nucleons is taken into account. With an elementary ω-meson cross section of 2.5 mb ($p_{\pi^-} = 1.3$ GeV/c) one could expect Z_{Pb}*2.5≈200 mb for a Pb nucleus. However the effective cross section results in only 33 mb. Because of the strong interaction of π^- with nuclear matter, only the hemisphere of the nucleus facing the beam takes part in the reaction (shadowing, Fig. 1). The mesons are produced with vacuum pole mass. In case of decay the mass of the meson is sampled according to the local baryon density at this "freezeout" point based on the spectral functions for infinite matter. The sampling is done in accordance with energy conservation. The spectral functions in the finite system (Fig. 2) are obtained by integration over the probability distribution of the meson decays. The majority of the ω-mesons decay outside the Pb nucleus and produce a narrow structure. The contributions from the inner part of the nucleus (full shift of the ω-meson mass) and the surface (reduced shift) increase the broadening of ω-mesons from 40 to about 80 MeV/c^2. This additional broadening is a consequence of the finite size of the system. The reaction $\pi^- Pb$ seems to be a promising experiment to probe the in-medium spectral distribibion of vector mesons. The predicted dilepton spectra could be measured with the HADES spectrometer [3]. In Fig. 2 the HADES resolution is taken into account.

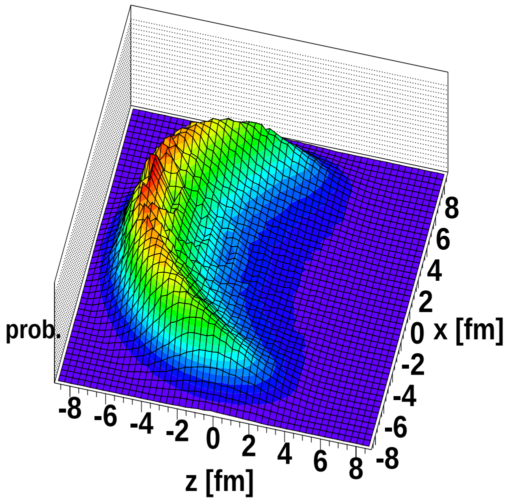

Figure 1: Spatial probability distribution of meson creation for $\pi^- Pb$ at p_π=1.3 [GeV/c].

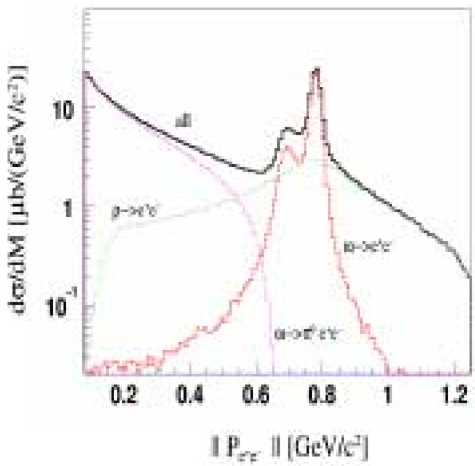

Figure 2: ρ- and ω-meson contributions to the dilepton specta for $\pi^- Pb$ at p_π=1.3 [GeV/c].

Below the η mass strong contributions from η Dalitz and other channels are expected. In the mass region of the (shifted) ω peak both πN Bremsstrahlung [4] and combinatorial background from π Dalitz decay [5] contribute still below the ρ-meson contribution.

References

[1] F.Klingl and W.Weise EPJ A4 (1999) 225
[2] E.Marco and W.Weise Phys. Lett. B482 (2000) 87
[3] J.Friese et.al. Nucl. Phys A654,(1999) 268
[4] W.Cassing et.al. Phys. Rep. 308, 65 (1999)
[5] W.Schön et.al. Act. Phys. Pol B27 Number 11 (1996)

Modifications in resonance life times and cross sections in a test-particle description of off-shell processes in transport theory

A.B. Larionov*, S. Leupold, U. Mosel
University of Giessen

For the understanding of heavy-ion collisions semi-classical transport theory has become an indispensable tool. While former works have focused their attention more or less on the quasi-particle regime the extension of the formalism to off-shell phenomena has become a topic of growing interest in the last few years since it has been realized that the collision rates present in high energetic nucleus-nucleus collisions typically are so large that an on-shell approximation seems to be inappropriate. In addition, the resonances excited during the reaction may have large decay widths. Therefore, a representation of these states by stable particles may not be a proper approximation. The usual approach to solve a transport equation is the representation of the phase-space density by test-particles. If not only asymptotically stable states but also resonances are simulated by test-particles, one has to attribute to those 'resonance test-particles' finite life times and arbitrary invariant masses (chosen according to their spectral distribution), i.e. the generalized test-particle representation is given by $\sum_i \delta^{(3)}(\vec{x}-\vec{x}_i(t))\,\delta(p_0^2 - E_i^2(t))\,\delta^{(3)}(\vec{p}-\vec{p}_i(t))$. Note that here in contrast to the quasi-particle approximation the test-particles are allowed to have arbitrary energies. The question which (in general energy- or mass-dependent) life time has to be attributed to the resonance test-particles is under present discussion. The commonly used recipe is to take the inverse of the decay width Γ of the resonance, evaluated for the respective invariant mass. Near threshold the width becomes small due to the available phase-space. Hence the life time — if identified with the inverse width — becomes large. In [1] it was suggested to rather calculate the life time from the time delay that the particles suffer which form the resonance. This time delay is given by the energy derivative of the scattering phase shift of these particles: $\tau = \partial\delta/\partial p_0$. This quantity vanishes near threshold. Hence the two expressions for the life time show a completely different behavior as functions of the invariant mass of the resonance as shown in Fig. 1 for the $\Delta(1232)$ resonance. Recently a novel approach to solve these questions has been presented [2, 3]. It has been shown there that the life time of an off-shell test-particle is indeed given by $\tau = \partial\delta/\partial p_0$. In addition, the cross section for any collision which involves an off-shell test-particle in the incoming channel is subject to an in-medium modification: the cross section has to be divided by $r = 2\sqrt{s}\Gamma\,\mathcal{A}\,(1-K)$ where Γ is the total width of the particle, $\mathcal{A}$ its spectral function and $1-K$ a renormalization factor (cf. [2, 3] for details).

To test the ideas above, we applied the BUU model in version [4] with the resonance production/absorption quenching [5]. The most sensitive observable for the Δ-resonance life time modifications turns out to be the invariant mass spectrum of the correlated proton-pion pairs.

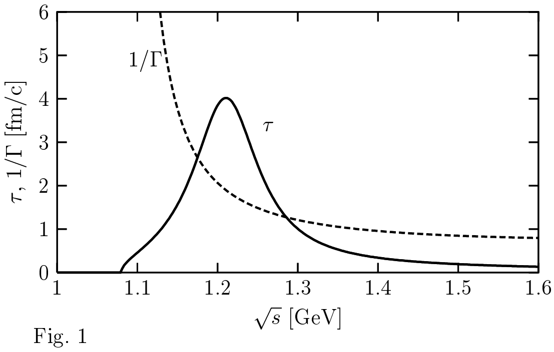

Fig. 1

Fig. 2 shows the invariant mass (p,π^+) spectra for a central Au+Au collision at 1.06 AGeV calculated without life time modifications (solid line), with modified Δ-resonance life time only (dashed line) and with both modified Δ-resonance life and $N\Delta \to NN$ cross section (dotted line). The life time modification leads to a sharper peaked spectrum at $M \simeq 1.2$ GeV due to longer life time of the Δ-resonances near the pole mass (Fig. 1). An additional modification of the $N\Delta \to NN$ cross section produces an even more sharp spectrum, since the absorption of the Δ-resonances near the pole mass gets reduced. Thus we conclude that the resonance life time modifications somewhat increase the deviation of the BUU calculation with the data [6] on the spectrum of the (p,π^+) pairs. Further studies will show if this effect could be counterbalanced by the off-shellness of the produced pions (work in progress).

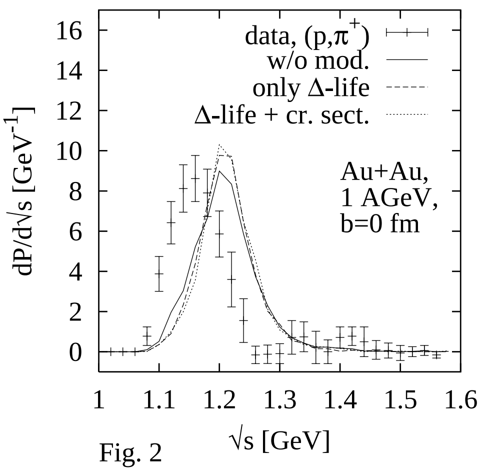

Fig. 2

References

[1] P. Danielewicz, S. Pratt, Phys. Rev. **C53**, 249 (1996).
[2] S. Leupold, Nucl. Phys. **A672**, 475 (2000).
[3] S. Leupold, nucl-th/0008036, subm. to Nucl. Phys. A.
[4] M. Effenberger, E.L. Bratkovskaya, U. Mosel, Phys. Rev. **C60**, 044614 (1999).
[5] A.B. Larionov, W. Cassing, S. Leupold, U. Mosel, contr. to this Annual Report.
[6] M. Eskef et al., Eur. Phys. J. **A3**, 335 (1998).

*On leave of absence from RRC "I.V. Kurchatov Institute", 123182 Moscow, Russia

Strange Particle Production and Equilibration at SIS energies within a Semiclassical Off-shell Transport Approach

W. Cassing, S. Juchem
University of Giessen

Recently we have formulated a novel transport approach that incorporates the propagation of particles off the mass-shell [1]. It goes beyond the conventional transport description within the on-shell quasiparticle limit to propagate particles with a finite lifetime by means of a dynamical spectral function. This spectral function is directly determined by the spacetime and momentum-dependent imaginary part of the particle self-energy. By this procedure it is guaranteed, that the actual spectral function is consistently adjusted to the scatterings and decays of the particle in the nuclear medium as well as in vacuum.

Within this off-shell transport approach we have studied strange meson production in the SIS energy regime. When treating baryons as well as antikaons off-shell we obtain an increase by a factor of about two for the production of K^- mesons in comparison to the on-shell calculation for $Ni + Ni$ at 1.8 A GeV (Fig. 1). This enhancement arises since antikaons couple strongly to nucleons such that they achieve a considerable collision width in the nuclear medium which leads to an effective lowering of their production threshold. So the antikaons might be produced at subtreshold energies and enhance the final K^--yield when becoming asymptotically on-shell. The inclusion of the off-shell propagation therefore gives a (partial) explanation for the high K^- abundancy that has been measured by the FRS, KaoS and FOPI Collaborations [2,3]. The data are still underestimated by the off-shell calculations that have been performed without any potentials for the strange mesons. Thus antikaon potenials will still be necessary to get a full description of the experimental results. We have also investigated the production of K^+ mesons in

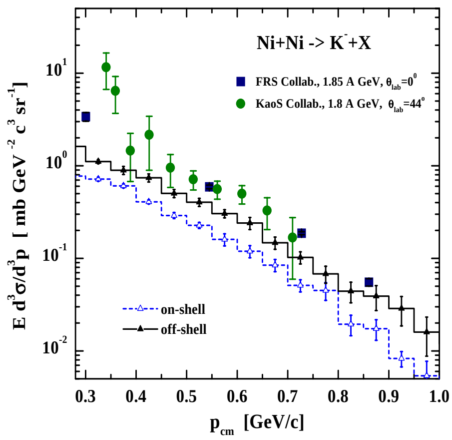

Figure 1: The inclusive spectra of K^- for $Ni + Ni$ at 1.8 A GeV within the off-shell transport approach (solid histogram, full triangles) and in the on-shell limit (dashed histogram, open triangles). The data are from [2] for $\theta_{lab} = 0^o$ (squares) and from [3] for $\theta_{lab} = 44^o$ (circles).

the same reaction, however, find only a small enhancement within the off-shell treatment relative to the on-shell limit which should be attributed to the weak coupling of kaons to nucleons [1b].

Furthermore, we have studied equilibration phenomena in the off-shell transport approach. For this aim we have confined the system to a box in coordinate space with periodic boundary conditions (using a density of $\rho = \rho_0$). We find that the off-shell generalization has practically no influence on the equilibration time of the nuclear system for various bombarding energies up to 1 A GeV [1c].

In order to study the equilibrium properties we compare the results of our transport (box) calculations with a simple statistical model for an ideal hadron gas . All hadron species that are propagated in the transport calculation (N,Δ,π) are also taken into account in the statistical model within the grand canonical ensemble. In Fig. 2 we

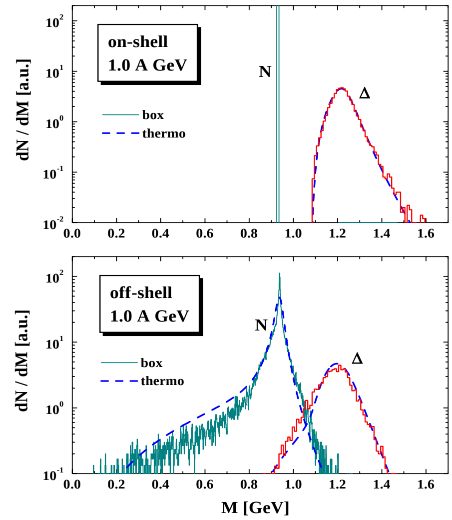

Figure 2: Differential distribution in mass for nucleons and Δ resonances for a bombarding energy 1 A GeV at $\rho = \rho_0$.

show the differential distributions in mass for nucleons and Δ resonances in the long time limit of the transport (box) calculations in comparison to the statistical model (dashed lines) for a bombarding energy of 1 A GeV. We find that the transport theoretical treatment yields nearly the same distributions in mass as the thermodynamical model, when for the latter the same spectral functions as in the transport calculation are employed. A temperature of 97 MeV (deduced from a transverse mass analysis of the particle spectra) has been used here. This result indicates that the actual realization of the off-shell dynamics guarantees the correct stationary solution in the long time limit.

References

[1] W. Cassing, S. Juchem, Nucl. Phys. A 665 (2000) 385; Nucl. Phys. A 672 (2000) 417; Nucl. Phys. A 677 (2000) 445.

[2] A. Schröter et al., Z. Phys. A 350 (1994) 101.

[3] P. Senger et al., Acta Phys. Pol. B27 (1996) 2993.

Probing the nuclear equation of state by K^+ production in heavy ion collisions

C. Fuchs, Amand Faessler, E. Zabrodin, Yu-Ming Zheng
Institut für Theoretische Physik, Universität Tübingen

From the very beginning kaons have been considered as one of the best probes to study dense and hot nuclear matter formed in relativistic heavy ion collisions. In particular at incident energies below the corresponding production thresholds in free space K^+ mesons are created in the early and high density phase of such reactions and – due to strangeness conservation – are not reabsorbed by the nuclear environment. Furthermore, there exist strong evidences that kaons change their properties inside the nuclear medium as predicted by effective chiral models. The aim of the present work is to study if decisive information on the nuclear EOS can be extracted from subthreshold kaon production by new high precision data [1]. The KaoS Collaboration has performed systematic measurements of the K^+ production far below threshold in heavy ($Au + Au$) and light ($C + C$) systems [2]. Looking at the ratios built from heavy and light systems possible uncertainties which might still exist in the theoretical calculations should cancel out to a large extent which allows to draw reliable conclusions. Furthermore, far below threshold the kaon production is a highly collective process and a particular sensitivity to the compression of the participant matter is expected. The present investigations are based on the Quantum Molecular Dynamics (QMD) transport model. For the nuclear EOS we adopt soft and hard Skyrme forces corresponding to a compression modulus of K=200 MeV and 380 MeV, respectively, and with a momentum dependence adjusted to the empirical optical nucleon-nucleus potential.

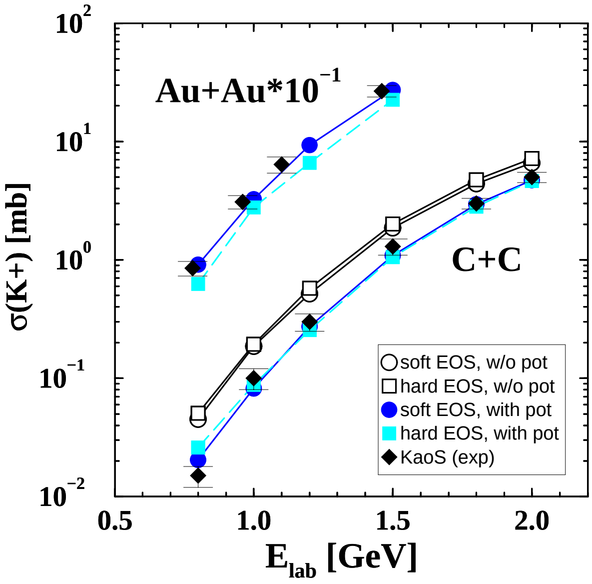

Figure 1: Excitation function of the K^+ cross section in $C+C$ and $Au + Au$ reactions. The calculations are performed with in-medium kaon potential and using a hard/soft nuclear EOS. For $C + C$ also results without in-medium kaon potential are shown.

In Fig. 1 the K^+ excitation function for $Au + Au$ and $C + C$ reactions starting from 0.8 A·GeV which is far below threshold (E_{thr} = 1.58 GeV) are shown. The calculations are performed for a soft/hard EOS including the in-medium kaon potential. For both systems the agreement with the KaoS data [3, 2] is very good when a soft EOS is used. In the large system there is a visible EOS effect which is absent in the light system. To estimate the influence of the in-medium kaon potential for $C + C$ also calculations without potential are shown. Already in the light system the K^+ yield is reduced by about **50%** by the influence of the potential which is essential to reproduce the yields [3]. The comparison to the new KaoS data [2] is made

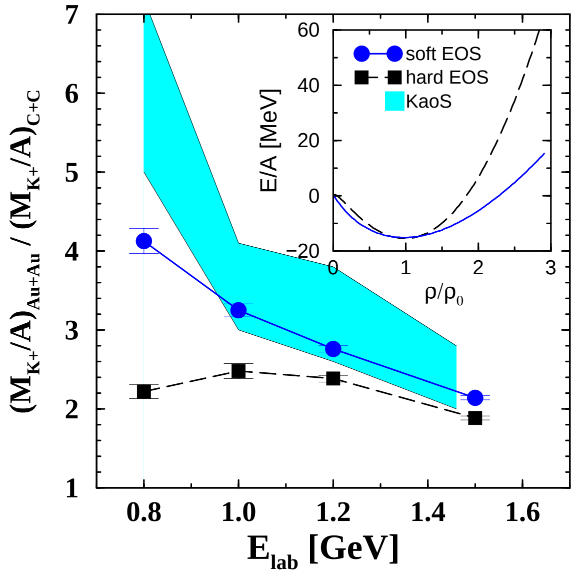

Figure 2: Excitation function of the ratio R of K^+ multiplicities obtained in inclusive $Au + Au$ over $C + C$ reactions. The calculations are performed with in-medium kaon potential and using a hard/soft nuclear EOS and compared to the experimental range of R (shaded area) given by the data from the KaoS Collaboration [2].

in Fig. 2. Here only calculations including the kaon potential are shown since it is already clear from Fig. 1 that without the potential one is not able to reproduce the experimental yields. The calculations are performed under minimal bias conditions with $b_{\mathbf{max}} = 11$ fm for $Au + Au$ and $b_{\mathbf{max}} = 5$ fm for $C + C$ and normalised to the experimental reaction cross sections [3, 2]. Both calculations show an increase of R with decreasing incident energy down to 1.0 A·GeV. However, this increase is much less pronounced using the stiff EOS. In the latter case R even drops for 0.8 A·GeV whereas the soft EOS leads to an unrelieved increase of R. Using the light system as reference frame there is a visible sensitivity on the EOS. Results for the K^+ excitation function in $Au + Au$ over $C + C$ reactions as measured by the KaoS Collaboration, strongly support the scenario with a soft EOS. The ratio itself is rather independent on the existance of the in-medium potential, but the potential is necessary to reproduce the total yields.

References

[1] C. Fuchs, A. Faessler, E. Zabrodin, Y.-M. Zheng, Phys. Rev. Lett. (2001) in press.

[2] C. Sturm *et al.*, Phys. Rev. Lett. **86**, 39 (2001).

[3] F. Laue et al., Phys. Rev. Lett. **82**, 1640 (1998).

Kaon Production via High Mass Resonances in UrQMD^{B,G}

H. Weber, S.A. Bass[‡] , S. Soff[§] , H. Stöcker and W. Greiner
Institut für Theoretische Physik, Universität Frankfurt am Main, Germany

The investigation of strange matter in heavy ion collisions is of great interest, as the s and $\bar{s}$-quarks are not present in the initial projectile and target matter. Therefore the measurement of strange particles might yield deep insight into the reaction dynamics during the high density phase.

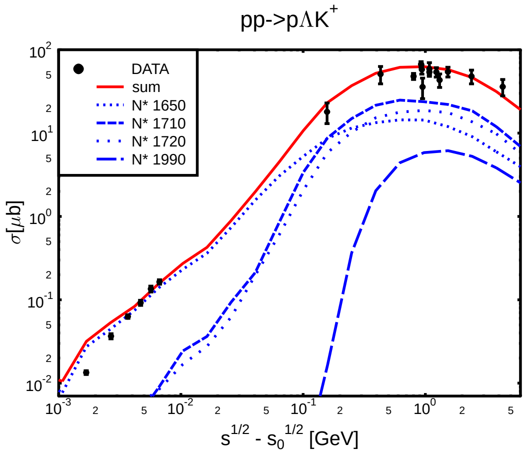

Figure 1: $pp \to p\Lambda K^+$ cross section in UrQMD compared to data.

For our investigation, we use the Ultrarelativistic Quantum Molecular Dynamics model (UrQMD) [1]. UrQMD provides a good description of NN and A+A collisions over a wide range of energies from a few hundred MeV/A up to hundreds of GeV/A. The production threshold for the lightest strange particle (K^+) via the process $NN \to N\Lambda K^+$ is 1.58 GeV. Particularly for SIS energies, the correct description of the production cross section near the threshold is very important. In contrast to most other models, UrQMD treats the elementary K^+ production via two-step processes

$$pp \to pB^* \to p\Lambda K^+, \qquad pp \to pB^* \to p\Sigma K$$

B^* are the high mass resonances N^*_{1650}, N^*_{1710}, N^*_{1720}, N^*_{1990} and Δ^*_{1920}. For the decay into the hyperon-kaon channel we use the experimental branching ratios, where available.

Figure 1 shows the cross section for the reaction $pp \to p\Lambda K^+$ as a function of energy above threshold. The dotted lines are contributions of the five resonances to the total cross section (solid line). With this approach we are able to describe the experimental data (dots) reasonably well, even a few MeV above the threshold (COSY data [2])

The $pp \to p\Sigma^0 K^+$ and the $pp \to p\Sigma^+ K^0$ channel can be described as well with this approach. Figure 2 shows these channels in UrQMD compared to data.

For higher collision energies, kaon production via string fragmentation becomes important. Figure 3 shows an excitation function of the K^+ to K^- ratio for central Pb+Pb

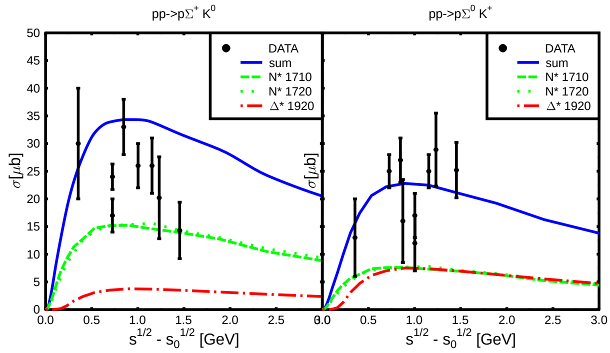

Figure 2: $pp \to p\Sigma^+ K^0$ and $pp \to p\Sigma^0 K^+$ cross section in UrQMD compared to data.

events calculated with the UrQMD model. The dots are experimental data from E802, E866/E917 [3] and NA49 [4, 5]. The model shows a good overall agreement with the experiments, except for the preliminary 40 GeV measurement from NA49 [5] which is slightly underestimated. Interestingly this good agreement for the K^+ to K^- ratio with the data can be obtained without invoking any medium dependent effects, such as in-medium masses.

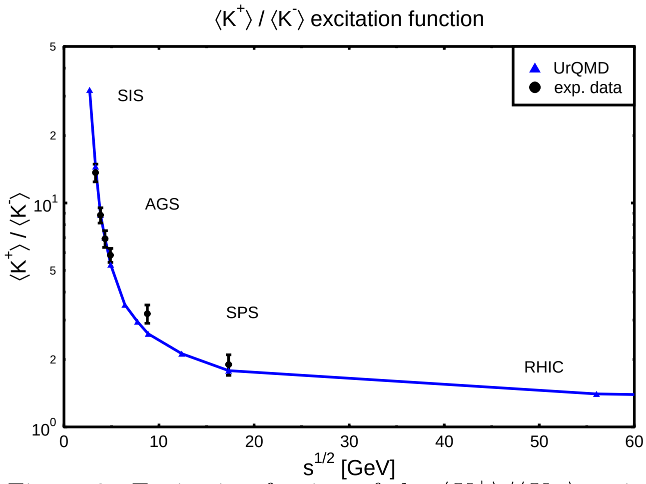

Figure 3: Excitation funtion of the $\langle K^+\rangle/\langle K^-\rangle$ ratio in central Pb+Pb or Au+Au collisions compared to data from E802, E866, E917 and NA49

References

[1] S. A. Bass *et al.*, Prog. Part. Nucl. Phys. **41**, 225 (1998)

[2] J. T. Balewski *et al.*, Phys. Lett. B **420**, 211 (1998)

[3] L. Ahle *et al.* [E866 Collaboration], Phys. Lett. B **490**, 53 (2000) [nucl-ex/0008010].

[4] J. Bachler *et al.* [NA49 Collaboration], Nucl. Phys. A **661**, 45 (1999).

[5] C. Blume *for the NA49 collaboration*, QM2001, to appear in the proceedings.

[‡] Duke University and RIKEN BNL Research Institute, USA
[§] LBL Berkeley, USA (Lynen-Fellow of the Humboldt-Foundation)

Collective flow in heavy ion collisions from SIS to SPS energies

E. Zabrodin, C. Fuchs, L. Bravina, and Amand Faessler, University of Tübingen

Collective effects, such as the transverse flow of particles produced in ultrarelativistic heavy ion collisions, are very important for the study of the nuclear equation of state (EOS) and for the search of a predicted transition to the quark-gluon plasma (QGP). At present the transverse flow is believed to be one of the most clear signals to detect the creation of the QGP in heavy-ion experiments. This explains the great interest of both experimentalists and theoreticians in the collective flow phenomenon [1].

The distribution of the particles in the azimuthal plane can be presented as [2]

$$\frac{dN}{d\phi} = a_0 \left[1 + 2 \sum_{n=1}^{\infty} v_n cos(n\phi) \right] , \qquad (1)$$

where ϕ is the azimuthal angle between the momentum of the particle and the reaction plane. The first two coefficients, v_1 and v_2, colloquially known as directed and elliptic flow, are the amplitudes of the first and second harmonics in the Fourier expansion of the azimuthal distribution, respectively. The directed and elliptic flow of hadrons in heavy-ion collisions is very sensitive to the EOS of the nuclear medium. The formation of small domains of a QGP phase might happen already at the SPS energies or even below. Accompanied by the hadronization this enforces a softening of the EOS due to the dropping pressure. Thus, the disappearance of the directed flow in midrapidity range can be considered as an indication of a new state of matter. This conclusion is supported by hydrodynamic simulations with and without the QGP phase.

Microscopic models, which do not imply the QGP formation, describe the dynamics of nuclear collisions at energies up to $\sqrt{s} \approx 2A$ GeV in terms of reactions between hadrons and their excited states, resonances. At higher energies additional degrees of freedom, strings, should be taken into account to describe correctly the processes of multiparticle production. We employ the quantum molecular dynamics (QMD) model [3] at the SIS energies, while at the AGS and SPS energies the quark-gluon string model (QGSM) [4] is applied. For the simulations at $1A$ GeV, $11.6A$ GeV, and $160A$ GeV, we choose light (S+S) and heavy (Au+Au and Pb+Pb) symmetric systems [5].

The deviations of the nucleon directed flow from the straight line behavior start to develop already at AGS energies (Fig. 1) due to the shadowing effect, which plays a decisive role in the competition between normal flow and antiflow in (semi)peripheral heavy-ion collisions. Hadrons, emitted with small rapidities at the onset of the collision in the antiflow area can propagate freely, while their counterparts will be absorbed by the flying massive spectators. The signal becomes stronger with the rise of the impact parameter and with the rise of the incident energy. In the latter case the spectators are more Lorentz-contracted and more hadrons can be emitted unscreened with small rapidities in the direction of antiflow. This effect should appear

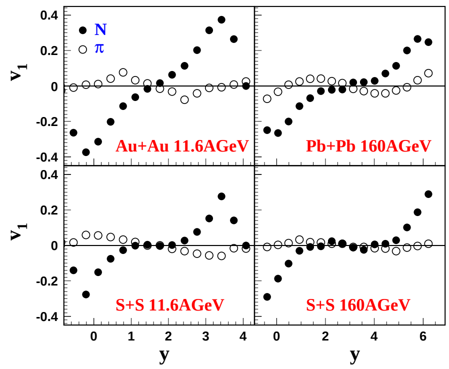

Figure 1: $v_1^{N,\pi}(y)$ in min. bias events at AGS and SPS.

in semicentral collisions with $b \leq 3$ fm at RHIC energies, and can mimic the softening of the EOS of hot and dense nuclear matter. However, the disappearance of directed flow due to shadowing is more distinct for light systems, such as S+S or Ca+Ca, while in the QGP case the effect should be more pronounced in heavy systems. Thus, one can distinguish between the two phenomena by the comparison of the directed flow of nucleons in the midrapidity range in light and heavy-ion collisions.

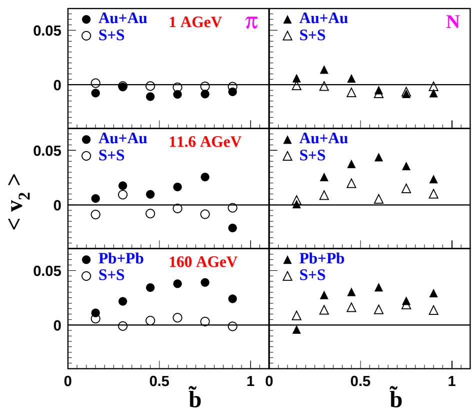

Figure 2: The mean elliptic flow of N's and π's in light and heavy system colliding at SIS, AGS, and SPS energies.

The elliptic flow of nucleons and pions is found to change its orientation from out-of-plane at $1A$ GeV to in-plane at $11.6A$ GeV (Fig. 2). The effect can be explained by stronger Lorentz-contraction of colliding nuclei. Also, at higher colliding energies the contracted spectators leave the reaction zone faster, thus giving space for the growth of elliptic flow in the reaction plane [5].

References

[1] Proc. of the QM'2001 conf.: Nucl. Phys. A (in press).

[2] S. Voloshin, Y. Zhang: Z. Phys. C 70 (1996) 665

[3] J. Aichelin: Phys. Rep. 202 (1991) 233;
C. Fuchs et al: J. Phys. G 22 (1996) 131

[4] N.S. Amelin et al: Phys. Rev. C 47 (1993) 2299

[5] L. Bravina, E. Zabrodin, C. Fuchs, Amand Faessler: Phys. Lett. B 470 (1999) 27; Phys. Rev. C 61 (2000) 064902; Phys. Rev. C 62 (2001) (in press).

Microscopic Interactions and Flow in Heavy Ion Collisions^B

T. Gaitanos[1], C. Fuchs[2], H. H. Wolter[1], Amand Faessler[2]
[1]Sektion Physik, Universität München, [2]Inst. für Theor. Physik, Universität Tübingen

Relativistic heavy ion collisions have been extensively investigated to determine the equation-of-state (eos) of nuclear matter using phenomenological effective fields of the non-relativistic Skyrme or the relativistic Walecka type. It is found generally that a soft eos with momentum dependence can decribe much of the data in the SIS energy range. It is, however, of fundamental interest to test also microscopic fields derived from NN- interactions by many-body theory. We have previously used self energies from relativistic Brueckner calculations (DB) and have shown that these satisfactorily explain the data for flow observables [1], however, only if non-equlibrium effects are considered, i.e. taking into account that the momentum distribution is not equilibrated during a large part of an energetic heavy ion collision, which changes the effective fields. The non-equlibrium effects effectively soften the eos.

However, different approximations have been used in DB calculations, which may lead to similar saturation properties and results for finite nuclei but to different behaviours for higher density and momentum. It may thus be possible to distinguish different DB models in heavy ion collisions. Here we have tested two particular DB models: one from the Groningen group (DBHM)[2], and a more recent one from the Tübingen group (DBT) [3]. The latter takes care to eliminate spurious contributions from negative energy states, and leads to a softer eos at higher densities and to less repulsion at higher momenta.

We have performed a detailed study of flow observables in $Au + Au$ collisions [4], which have been investigated extensively by the FOPI collaboration [5]. We discuss differential flow observables: stopping or longitudinal flow and transverse in-plane and out-of-plane flow. We have used the common description in terms of the Fourier coefficients of the azimuthal distributions: v_1 (flow) and v_2 (elliptic flow), as functions of the normalized rapidity $Y^{(0)}$ and the total transverse momentum $p_t^{(0)}$. As an example in fig.1 we show for forward rapidities and different fragments the flow as a function of the transverse momentum. It is seen that the two DB models yield different results and that the DBT model reproduces preliminary FOPI data [5] better, which was not so clearly seen in global observables, like the directed flow (not shown here [4]). Similar in fig.2 we show an excitation function of the elliptic flow compared to data from different sources. We see that the DBT model reproduced the data considerably better, in particular the recent FOPI data between 400 Mev and 1 GeV. Similar results are found for other flow observables: above 400 MeV the softer and less repulsive DBT model seems to be preferred, below in some cases the DBHM model has advantages.

Thus we generally find that microscopic fields succeed also to reproduce more exclusive flow variables, thus leading to a rather unified picture of nuclear fields for nuclear matter, finite nuclei and heavy ion collisions. In the more detailed comparisons it was shown that different DB approximations can indeed be distinguished by looking at differential flow observables.

References

[1] T. Gaitanos, C. Fuchs, H.H. Wolter, Nucl. Phys. **A650** (1999) 97.

[2] B. ter Haar, R. Malfliet, Phys. Rep. **149** (1987) 207.

[3] C. Fuchs, T. Waindzoch, A. Faessler, D.S. Kosov, Phys. Rev. **C58** (1998) 2022; T. Gross-Boelting, C. Fuchs, A. Faessler, Nucl. Phys. **A648** (1999) 105.

[4] T. Gaitanos, C. Fuchs, H.H. Wolter, A. Faessler, EPJ submitted, nucl-th/0102010.

[5] A. Andronic, FOPI collaboration, Nucl. Phys. **A661** (1999) 333c, and refences cited there.

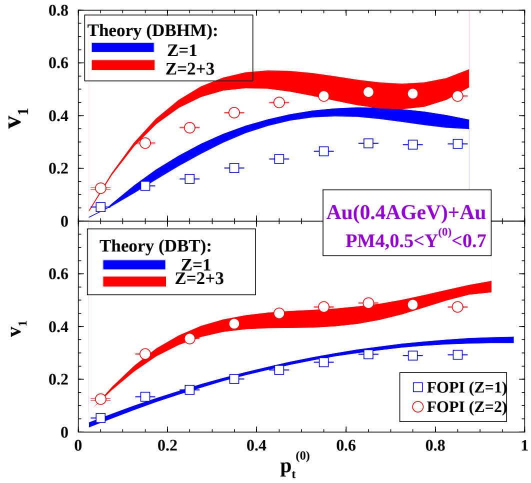

Figure 1: In-plane flow for semi-central Au+Au collisions at 400 AMeV for protons and light fragments [5] in comparisons to calculations using different DB fields. Statistical errors of the calculation are indicated by bands.

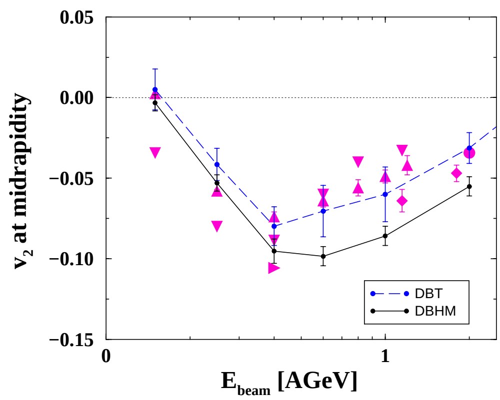

Figure 2: Energy dependence of the elliptic flow v_2 at mid-rapidity. The data denoted by upright triangles are taken from the FOPI collaboration [5], the others from others sources [4].

Directed Flow of Baryons in Heavy-Ion Collisions^{G}

Yu.B. Ivanov, E.G. Nikonov, W. Nörenberg, A.A. Shanenko and V.D. Toneev
GSI Darmstadt

The collective motion of nuclear matter observed in heavy-ion interactions is essentially caused by the pressure gradients arising during the time evolution in the collision, and hence opens a promising way for obtaining information on the equation of state (EoS) and, in particular, on a possible phase transition. We analyze the collective motion of nucleons from high-energy heavy-ion collisions within a relativistic two-fluid model for different equations of state [1].

Our consideration is essentially based on the recently proposed Mixed-Phase (MP) model [2]. The underlying assumption of the MP model is that unbound quarks and gluons *may coexist* with hadrons forming a *homogeneous* quark/gluon–hadron phase. Since the mean distance between hadrons and quarks/gluons in this mixed phase may be of the same order as that between hadrons, the interaction between all these constituents (unbound quarks/gluons and hadrons) plays an important role and defines the order of the phase transition. For the case of quarks of two light flavors at zero baryon density ($n_B = 0$), the MP model is consistent with lattice QCD data providing a continuous phase transition of the cross-over type with a deconfinement temperature $T_{dec} = 153$ MeV. In a two-phase approach based on the bag model a first-order deconfinement phase transition occurs with a sharp jump in energy density ε at T_{dec} close to the value obtained from lattice QCD. A particular feature of the MP model is that, for $n_B = 0$ the *softest point* of the EoS, defined as a minimum of the function $p(\varepsilon)/\varepsilon$, is not very pronounced and located at comparatively low values of the energy density: $\varepsilon_{SP} \approx 0.45$ GeV/fm^3, which roughly agrees with the lattice QCD value. In contrast, the bag-model EoS exhibits a very pronounced softest point at large energy densities $\varepsilon_{SP} \approx 1.5$ GeV/fm^3.

We have studied experimental consequences of these differences in EoS within the hydrodynamic approach. We use the 3D relativistic two-fluid model with a finite stopping power [3]. These two fluids, initially associated with target and projectile nucleons, are described by a set of hydrodynamic equations with the coupling term, which characterizes friction between the counter-streaming fluids. The friction term originates from both elastic and inelastic NN collisions and gives rise to a direct emission of mesons in addition to the thermal mesons in the fluids [3].

The average directed flow is defined by

$$\langle P_x \rangle = \frac{\displaystyle\int dp_x dp_y dy \; p_x \left(E\frac{d^3N}{dp^3} \right)}{\displaystyle\int dp_x dp_y dy \left(E\frac{d^3N}{dp^3} \right)} \, ,$$

where the integration in the c.m. system runs over the rapidity region $[0, y_{cm}]$. The calculated excitation functions for $\langle P_x \rangle$ of baryons within different models are shown in the figure for $Au{+}Au$ collisions at the impact parameter $b = 3$ fm. As shown in the upper panel, conventional one-fluid (1F) hydrodynamics for pure hadronic matter [4] results in a very large directed flow due to the inherent instantaneous stopping of the colliding matter. This instantaneous stopping is unrealistic at high beam energies. If the deconfinement phase transition (PT), based on the bag-model EoS [4], is included, the excitation function of $\langle P_x \rangle$ exhibits a deep minimum near $E_{lab} \approx 6$ A·GeV, which is a manifestation of the strong softest-point effect in the bag-model EoS.

The result of two-fluid (2F) hydrodynamics with the MP EoS noticeably differs from the one-fluid calculations. After a maximum around 1 A·GeV, the average directed flow decreases slowly and smoothly. This difference is caused by the fact that the softest point of the MP EoS is washed out for $n_B \gtrsim 0.4$ and also by dynamical reasons, i.e. the finite stopping power and direct pion emission change the evolution pattern. The latter point is confirmed by comparison to three-fluid calculations with the bag EoS [5] plotted in the lower panel of the figure. As seen, the minimum of the directed flow excitation function, predicted by the one-fluid hydrodynamics with the bag EoS, survives in the three-fluid (nonunified) regime, but its value decreases and its position shifts to higher energies. If one applies the *unification procedure* of [5], which favors fusion of two fluids into a single one, and thus making stopping larger, three-fluid hydrodynamics gives results, which are very similar to those of the one-fluid model, and predicts in addition a bump at $E_{lab} \approx 40$ A·GeV.

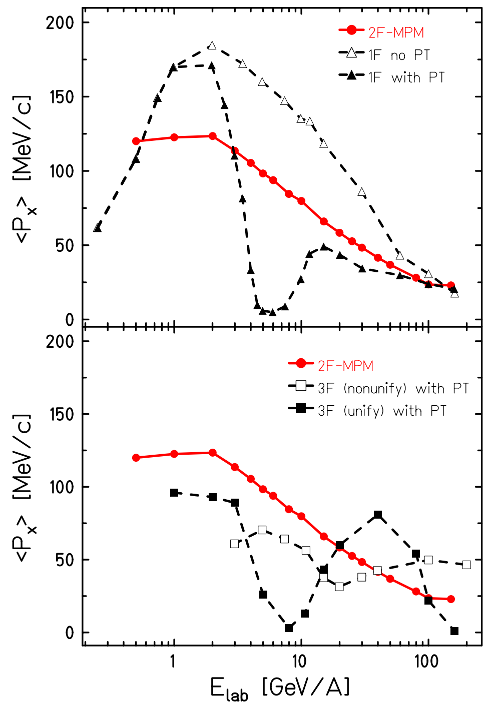

Recent experimental results confirm that the excitation function of the directed baryonic flow is a smooth function in the 2-8 A·GeV energy range [6], which is in agreement with our MP EoS.

[1] Yu.B. Ivanov, E.G. Nikonov, W. Nörenberg, A.A. Shanenko and V.D. Toneev, GSI Preprint 2000-39; nucl-th/0011004.

[2] E.G. Nikonov, A.A. Shanenko, and V.D. Toneev, Heavy Ion Phys. **8** (1998) 89; nucl-th/9802018. V.D. Toneev, E.G. Nikonov, and A.A. Shanenko, Preprint GSI 98-30, Darmstadt, 1998.

[3] I.N. Mishustin, V.N. Russkikh, and L.M. Satarov, Nucl. Phys. **A494** (1989) 595; Yad. Fiz. **54** (1991) 429.

[4] D.H. Rischke, Y. Pürsün *et al.*, Heavy Ion Phys. **1** (1996) 309; D.H. Rischke, Nucl. Phys. **A610** (1996) 88c.

[5] J. Brachmann *et al.*, Phys. Rev. C **61** (2000) 024909.

[6] E895 Collaboration, H. Liu *et al.*, Phys. Rev. Lett. **84** (2000) 5488.

Maximum Strangeness Content in Heavy Ion Collisions Around 30 A·GeV^{B,G}

J. Cleymans, University of Cape Town, South Africa
H. Oeschler, Technische Universität Darmstadt
K. Redlich, University of Wrocław, Poland and GSI, Darmstadt

Strangeness production in heavy ion collisions at relativistic energies provides one of the key information about the reaction mechanism and could indicate the onset of new phenomena.

The attempts to describe the measured particle ratios including strange hadrons at AGS and SPS and recently also at RHIC using a strangeness fugacity are very successful [1, 2, 3, 4, 5]. However, the usual grand-canonical treatment of strangeness conservation is not sufficient, if the number of strange particles is small [6]. This requires local strangeness conservation which is done in the statistical model using the canonical formulation of strangeness conservation [7].

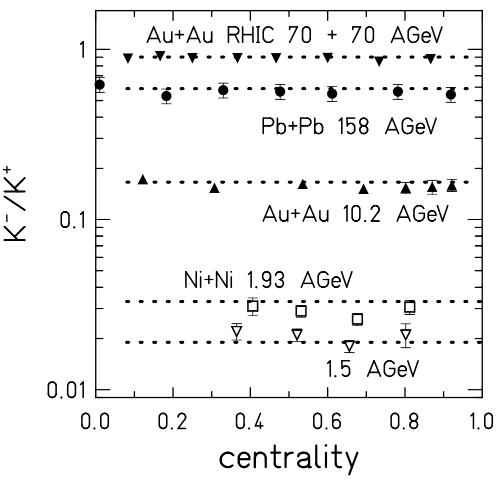

Figure 1: *K^+/K^- ratio is independent of the number of participating nucleons at incident energies from 1.5 A·GeV up to RHIC energies. The dashed lines show the values of the statistical model.*

The canonical approach describes the measured particle ratios at SIS energies and is able to explain the different excitation functions of K^+ and K^- in heavy ion collisions which – when plotted as a function of $\sqrt{s} - \sqrt{s}_{threshold}$ – cross around 1 A·GeV [8]. The canonical description also explains that $M(K^+)/A_{part}$ rises linearly with A_{part} as observed in Au+Au collisions at 1 A·GeV [7, 9] which is in contrast to the behavior of $M(\pi)/A_{part}$ which is independent of A_{part}. This difference is due to the volume term in the canonical description [7]

$$n_{K^+} \sim \exp\left(-\frac{E_{K^+}}{T}\right)\left[g_\Lambda V \int \frac{d^3p}{(2\pi)^3} \exp\left(-\frac{(E_\Lambda - \mu_B)}{T}\right)\right]$$

which takes care of the fact that strange particles are produced associately with another strange particle (e.g. a K^+ together with a Λ). The volume term V, however, drops out when studying the ratio of K^-/K^+ as for the production of K^- an analoguous formula holds

$$n_{K^-} \sim \exp\left(-\frac{E_{K^-}}{T}\right)\left[g_{K^+} V \int \frac{d^3p}{(2\pi)^3} \exp\left(-\frac{E_{K^+}}{T}\right)\right].$$

Indeed, the measured ratios do not vary with the number of participating nucleons in Ni+Ni collisions [10]. This feature is found at all incident energies from 1.5 A·GeV up to RHIC energies as shown in fig. 1 [11, 12, 13]. The above result is especially interesting since between 1.5 and 2.5 A·GeV K^+ production is above while K^- production is below the corresponding NN thresholds.

The enhancement of multi-strange baryons from p+A to $A + A$ collisions might be explainable by a transition from canonical to grand-canonical description as demonstrated in [14].

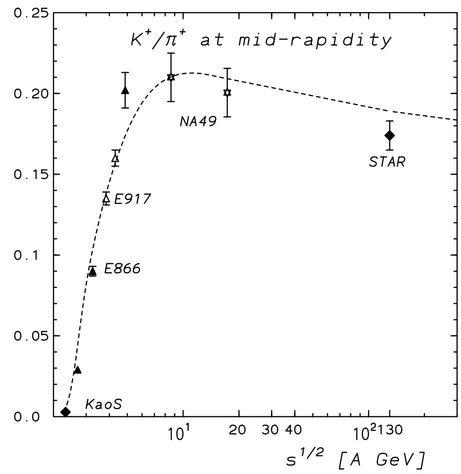

Figure 2: *K^+/π^+ ratio obtained around midrapidity as a function of $\sqrt{s}$ from the various experiments. The dashed line shows the calculation with the statistical model.*

Recently, the evolution of the K^+/π^+ ratio as a function of $\sqrt{s}$ has attracted great interest as a maximum seemed to appear around 40 A·GeV. Figure 2 shows this ratio obtained at midrapidity from SIS energies up to RHIC [12, 13, 15]. Indeed, a maximum around the data point obtained at 40 A·GeV is seen. In general, statistical-model calculations should be compared with 4π integrated results. Then the maximum is even more pronounced. The extrapolation to 4π is, however, in some cases not well established.

The fact that the statistical model based on the general freeze-out curve [16] (dashed line in Fig. 2 exhibits a maximum, too, might appear surprising. Intuitively, one expects that the fraction of strange particles increases with increasing incident energy. So, the question arises whether the maximum is caused by the distribution of strange quarks among the hadrons at freeze out or whether

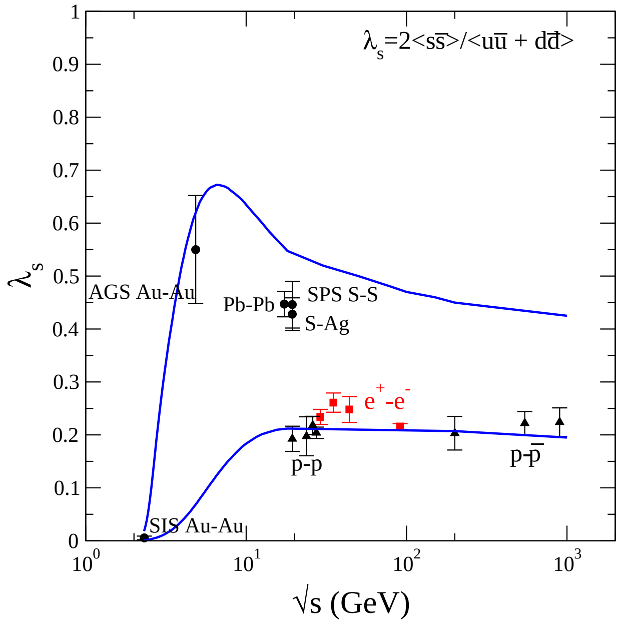

Figure 3: *The Wroblewski ratio λ_S as a function of $\sqrt{s}$. The points refer to measured values (not measured particles species with generally rather small cross sections are added according to the statistical model). The solid lines shows the statistical model results for PbPb and pp collisions.*

less strange quarks are produced in total above a certain incident energy.

To clarify this point, we study next the Wroblewski ratio [17], which is a measure of the strangeness content produced in the collisions. It is defined as

$$\lambda_S = \frac{2N(s\bar{s})}{N(u\bar{u}) + N(d\bar{d})}$$

where $N(q\bar{q})$ is the number of produced quark-antiquark pairs of the given species. The Wroblewski ratio varies from 0 at low incident energies, where no strange particle are produced to a upper limit of 1 for infinite temperature where the difference in masses can be neglected.

Figure 3 shows the values of λ_S extracted from the experimental data. The solid lines in Fig. 3 are the results of the statistical model based on the general freeze-out curve [16]. The results for pp, p$\bar{\text{p}}$, e$^+$e$^-$ are also included. The lower values of λ_S in elementary compared to AA collisions are due to canonical suppression [18]. From Fig. 3 we conclude that around 30 A·GeV the strangeness content in heavy ion collisions reaches a maximum and decreases slightly towards higher incident energies. This is evidenced in Fig. 4 which shows contour lines of constant λ_S in the $T - \mu_B$ plane. As expected λ_S rises with increasing T. With decreasing μ_B, μ_S decreases and hence λ_S. Following the general freeze-out curve, shown as full line in Fig. 4, λ_S rises quickly at SIS and AGS energies, reaches then a maximum around 30 A·GeV.

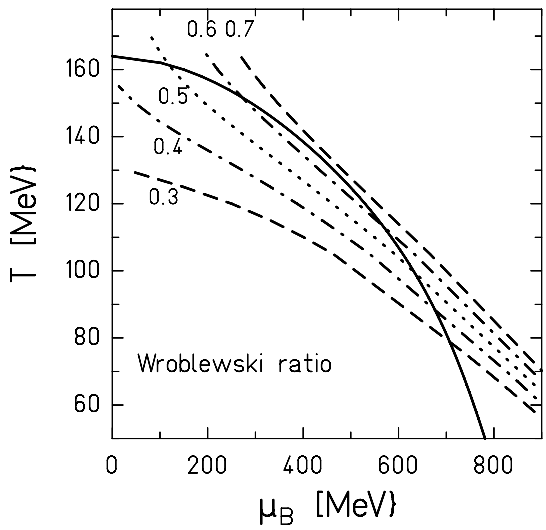

Figure 4: *Lines of constant strangeness content λ_S in the $T - \mu_B$ plane together with the general freeze-out curve (full line) [16].*

References

[1] J. Cleymans and H. Satz, Z. Phys. **C57** (1993) 135.

[2] P. Braun-Munzinger, J. Stachel, J.P. Wessels and N. Xu, Phys. Lett. **B344** (1995) 43.

[3] J. Sollfrank, J. Phys. G: Nucl. Part. Phys. **23** (1997) 1903.

[4] P. Braun-Munzinger, I. Heppe, J. Stachel, Phys. Lett. **B465** (1999) 15.

[5] V.D. Toneev et al., submitted to J. Phys. G: Nucl. Part. Phys.

[6] R. Hagedorn and K. Redlich, Z. Phys. **A27** (1985) 541.

[7] J. Cleymans, H. Oeschler and K. Redlich, Phys. Rev. **C59** (1999) 1663.

[8] J. Cleymans, H. Oeschler and K. Redlich, Phys. Lett. **B485** (2000) 27.

[9] M. Mang, Dissertation, University of Frankfurt, (KaoS Collaboration), 1997.

[10] M. Menzel, Dissertation, U. Marburg, (KaoS Collaboration), 2000.

[11] L. Ahle et al., (E802 Collaboration), Phys. Rev. **C60** (1999) 044904.

[12] C. Blume, (NA49 Collaboration), Conference on “Quark Matter 2001”, Stony Brook, Jan. 2001....

[13] J. Harris, (STAR Collaboration), idem.

[14] S. Hamieh, K. Redlich, A. Tounsi, Phys.Lett. **B486** (2000) 61.

[15] L. Ahle et al., (E866/E917 Collaboration), Phys. Lett. B476 (2000) 1.

[16] J. Cleymans and K. Redlich, Phys. Rev. Lett. **81** (1998) 5284; Phys. Rev. **C60** (1999) 054908.

[17] A. Wroblewski, Acta Physica Polonica **B16** (1985) 379.

[18] F. Becattini et al., hep-ph/0002267.

A model for dilepton production from an expanding fireball

R.A. Schneider, T.Renk and W. Weise, TU München

The search for the quark-gluon plasma (QGP) at CERN and RHIC requires a detailed understanding of the properties of hot QCD. It has become clear over the last years that a perturbative approach to thermal QCD is insufficient to calculate properties of the QGP because of the occurrence of infrared divergences and gauge dependencies of physical quantities. Even the Hard Thermal Loop resummation is likely to be applicable only for very large temperatures far outside the scope of present and future experiments. Clearly, nonperturbative input, e.g. from lattice simulations of QCD is needed to improve the situation.

Lattice results indicate that the equation of state (EOS) of a QGP can be fit with a relatively simple quasiparticle model, where quarks and gluons acquire thermal masses. For these quasiparticle masses, the ansatz $m_{th} \sim g(T)T$ is used, where the coupling $g(T)$ is fit to the lattice data. One finds effective quark masses of $\sim$ 300 MeV.

Figure 1: Different quasiparticle scenarios [2] in comparison to the CERES Pb-Au data

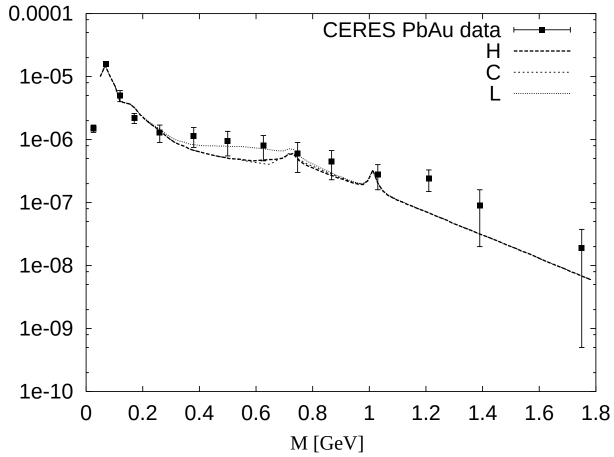

We employ this model for the calculation of the dilepton production in a fireball produced by a heavy ion collision and compare to data taken by the CERES collaboration at the SPS. The relevant degrees of freedom in the model above the phase transition temperature T_C are now quarks and antiquarks as thermal quasiparticles which couple to the photon with the standard quark charge, whereas all QCD corrections are already incorporated in the quasiparticle masses. Several scenarios are discussed for the quasiparticle masses close to T_C. In some models, these thermal masses appear to become heavy near T_C. On the other hand, chiral restoration at T_C would imply that the quark masses drop close to the transition. We therefore investigate three cases as to their influence on the spectra of the produced dileptons: a 'heavy' mass scenario (H), a 'light' one (L) which simulates the dropping of effective quark masses near T_C and a 'constant' one (C) in which the quasiparticle mass is kept at $\sim$ 300 MeV at all temperatures.

Figure 2: Time evolution of the dilepton production yield under CERES conditions in the 'light' quasiparticle scenario, as function of the e^+e^- invariant mass M.

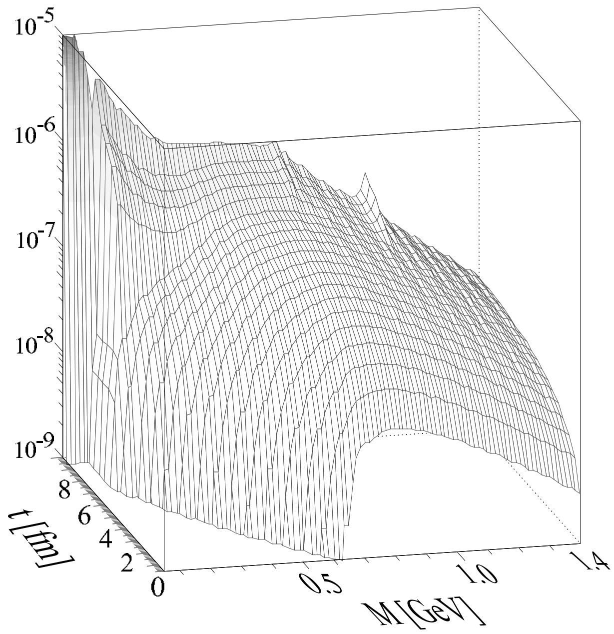

We use a model specified in [1] for the expansion of the fireball. For the hadronic phase below T_C, we use an improved Vector Meson Dominance model with ρ, ϕ and ω as the dominant degrees of freedom, combined with pionic excitations carrying the same quantum numbers. We assume factorization of finite baryon density effects and thermal effects and calculate the spectral function using perturbative methods.

The result describes the CERES data nicely (Fig. 1). The simple model for the fireball allows detailed insight into the expansion including its time evolution, this is shown for the 'light' scenario in Fig. 2. The low-mass region between 0.3 - 0.7 GeV is quite insensitive to the detailed parametrization of the thermal quark masses.

In conclusion, we have shown that a quasiparticle model of the QGP phase and, at $T < T_C$, a hadronic theory with finite density and temperature effects lead to a successful description of the CERES data, whereas a purely hadronic description fails in the low invariant mass region as well as in the high mass region.

References

[1] R.A. Schneider, and W. Weise, Eur. Phys. J. **A9** (2000) 357

[2] R.A. Schneider, T. Renk and W. Weise; in preparation

Work supported in part by BMBF and GSI.

The color dipole approach to the Drell-Yan process

B.Z. Kopeliovich[1], J. Raufeisen[2], A.V. Tarasov[1,3]
[1]MPI K Heidelberg, [2]LANL, [3]University of Heidelberg

The high center of mass energies at RHIC and LHC will allow one to study the Drell-Yan(DY) process in a kinematical region, where the dilepton mass M is much smaller than the center of mass energy $\sqrt{s}$. This region is the DY analog to small Bjorken-x_{Bj} DIS. In addition, coherence effects due to multiple scattering in proton-nucleus (pA) collisions can also be studied.

We developed an approach [1, 2], in which the DY cross section is expressed in terms of the same color dipole cross section as DIS. Our approach is formulated in the rest frame of the target, where DY dilepton production looks like bremsstrahlung of massive photons, rather than parton annihilation, fig. 1. The projectile quark is decomposed into a series of Fock states,

$$|q\rangle = \sqrt{Z_2}|q_{bare}\rangle + \Psi_{\gamma^* q}|\gamma^* q\rangle + \dots . \tag{1}$$

The cross section for production of a virtual photon in quark-proton scattering reads then [1, 3]

$$\frac{d\sigma(qp \to \gamma^* X)}{d\ln\alpha} = \int d^2\rho\, |\Psi_{\gamma^* q}(\alpha,\rho)|^2 \sigma_{q\bar{q}}(\alpha\rho). \tag{2}$$

Here, $\sigma_{q\bar{q}}$ is the cross section for scattering a $q\bar{q}$-dipole off a proton which depends on the $q\bar{q}$ separation $\alpha\rho$. The photon-quark transverse separation is denoted by ρ and α is the fraction of the light-cone momentum of the initial quark taken away by the photon.

This approach is especially suitable to describe nuclear effects, since it allows one to apply Glauber multiple scattering theory. At very high energy, the transverse separation between γ^* and q in the $|\gamma^* q\rangle$ state is frozen during propagation through the nucleus, due to Lorentz time dilatation. Therefore, partonic configurations with fixed separations in impact parameter space are eigenstates of the interaction and one can generalize (2) to nuclear targets by replacing $\sigma_{q\bar{q}}(\alpha\rho)$ with

$$\sigma^A_{q\bar{q}}(\alpha\rho) = 2\int d^2b \left\{1 - \exp\left(-\frac{\sigma_{q\bar{q}}(\alpha\rho)}{2}T(b)\right)\right\}. \tag{3}$$

Here $T(b)$ is the nuclear thickness at impact parameter b.

The frozen approximation (3) is however not well justified at presently achievable fixed target energies, where the size of the $|\gamma^* q\rangle$-state may fluctuate on length scales of the order of the nuclear radius. In pA scattering, this leads to transitions between states which are eigenstates in proton-proton (pp) scattering. We go beyond the frozen approximation by summing over all possible trajectories of the quark in the $|\gamma^* q\rangle$-state. This summation can be formulated in terms of the Green function for a two dimensional Schrödinger equation with an imaginary potential proportional to $\sigma_{q\bar{q}}(\alpha\rho)$ [3, 4]. In the limit of very high energy of the projectile quark, one recovers the frozen approximation (3). The formulae are however too complicated to be displayed here.

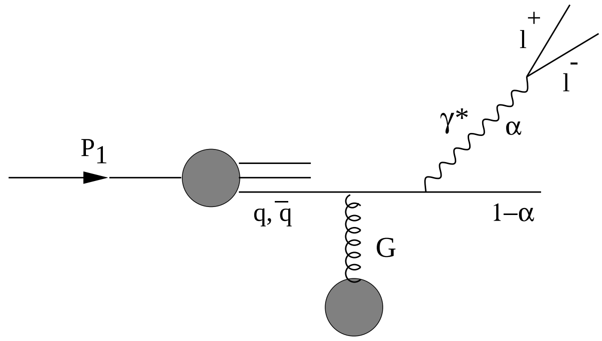

Figure 1: In the target rest frame, DY dilepton production looks like bremsstrahlung. A quark or an antiquark inside the projectile hadron scatters off the target color field and radiates a massive photon, which subsequently decays into the lepton pair. The photon can also be radiated before the quark hits the target.

Before calculating nuclear effects, we checked that the dipole approach is in agreement with DY data from pp collisions. We are able to reproduce E772 data well, without K factor [5]. The transverse momentum distribution of DY pairs in pp collisions is also calculated. The result does not diverge at zero transverse momentum due to the saturation of the dipole cross section at large separations. Note that first order pQCD leads to a divergent result.

The shadowing for DY in pA collisions at large Feynman-x_F measured at FNAL is then also well reproduced [4]. Nuclear effects on the transverse momentum distribution of the pairs are studied, too. While shadowing is predicted for dileptons with low transverse momenta, an enhancement at intermediate transverse momentum $q_\perp \sim 2$ GeV is expected. Nuclear effects vanish at very large $q_\perp$ For pA collisions at RHIC energies, considerable shadowing of DY dileptons is predicted for the whole x_F-range.

References

[1] B.Z. Kopeliovich, proc. of the workshop Hirschegg '95: Dynamical Properties of Hadrons in Nuclear Matter, Hirschegg January 16-21, 1995, ed. by H. Feldmeyer und W. Nörenberg, Darmstadt, 1995, p. 102 (hep-ph/9609385).

[2] S. J. Brodsky, A. Hebecker, and E. Quack, Phys. Rev. **D55** (1997) 2584.

[3] B.Z. Kopeliovich, A. Schäfer and A.V. Tarasov, Phys. Rev. **C59** (1999) 1609, extended version in hep-ph/9808378.

[4] J. Raufeisen, Ph.D. thesis, hep-ph/0009358.

[5] B.Z. Kopeliovich, J. Raufeisen and A.V. Tarasov, hep-ph/0012035, submitted to Phys. Lett. B.

Particle ratios in Pb+Pb at SPS in a chiral $SU(3) \times SU(3)$ model^{B,G}

D. Zschiesche[a], C. Beckmann[a], K. Balazs[a], S. Schramm[a], J. Schaffner-Bielich[b]
H. Stöcker[a], W. Greiner[a]
[a] *Institut für Theoretische Physik J.W. Goethe Universität, D-60054 Frankfurt am Main*
[b] *Riken BNL Research Center, Brookhaven National Lab, Upton, New York 11973*

Ideal gas model calculations have been used for a long time to calculate particle production in relativistic heavy ion collisions, (see e.g. [1, 2] and references therein). Fitting the particle ratios as obtained from those noninteracting gas calculations to the experimental measured ratios at SIS, AGS and SPS for different energies and different colliding systems yields a curve of chemical freeze-out in the $T - \mu$ plane. Now the question arises, how much the deduced temperatures and chemical potentials depend on the model employed. Especially the influence of changing hadron masses and effective potentials should be investigated, as has been done for example in [3, 4, 5, 6]. This is of special importance for the quest of a signal of the formation of a deconfined phase, i.e. the quark-gluon plasma. As deduced from lattice data [7], the critical temperature for the onset of a deconfined phase coincides with that of a chirally restored phase. Chiral effective models of QCD therefore can be utilized to give important insights on signals from a quark-gluon plasma formed in heavy-ion collisions.

We compare experimental measurements for Pb+Pb collisions at SPS with the results obtained from a chiral $SU(3) \times SU(3)$ model [6, 8]. This effective hadronic model predicts a chiral phase transition at $T \approx 150\,\text{MeV}$. Furthermore the model predicts changing hadronic masses and effective chemical potentials, due to strong scalar and vector fields in hot and dense hadronic matter, which are constrained by chiral symmetry.
In [2] the noninteracting gas model was fitted to particle ratios measured in Pb+Pb collisions at SPS. The lowest χ^2 is obtained for $T = 168\,\text{MeV}$ and $\mu_q = 88.67\,\text{MeV}$. Using these values as input for the chiral model leads to dramatic changes due to the changing hadronic masses in hot and dense matter [6] and therefore the freeze-out temperature and chemical potential have to be readjusted to account for the in-medium effects of the hadrons in the chiral model. We call the best fit the parameter set that gives a minimum in the value of χ^2, with $\chi^2 = \sum_i \frac{(r_i^{exp} - r_i^{model})^2}{\sigma_i^2}$. Here r_i^{exp} is the experimental ratio, r_i^{model} is the ratio calculated in the model and σ_i represents the error in the experimental data points as quoted in [2]. In all calculations μ_s was chosen such that the overall net strangeness f_s is zero. The best values for the parameters are $T = 144\,\text{MeV}$ and $\mu_q \approx 95\,\text{MeV}$. While the value of the chemical potential does not change much compared to the noninteracting gas calculation, the value of the temperature is lowered by more than 20 MeV. Using the best fit parameters a reasonable description of the particle ratios used in the fit procedure can be obtained (see fig.1, data from [2]).

This shows, that in spite of the strong assumption of

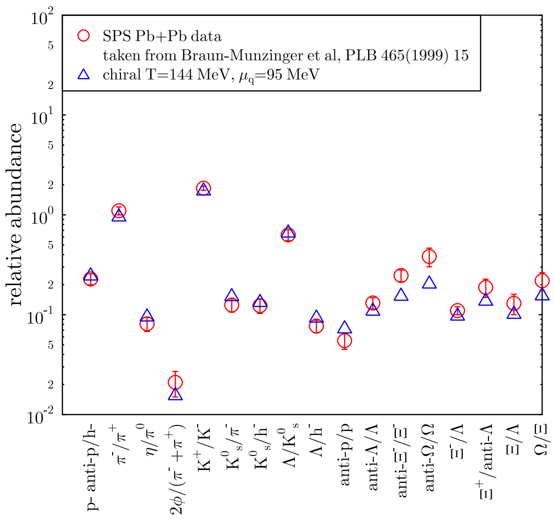

Figure 1: Particle ratios as predicted by the chiral $SU(3) \times SU(3)$ model ($T = 144\,\text{MeV}$ and $\mu_q \approx 95\,\text{MeV}, \mathrm{f_s} = 0$) compared to SPS Pb+Pb data (taken from [2]).

thermal and chemical equilibrium the obtained values for T and μ differ significantly depending on the underlying model, i.e. whether and how effective masses and effective chemical potentials are accounted for. Note that we assume implicitly, that the particle ratios are determined by the medium effects and freeze out during the late stage expansion - no flavor changing collisions occur anymore, but the hadrons can take the necessary energy to get onto their mass shall by drawing energy from the fields. Rescattering effects will alter our conclusion but are presumably small when the chemical potentials are frozen.

References

[1] D. Hahn and H. Stöcker, Nucl. Phys. **A452**, 723 (1986).

[2] P. Braun-Munzinger, J. Heppe, and J. Stachel, Phys. Lett. B **465**, 15 (1999).

[3] H. Stöcker, W. Greiner, and W. Scheid, Z. Phys. A **286**, 121 (1978).

[4] J. Theis *et al.*, Phys. Rev. D **28**, 2286 (1983).

[5] J. Schaffner, I. N. Mishustin, L. M. Satarov, H. Stöcker, and W. Greiner, Z. Phys. **A341**, 47 (1991).

[6] D. Zschiesche *et al.*, Springer Tracts in Modern Physics **163**, 129 (2000).

[7] F. Karsch, hep-lat/9903031 (1998).

[8] P. Papazoglou *et al.*, Phys. Rev. C **59**, 411 (1999).

Effects of coherence in nuclear and hadronic collisions

J.Hüfner[1,2], B.Z. Kopeliovich[2,3], J. Raufeisen[4], A.V. Tarasov[2,3]
[1]University of Heidelberg, [2]MPI-K Heidelberg, [3]University of Regensburg, [4]LANL

The light-cone QCD approach incorporating the effects of the nonperturbative interaction between produced quarks and gluons suggested in [1] is applied in [2] to calculation of nuclear shadowing for longitudinal and transverse photons. This work was motivated by the results of the HERMES experiment observed unusual shadowing at small Q^2 where perturbative methods cannot be used. Although an exciting effect of strong dependence of the coherence length on the photon polarization was discovered in [2], data of HERMES remain unexplained.

The strong nonperturbative interaction of radiated gluons leads not only to a substantially weaker shadowing in heavy ion collisions, but also for the first time explains the observed smallness of large mass diffraction and allows to explain in a parameter free way the energy dependence of elastic scattering of hadrons [3, 4] in a good agreement with data.

The phenomena related to propagation of fast partons through medium are important for prediction of the initial condition in heavy ion collisions and also for the so called jet quenching probe for the produced matter. Broadening of the transverse momentum of a quark propagating through nuclear medium is calculated in [5]. It is found to be a color filtering effect and expressed in terms of the universal color dipole cross section which is fitted to data for the proton structure function. The calculated broadening of p_T for a quark propagating through a nucleus is somewhat larger than what was measured in Drell-Yan reaction on nuclei.

Energy loss of a quark propagating through nuclear matter can be also measured in Drell-Yan reaction. The main problem is to discriminate between this effect and nuclear shadowing. This is done in [6] employing our experience in parameter free calculation of shadowing. The analysis of data for Drell-Yan reaction from the E772 and E866 experiments at Fermilab resulted in a rather large rate of energy loss $dE/dz \approx -2\,GeV/fm$. This is the first observation of a nonzero energy loss effect.

It is usually believed that energy loss leads to baryon stopping in heavy ion collisions. A different point of view is presented in [7] where it is shown that the dominant mechanism of stopping is baryon number transfer by gluons. Nearly the same stopping is expected at RHIC as at SPS, as is confirmed by the preliminary data from RHIC.

Charmonium suppression is considered as one of the main probes for creation of a hot deconfined matter in relativistic heavy ion collisions. The conventional base line for search of new physics relates charmonium suppression to simple absorption in cold nuclear matter. First of all, one needs to know the charmonium-nucleon cross section. It is predicted in [8] quite reliably employing the light-cone dipole formalism with the realistic charmonium wave functions and phenomenological dipole cross section fitted to DIS data. This method is tested comparing to data on charmonium photoproduction. The important effect missed in previous calculations is the relativistic spin rotation which increases the production rate of Ψ' by factor of 2-3. The cross sections are predicted for J/Ψ, Ψ' and χ, and with a proper mixture of these states the effective absorption cross section in cold nuclear matter is found.

In heavy ion collisions all nucleons which the produced charmonium interacts with, have already had a chance to interact with other nucleons and are in color-excited states. It is found in [9] that the colored 3-quark system interacts up to about 60% stronger than colorless one. Although this effect is not sufficiently strong to explain the observed anomalous E_T dependence of J/Ψ absorption, it must be included together with other missed effects in the interpretation of the experimental results. In particular, fluctuations of transverse energy should be taken into account, especially for most central collisions. It is demonstrated in [10] that they strongly correlate with fluctuation of charmonium suppression by interaction with the produced medium.

Coherent effects in elastic proton-nucleus scattering are proved to keep unchanged compared to pp scattering the ratio of spin-flip to non-flip amplitudes. This allows to use coulomb-nuclear interference in polarimetry as a basis for polarimetry. This method suggested in [11, 12] is accepted for polarimetery at RHIC.

References

[1] B.Z. Kopeliovich, A. Schaefer, A.V. Tarasov, Phys. Rev. D62 (2000) 054022

[2] B.Z. Kopeliovich, J. Raufeisen, A.V. Tarasov, Phys. Rev. C62 (2000) 035204

[3] B.Z. Kopeliovich, I.K. Potashnikova, B. Povh, E. Predazzi, Phys. Rev. Lett. 85 (2000) 507

[4] B.Z. Kopeliovich, I.K. Potashnikova, B. Povh, E. Predazzi, Phys. Rev. D63 (2001) 054001

[5] M.B. Johnson, B.Z. Kopeliovich, A.V. Tarasov, Phys. Rev. C63 (2001) 035203

[6] M.B. Johnson, B.Z. Kopeliovich, I.K. Potashnikova and the E772 Collaboration, hep-ex/0010051, submitted to Phys. Rev. Lett.

[7] G.T. Garvey, B.Z. Kopeliovich, B. Povh, hep-ph/0006325, accepted in Comments Nucl. Part. Phys.

[8] J. Hüfner, Yu.P. Ivanov, B.Z. Kopeliovich, A.V. Tarasov, Phys. Rev. D62 (2000) 094022

[9] J. Hüfner, B.Z. Kopeliovich, A. Polleri, hep-ph/0010282, accepted in Eur. Phys. J. A.

[10] J. Hüfner, B.Z. Kopeliovich, A. Polleri, nucl-th/0012003, submitted to Phys. Lett.

[11] B.Z. Kopeliovich, T.L. Trueman, hep-ph/0012091, submitted to Phys. Rev. D

[12] B.Z. Kopeliovich, A.V. Tarasov, Phys. Lett. B497 (2001) 44

Production of hard partons from soft gluonic fields^{B+G}

Dennis D. Dietrich, Gouranga C. Nayak, Walter Greiner, Johann Wolfgang Goethe Universität

We study parton-pair production from a space-time dependent chromofield via vacuum polarization by using the background field method of QCD. The processes we consider are both leading and higher order in gA but first order in the action. We derive general expressions for the corresponding probabilities. Parton production from a space-time dependent chromofield will play a crucial role in the production and equilibration of the quark-gluon plasma in ultra relativistic heavy-ion collisions at RHIC and LHC. In ultra relativistic heavy-ion collisions, when two highly Lorentz contracted nuclei pass through each other a chromofield is formed between them due to the exchange of soft gluons [1]. The chromofield so formed polarizes the QCD vacuum and produces $q\bar{q}$-pairs and gluons via a Schwinger-like mechanism [2]. As seen in numerical studies [3], the chromofield acquires a strong space-time dependence due to a combination of such effects as expansion, background acceleration, color rotation, collision and parton production. In situations like this, the parton production from a constant chromofield is not justified and one has to find the corresponding expression for a general space-time dependent chromofield.

The e^+e^- pair production from a weak space-time dependent classical field is studied by Schwinger [2]. Because of the same structure of the interaction lagrangian density the production of a $q\bar{q}$ pair is similar to the e^+e^- case except for color factors [5]. (*N.B.*: Only the real parts of the following expressions are to be taken.) Details are given in [6]:

$$\frac{dW_{q\bar{q}}}{d^4xd^3k} = \frac{g^2m}{(2\pi)^5k^0}\ A^a_\mu(x)\ e^{ik\cdot x}\int d^4x_2\ A^a_\nu(x_2)\ e^{-ik\cdot x_2}$$
$$(i[k^\mu(x-x_2)^\nu + (x-x_2)^\mu k^\nu + k\cdot(x-x_2)g^{\mu\nu}]$$
$$(\frac{K_0(m\sqrt{-(x-x_2)^2})m\sqrt{-(x-x_2)^2} + 2K_1(m\sqrt{-(x-x_2)^2})}{[\sqrt{-(x-x_2)^2}]^3})$$
$$-m^2g^{\mu\nu}\frac{K_1(m\sqrt{-(x-x_2)^2})}{\sqrt{-(x-x_2)^2}}).$$

The computation of the probability for the production of gluons is not straight forward and there is no counter part to this in QED. The processes which in leading order of the action contribute to gluon pair production are evaluated following the background field method of QCD [7] which, in a gauge invariant manner incorporates a classical background field and a quantum gluonic field simultanously. The probability is obtained by spin-summing the phase-space integral over the absolute square of the amplitudes. The Feynman rules for the production of two gluons by coupling to the A-field once or twice can be read from the Lagrangian density and are given in [8, 6]. To obtain the correct physical gluon polarizations in the final state we put the sums over the polarizations of the outgoing gluons equal to the negative of the metric tensor and afterwards deduct the corresponding ghost contributions. The vertices involving two ghosts and one classical field and two ghosts and two classical fields respectively can again be read from the lagrangian density and are also found in [8, 6]. We obtain the probability per unit time and unit volume of the phase space for the production of a real gg pair from a space-time dependent classical chromofield A [6]:

$$\frac{dW_{gg}}{d^4xd^3k} = \frac{1}{(2\pi)^5k^0}\int d^4x' e^{ik\cdot(x-x')}\frac{1}{(x-x')^2}$$
$$\{\frac{3}{4}g^2A^{a\mu}(x)A^{a\mu'}(x')[3k_\mu k_{\mu'} - 8g_{\mu\mu'}k^\nu i\frac{(x-x')_\nu}{(x-x')^2} + 6\frac{g_{\mu\mu'}}{(x-x')^2}$$
$$+5(k_\mu i\frac{(x-x')_{\mu'}}{(x-x')^2} + k_{\mu'}i\frac{(x-x')_\mu}{(x-x')^2}) - 12\frac{(x-x')_\mu(x-x')_{\mu'}}{(x-x')^4}]$$
$$-3ig^3A^{a\mu}(x')A^{c\lambda}(x')A^{a'\mu'}(x)f^{a'ac}K_\lambda g_{\mu\mu'}$$
$$-\frac{1}{16}g^4A^{a\mu}(x)A^{c\lambda}(x)A^{a'\mu'}(x')A^{c'\lambda'}(x')[24g_{\mu\mu'}g_{\lambda\lambda'}f^{acx}f^{a'c'x}$$
$$+g_{\mu\lambda}g_{\mu'\lambda'}(f^{abx}f^{xcd} + f^{adx}f^{xcb})(f^{a'bx'}f^{x'c'd} + f^{a'dx'}f^{x'c'b})]\}.$$

As a simple example we choose the field to be

$$A^{a3}(t) = A_{in}e^{-|t|/t_0},\ t_0 > 0,\ a = 1,...,8.$$

The exponential decay of the source terms originates from the decay of the model-field. Their oscillatory behavior is due to the exponential factor,already present in the general formula.

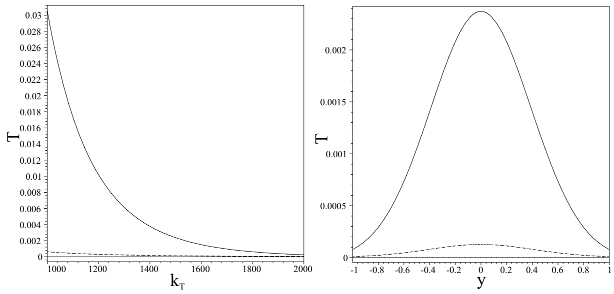

Fig. 1 Dimensionless time-integrated source terms for quarks (dash) and gluons (solid) versus transverse momentum kT in MeV and rapidity y for the parameters $\alpha_S = 0.15$, $A_{in} = 1.5GeV$, $t_0 = 0.5fm$, $k_T = 1.5GeV$, $y = 0$.

The decay behavior with the transverse momentum k_T in MeV is mostly due to the choice of the field. Only in the second contribution to the gluon source term there is already a factor $1/(k^0)^2$ present in the general formula. As the momentum structure of the general equations is mostly based on the k^0-component, the origin for the typical rapidity y behavior is mainly linked to the behavior for changing transverse momentum. For this model field, a stronger coupling, a stronger chromofield and/or a slowlier varying field emphasize dominance of the gluon-pair production over the production of $q\bar{q}$ pairs even more.

References

[1] F. E. Low, Phys. Rev. **D12** (1975) 163; S. Nussinov, Phys. Rev. Lett. **34** (1975) 1286; K. Kajantie and T. Matsui, Phys. Lett. **B164** (1985) 373; A. Karman, T. Matsui and B. Svetitsky, Phys. Rev. Lett. **56**, 219 (1986): G. Gatoff, A. K. Kerman and T. Matsui, Phys. Rev. **D36** (1987) 114; A. Bialas, W. Czyz, A. Dyrek and W. Florkowski, Nucl. Phys. **B296** (1988) 611; B. Banerjee, R. S. Bhalerao and V. Ravishankar, Phys. Lett. **B224** (1989) 16; M. Asakawa and T. Matsui, Phys. Rev. **D43** (1991) 2871; K. J. Eskola and M. Gyulassy, Phys. Rev. **C47** (1993) 2329; J. M. Eisenberg, Found. Phys. **27** (1997) 1213.

[2] J. Schwinger, Phys. Rev. **82**, 664 (1951).

[3] G. C. Nayak and V. Ravishankar, Phys. Rev. **D55** (1997) 6877; Phys. Rev. **C58** (1998) 356; R. S. Bhalerao and G. C. Nayak, Phys. Rev. **C61**, 054907 (2000)

[4] C. Itzykson and J. Zuber, *Quantum Field Theory* (McGraw-Hill Inc., 1980), R. S. Bhalerao and V. Ravishankar, Phys. Lett. **B409**, 38 (1997).

[5] G. C. Nayak and W. Greiner, *hep-th*/0001009

[6] D. D. Dietrich, G. C. Nayak and W. Greiner, hep-ph/0009178; hep-th/0007139.

[7] B. S. DeWitt, Phys. Rev. **162**, 1195 and 1239 (1967); *in* Dynamic theory of groups and fields (Gordon and Breach, 1965); G. 't Hooft, Nucl. Phys. **B62**, 444 (1973).

[8] L. F. Abbott, Nucl. Phys. **B185**, 189 (1981).

Nonequilibrium quark dynamics in ultrarelativistic heavy ion collisions^{B,G}

S. Scherer[1], M. Hofmann[1], M. Bleicher[2], L. Neise[1], H. Stöcker[1], W. Greiner[1]
[1] Institut für Theoretische Physik, J. W. Goethe-Universität Frankfurt am Main, Germany,
[2] Nuclear Science Division, Lawrence Berkeley Laboratory, Berkeley, U.S.A.

Heavy ion collisions at the CERN-SPS are supposed to reach the transition form hadronic matter to the quark-gluon plasma. The analysis of collective observables such as flow allows to speculate that this transition may show up even down to AGS energies. The description of such a collision by microscopic models thus must treat properly the degrees of freedom emerging from soft QCD.

Such a model can be realized by treating quarks as classical particles interacting according to a two-body color potential [1]. The Hamiltonian of this quark molecular dynamics (qMD) reads

$$\mathcal{H} = \sum_{i=1}^{N} \sqrt{\mathbf{p}_i^2 + m_i^2} - \frac{1}{2}\sum_{i,j} C_{ij}^{\mathrm{c}} \left(\frac{3}{4}\frac{\alpha_s}{|\mathbf{r}_i - \mathbf{r}_j|} + \kappa\, |\mathbf{r}_i - \mathbf{r}_j| \right)$$

where the well known Cornell-potential is used to describe the quark interaction. Sign and relative strength of the interaction are described by the color factor C_{ij}^{c}, depending on the color combination of each pair. Confining properties are ensured by the linear increase of $V(r)$ at large distances. The time evolution of such a system yields colorless quark clusters which are mapped to hadrons.

When coupled to a hadronic transport model such as UrQMD[2] to create the initial quark distribution, the qMD can provide us with detailed information about the dynamics of the quark system and the parton-hadron conversion. Correlations between the quarks clustering to build new hadrons can be studied [3].

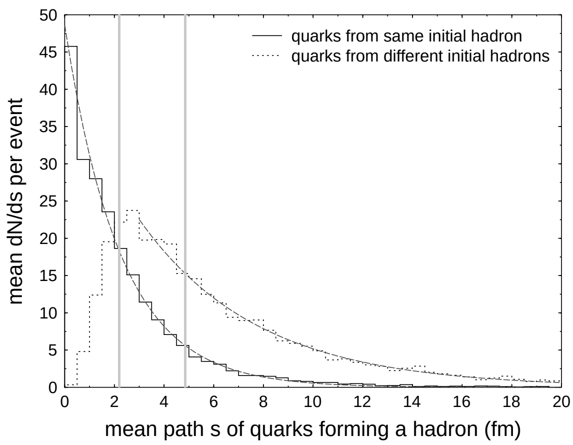

Figure 1: Hadronization in S+Au collisions at 200 GeV/N: Mean diffusion path of quarks forming a hadron from the same initial hadron (solid line) and from different initial hadrons (dashed line) within qMD. Fitting the decay profiles yields diffusion lengths of 2.2 fm and 4.8 fm.

Hadrons of the colliding nuclei are propagated in UrQMD, producing new hadrons in inelastic collisions and preformed hadrons in string excitations. Once complete overlap of the impinging nuclei is reached, all hadrons with at least one collision or within their formation time are broken up in their (valence) quark content. These quarks are then propagated in qMD, finally hadronizing again.

Figure 1 shows (for S+Au collisions at SPS energies of 200 GeV/N) the distribution for the mean path travelled by quarks forming a hadron (a) from the same initial hadron (solid line) and (b) from different initial hadrons (dotted line).

A measure of the relative mixing within the quark system and thus for thermalization is the relative number of hadrons formed by quarks from the same initial hadron versus hadrons formed by quarks from different initial hadrons. This ratio is $r = 0.574 \pm 0.008$ for the S+Au collision (spectators are not included). Since a value of $r = 1$ indicates complete rearrangement of quarks and thus complete loss of correlations in the quark system, one would expect a much larger value of r, considering the presumed transition to the quark-gluon plasma in Pb+Pb collisions at 160 GeV/N,

First results for the excitation function of this ratio in Pb+Pb collisions, however, shows a different picture (Figure 2): a nearly constant value of about 0.3 is obtained for energies in the range from 20 to 160 GeV/N, nearly independent of the impact parameter. This surprising behavior needs clarification by further investigations.

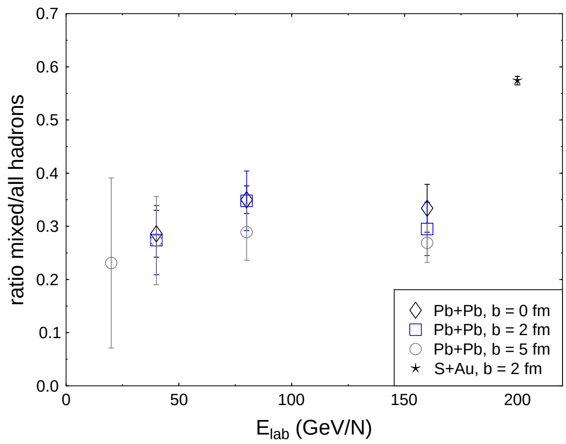

Figure 2: Excitation function of ratio of mixed to total hadrons for Pb+Pb collisions. The value for S+Au collision at 200 GeV/N is also shown.

References

[1] M. Hofmann et al., Phys. Lett. **B478** (200) 161 (nucl-th/9908030); nucl-th/9908031.

[2] S. A. Bass et al., Phys. Rev. C **60** (1999) 021902 [nucl-th/9902062].

[3] S. Scherer et al., N. Journ. Phys. *to be publ.*

Deconfinement, Color Screening and Quarkonium Suppression

S. Digal, M. Nardi, P. Petreczky and H. Satz, Universität Bielefeld

The study of color deconfinement in strongly interacting matter leads to challenging problems of theoretical as well as of more phenomenological nature. How does the transition from hadronic matter to a quark-gluon plasma take place - is it a genuine phase transition or some less 'singular' cross-over, and what are the basic properties of the new deconfined medium? In the chiral limit ($m_q = 0$) and in the limit of pure gauge theory ($m_q = \infty$) we do have critical behavior in the classical sense, with well-defined order parameters and singularities in the partition function and hence in thermodynamic observables. Is there some way to really 'define' the transition in full QCD with light but not massless quarks? On the other hand, the aim of high energy nuclear collisions is to investigate the transition and the predicted new deconfined state of matter in the laboratory. What probes exist for these tasks? Is there an experimentally accessible deconfinement order parameter, and how can the temperature dependence of the hot deconfined medium be tested?

The role of the effective quark mass in QCD is similar to that of an ordering external field H in spin theories [1]. For $H = 0$, spin systems show at $T = T_c$ the familiar order-disorder transition, which disappears for $H \neq 0$. The critical behavior at $T = T_c$ can be described either in terms of singularities of thermal observables, or equivalently, as singular behavior of suitably defined geometric cluster variables. Such singular cluster percolation features persist, however, even for $H \neq 0$. It is thus of particular interest to see if the deconfinement transition can in some way be associated to the onset of percolation of clusters of deconfined medium. The answer to this question requires a systematic study of percolation in QCD. First steps had indicated that in the strong coupling limit Polyakov loop percolation indeed led to the correct deconfinement transition in pure Gauge theory [2]. In recent work it was shown that this conclusion can in fact be extended to $SU(2)$ gauge theory in general [3]. Studies of full QCD with dynamical quarks are under way. They could eventually check if the cross-over line between confined and deconfined matter in the $m_q - T$ plane coincides with the line of singular behavior defined through cluster percolation [1].

The behavior of a deconfined medium can be tested by studying the dissociation of quarkonium states through color screening [4]. A prerequisite for this is an understanding of the heavy quark potential in a hot medium, which can in principle be obtained through finite temperature lattice studies. Such studies, however, require extensive computational efforts which have become possible only recently; hence the past year has led to pioneering work in this field [5, 6]. The results of this work will certainly have an impact on the application of quarkonium dissociation as deconfinement probe in nuclear collisions.

The results of experimental studies of J/ψ production in nuclear collisions at the CERN-SPS have made this a particularly interesting as well as challenging probe [7]. While peripheral $Pb-Pb$ collisions lead only to the pre-resonance absorption, already seen in pA and light ion interactions, there appears at a certain centrality a rather sudden onset of an additional 'anomalous' suppression, and for very central collisions a second further drop of the production rate occurs (see Fig. 1). Such a pattern is in fact expected from sequential charmonium suppression, leading first to the dissociation of the χ_c state and of its J/ψ decay products, then to the dissociation of the directly produced J/ψ [8]. More detailed recent investigations have led to a behavior which is qualitatively in accord with data [9, 10]; in particular, however, the central second drop appears to be much stronger than predicted by an onset of direct J/ψ suppression. The possible effects of fluctuations must therefore be taken into account in more detail [9, 11]. Such work is under way.

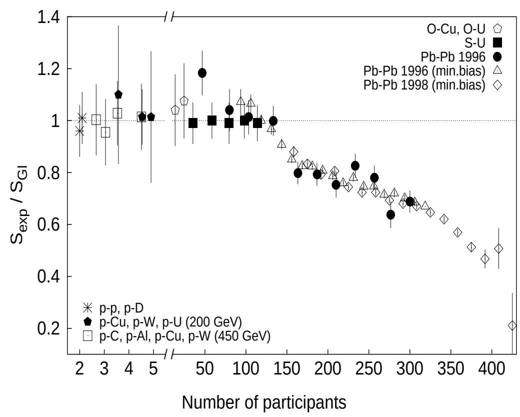

Figure 1: J/ψ production in different interactions

References

[1] H. Satz, Nucl. Phys. A642 (1998) 130.
[2] H. Satz and S. Fortunato, Phys. Lett. B475 (2000) 311.
[3] S. Fortunato, F. Karsch, P. Petreczky, H. Satz, hep-lat/0011084, to appear in Nucl. Phys. B.
[4] T. Matsui and H. Satz, Phys. Lett. 178 B (1986) 416.
[5] A. Cucchieri, F. Karsch and P. Petreczky, Phys. Lett. B497 (2001) 80.
[6] F. Karsch, E. Laermann and A. Peikert, hep-lat/0012023.
[7] see M. Abreu et al. (NA50), Nucl. Phys. A663 (2000) 721.
[8] S. Gupta and H. Satz, Phys. Lett. B383 (1992) 439.
[9] H. Satz, Nucl. Phys. A 661 (1999) 104c.
[10] M. Nardi and H. Satz, Phys. Lett. B442 (1998) 14.
[11] J.-P. Blaizot M. Dinh and J.-Y. Ollitrault, Phys. Rev. Lett. 85 (2000) 4012.

Quarkonium at Collider Energies^{B+G}

L. Gerland, H. Stöcker, W. Greiner
J.W.G. Universität, D-60054 Frankfurt a. M., Germany

There are different time scales relevant for the production of quarkonium states:
1) the time needed to produce a heavy quark pair in a hard collision,
2) the time needed for a $Q\bar{Q}$ pair to form a bound state.

The production time of a $Q\bar{Q}$ pair in its rest frame is given by $\tau_p = \frac{1}{m_Q}$. This is 0.13 fm/c for $c\bar{c}$ and 0.05 fm/c for $b\bar{b}$. The Lorentz factor of the pair at midrapidity in the rest frame of the target is $\gamma \approx 10$, 100 and 3000 for a Quarkonium state at SPS, RHIC and LHC energies. At SPS fixed target energies $\gamma c \tau_p$ is smaller than the average internucleon distance in nuclei $r_{NN} \approx 1.8$ fm. Thus, the production of heavy quark pairs is incoherent. At RHIC the production distance of $c\bar{c}$ pairs is already as large as the diameter of a gold nucleus, and for $b\bar{b}$ pairs $c\tau_p > 1.8$ fm, but this is still small as compared to the nuclear radius. At LHC both production distances exceed the diameter of a lead nucleus by an order of magnitude. The hadronisation time t_H resp. the coherence length l_c of heavy Quarkonium is $l_c = c \cdot t_H = \frac{1}{\Delta E} \approx \frac{\gamma}{\Delta M}$ with:
$\Delta E = \sqrt{p^2 + (M_{Q\bar{Q}} + \Delta M)^2} - \sqrt{p^2 + M_{Q\bar{Q}}^2} \approx \frac{(M_{Q\bar{Q}}+\Delta M)^2 - M_{Q\bar{Q}}^2}{2p} \approx \frac{M_{Q\bar{Q}} \Delta M}{p} = \frac{\Delta M}{\gamma}$.
p is the momentum of the Quarkonium in the rest frame of the target, $M_{Q\bar{Q}}$ is the mass of the $Q\bar{Q}$-pair and $\Delta M = \int \psi^2(k) \frac{k^2}{M_Q} \mathrm{d}^3k / \int \psi^2(k) \mathrm{d}^3k$, $\psi(k)$ is the wavefunction of the Quarkonium state in momentum space, we use here the wave functions from the refs. [1, 2]. ΔM is the average kinetic energy of the $Q\bar{Q}$-pair in the bound state and $l_c/\gamma = 0.44(0.34)$ fm for the J/Ψ (Υ).

Thus, for charm and bottom production at RHIC and LHC $l_c > 2 \cdot R_A$ (R_A is the nuclear radius), $l_c < 2 \cdot R_A$ for fixed target SPS energies. The applicability of the approach developed in this paper requires that $l_c > 2 \cdot R_A$ which is fulfilled at RHIC and LHC.

We assume here that $Q\bar{Q}$ pairs are produced in AB collisions predominantly in hard collisions. The basic quantity is the cross section of production of $Q\bar{Q}$ pairs with light cone momenta z_i, k_i, which we parametrize as $\frac{d\sigma(AB \to Q\bar{Q}+X)}{\mathrm{d}^2k_1 \mathrm{d}z_1 \mathrm{d}z_2 \mathrm{d}^2k_2} = D_{AB}(z_1, z_2) \cdot \exp(-B(AB)(k_1^2 + k_2^2))$. Here k_i $\{i = 1, 2\}$ are the transverse momenta of the Q and the $\bar{Q}$ quark and z_i $\{i = 1, 2\}$ are the fractions of their longitudinal momenta. Such a factorization does not contradict the data in pp collisions [3].

To evaluate the suppression of hidden heavy flavour production resulting from the broadening of the transverse momentum distributions of Q quarks due to final state interaction, we deduce first a relationship between the slopes for the various processes of heavy quark production. In the following we use the relative transverse momentum $k_t = \frac{k_1 - k_2}{2}$ and the total transverse momentum $p_t = k_1 + k_2$ of the pair, writing $\frac{d\sigma(AB \to Q\bar{Q}+X)}{\mathrm{d}^2k_t \mathrm{d}^2p_t \mathrm{d}z_1 \mathrm{d}z_2} = D_{AB}(z_1, z_2) \exp\left(-B(AB)\left(-\frac{p_t^2}{2} - 2k_t^2\right)\right)$.

To take into account possible nuclear effects on the longitudinal momentum distribution we make the ansatz $D_{AB}(z_1, z_2) = D(AB) \cdot f_{AB}(p_z) \cdot \exp\left(-\frac{k_z^2}{C_{AB}^2}\right)$, where p_z and k_z are the total and relative longitudinal momentum. We further assume that $f_{AB}(p_z) = f_{pp}(p_z)$, which means that we neglect parton energy losses of the pair, this effect will be discussed later on. The normalization condition follows from the QCD factorization theorem [4] for the total cross section: $\frac{D(AB)}{B(AB)^2 \cdot C_{AB}} = \frac{AB \cdot D(pp)}{B(pp)^2 \cdot C_{pp}}$ The differential cross sections are proportional to the square of the two body wave functions ϕ.

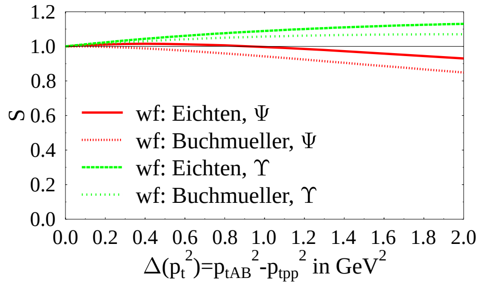

Figure 1: The righthandside of eq.(1) vs. the transverse momentum broadening for the J/Ψ and the Υ is plotted.

The production cross section of bound states of heavy quarks is proportional to the overlap integral of the two-body wave function and the wave function of the bound $\psi(k_t)$ state to get $\frac{\mathrm{d}^3\sigma(AB \to Quarkonium+X)}{\mathrm{d}^2p_t \mathrm{d}p_z} \propto |\langle \psi(k_t, k_z) | \phi_{AB}(k_t, p_t, k_z, p_z) \rangle|^2$. Here we neglected the difference between the current quark mass in the two body wave function and the constituent quark mass in the wave function of the bound state. With this one can evaluate the survival probability:
$S \equiv \frac{\sigma(A+B \to Quarkonium+X)}{AB \cdot \sigma(p+p \to Quarkonium+X)}$. Our final result is then

$$S = \frac{B(AB)C_{AB}}{B(pp)C_{pp}} \left| \frac{\int \mathrm{d}^3k \psi(k) \exp(-B(AB)k_t^2) \exp\left(-\frac{k_z^2}{2C_{AB}^2}\right)}{\int \mathrm{d}^3k \psi(k) \exp(-B(pp)k_t^2) \exp\left(-\frac{k_z^2}{2C_{pp}^2}\right)} \right|^2 \tag{1}$$

up to nuclear effects in the parton distribution functions.

Note that if one defines the survival probability as the ratio of the differential cross section $\frac{\mathrm{d}^2\sigma}{\mathrm{d}^2p_t}$ for nuclear and nucleon targets their p_t dependence would be a factor $\exp\left(-\frac{B(AB)-B(pp)}{2} p_t^2\right)$. That means that the p_t dependence of J/Ψ suppression is due to the broadening of the transverse momentum distribution as a result of the final state interactions of the Q quarks in the nuclear medium.

In fig. 1 the result of eq. (1) is plotted versus the transverse momentum broadening of the J/Ψ's: $\Delta p_t^2 = 2/B(pp) - 2/B(AB)$. E.g. $\Delta p_t^2 = 0.48$ GeV^2 was found at Fermilab energies in pAu. $C_{AB}^2 = C_{pp}^2$ is used as a first approximation. $S \approx 1$ for the J/Ψ. That means there is practically no change due to the broadening of the transverse momentum distribution. The parameters used for the calculation are explained in ref. [5]. As one can see we obtain even a slight enhancement for the Υ meson production. This model neglects a lot of effects that might occur in AB-collisions, but predicts that the J/Ψ is less suppressed in pA collisions at collider energies than at fixed target energies.

References

[1] E. Eichten et al., Phys. Rev. **D21** (1980), 203
[2] W. Buchmüller and S. Tye Phys. Rev. **D24** (1981) 132
[3] M.J. Leitch et al., Phys. Rev. Lett. **72** (1994) 2542
[4] G.T. Bodwin, Phys. Rev. **D31**(1985) 2616
[5] L. Gerland et al., J. Phys. G in Print and eprint nucl-th/0009008

Shadowing Effects on Vector Boson Production*

R. Vogt (LBNL and UC Davis)

The Z^0 was proposed as an alternative reference process for quarkonium suppression at the LHC. There are two difficulties with using the Z^0 as a baseline for quarkonium suppression: the large mass differences, $m_{Z^0} \gg m_\Upsilon, m_{J/\psi}$, and the difference in production mechanisms, predominantly $q\overline{q}$ for the Z^0 and gg for quarkonium. Both these differences are important as far as nuclear effects are concerned. However, the differences that reduce the value of the Z^0 as a baseline process are the same that make it an interesting object of study itself—the Z^0 provides a unique opportunity to study quark shadowing at high Q^2. Therefore, we examine the possible effects of shadowing on Z^0 production as well as W^+ and W^- production which are also quark dominated. The impact parameter dependence of the shadowing effect will also be shown.

The electroweak production and decay channels of the massive vector bosons make them excellent candidates for shadowing studies since no hadronic final-state rescattering is possible. The Z^0 itself, with a 3.37% branching ratio to lepton pairs, will be easily observable by reconstructing the peak. Full reconstruction of the leptonic $W^\pm$ decays, $W^\pm \rightarrow l^\pm \nu$, is not possible due to the missing energy given to the undetected neutrino but charged leptons with momenta greater than 40 GeV should be prominent. This technique has been used at the Tevatron to measure the asymmetry between W^+ and W^- production through their lepton decays since this asymmetry is sensitive to the ratio f_d^p/f_u^p at intermediate values of x and high Q^2. If the charged leptons from $W^\pm$ decays can be identified in heavy ion collisions, such asymmetry measurements may also be employed at the LHC to reduce systematics and obtain a more meaningful determination of the Q^2 dependence of quark shadowing in the nucleus.

The table gives the total cross sections in the CMS and ALICE central acceptances $|y| < 2.4$ and $|y| < 1$ respectively for no shadowing and with three shadowing parameterizations. The cross sections are larger than the virtual photon mediated Drell-Yan cross sections at lower masses. The results, given for Pb+Pb collisions, are integrated over impact parameter in units of nb/nucleon pair.

Detector	σ_1 (nb)	σ_{S_1} (nb)	σ_{S_2} (nb)	σ_{S_3} (nb)
		Z^0		
CMS	15.41	10.87	10.96	14.26
ALICE	6.22	4.35	4.49	5.86
		W^+		
CMS	20.85	14.39	14.54	18.93
ALICE	8.13	5.52	5.73	7.44
		W^-		
CMS	21.84	15.08	15.26	19.83
ALICE	8.35	5.66	5.89	7.64

The figure compares the ratios of Z^0 production in Pb+Pb collisions with three shadowing parameterizations to Pb+Pb collisions with no shadowing as a function of rapidity. The isospin effects wash out the differences between the W^+ and W^- distributions in the ratios so that the results are essentially identical for the two charged vector bosons. Therefore the ratios are shown only for the W^+. The results are shown for several impact parameter bins, the most central bin, $b < 0.2R_A$, an intermediate impact parameter bin around $b \sim R_A$, and a peripheral bin around $b \sim 2R_A$. It is clear that by neglecting the impact parameter dependence of shadowing, one may make an overestimate of the effect in peripheral collisions, an important point if using the Z^0 as a baseline in different transverse energy bins. Note also that the integration over all impact parameters is equivalent to the average shadowing.

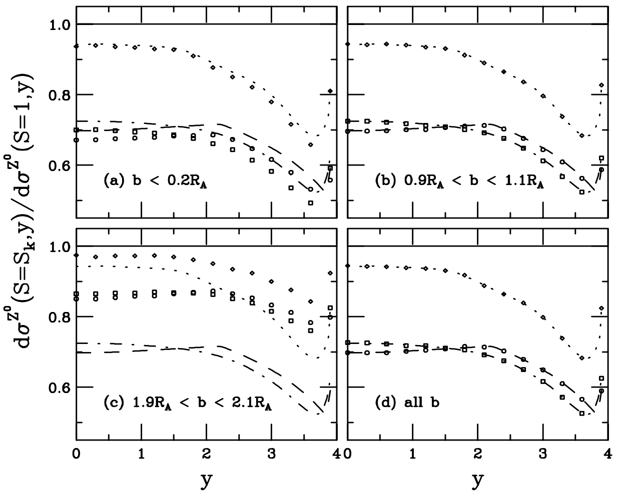

Once the basic nuclear shadowing effects on vector boson production have been understood, they can perhaps be used to study other medium effects in heavy ion collisions by comparing the leptonic and hadronic decay channels. The hadronic decays of the vector bosons, $\sim 70\%$ of all decays of each boson, may be more difficult to interpret. While the width of the Z^0 decay to l^+l^- is not expected to be modified in the quark-gluon plasma, the Z^0 has a 2.49 GeV total width and will decay in any quark-gluon plasma to two jets through $Z^0 \rightarrow q\overline{q} \rightarrow$ jet + jet in ~ 0.1 fm. Therefore, the decay jets could be modified in the medium which may still be progressing toward thermalization and will be subject to rescattering and jet quenching. Thus a comparison of a reconstructed Z^0 in the dilepton channel where no nuclear effects are expected since leptons do not interact strongly and medium-modified jets should result in a broader width for the $q\overline{q}$ channel than the l^+l^- channel. In addition, the Z^0 could be used to tag jets through the $q\overline{q} \rightarrow Z^0 g$ and $gq \rightarrow Z^0 q$ channels to study the jet properties in the quark-gluon plasma.

*Condensed from GSI-Preprint 2000-49, hep-ph/0011242.

Probing chiral dynamics by charged-pion correlations*

Jørgen Randrup (LBNL)

High-energy nuclear collisions are expected to produce transient systems within which chiral symmetry is approximately restored and the matter is partially deconfined. The identification and exploration of such a novel matter phase is a major experimental goal and the efforts have intensified with the recent commisioning of the Relativistic Heavy Ion Collider at BNL.

Through the past decade, it has been speculated that the rapid expansion of the collision zone, after an approximate restoration of chiral symmetry has occurred, may produce long-wavelength isospin-polarized agitations of the pionic field, commonly referred to as disoriented chiral condensates (DCC), which in turn should lead to anomalies in the resulting pion multiplicity distribution. However, the experimental search for the phenomenon has been hampered by the lack of signatures that are practically observable.

The present work identifies a novel observable that may be particularly suitable as an indicator of the DCC phenomenon, namely the approximate back-to-back correlation between oppositely charged soft pions.

The pionic degrees of freedom experience a rapidly changing environment that can be approximately accounted for by an in-medium effective mass depending both on the degree of agitation and on the chiral order parameter. Since the system is steadily cooling down while the order parameter reverts from its initial small value to its large vacuum value in a non-equilibrium fashion, the effective pion mass has then a correspondingly intricate evolution, displaying an overall decay towards the free mass overlaid by the effect of the rather regular oscillations by the relaxing order parameter. This time modulation of the effective mass may lead to parametric amplification those soft pionic modes with an energy near half the σ mass.

The effect is brought out most clearly in the simple case where the environment, and hence the effective mass, is spatially uniform, as is approximately the case in the interior of the collision zone. It is then obvious that although the time dependence of the mass may generate considerable agitation, this agency cannot add any net momentum. Thus the any pions produced by the mechanism must be formed pairwise and moving in opposite directions. Furthermore, by a similar reasoning, the time dependence of the mass does not add any change, so the produced pairs must be oppositely charged. Thus, the particles generated by an arbitrary time dependence in a uniform medium are charge-conjugate back-to-back pairs. This basic feature may be exploited as a probe of the chiral dynamcis.

When the environment has a spatial dependence, as is more realistic, the pions experience forces that tend to erode the clear back-to-back correlation pattern. We have examined this effect with a quantum-field treatment of a one-dimensional scenario, using a mass function that emulates the profiles obtained in more elaborate numerical simulations with the linear σ model. The resulting two-body correlation function for charge-conjugate pions is shown in the figure. The characteristic correlation structure is seen to be rather robust and so there is reason to hope that this signature may be experimentally observable.

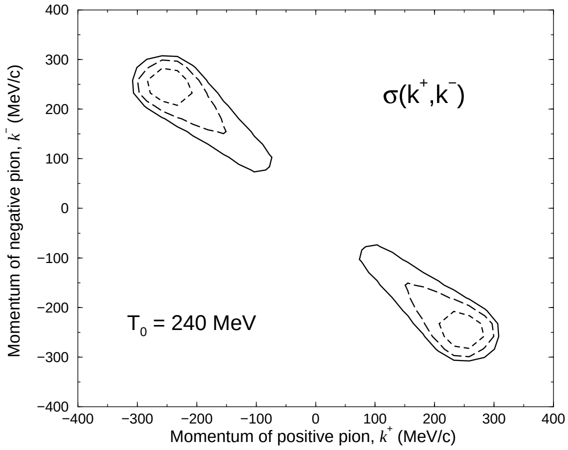

Of course, this "signal" is partially obscured or eroded by a number of other processes and thus any attempt to extract it from the experimental data must take careful account of such "background" contributions.

One important issue concerns the possible presence of other agencies that may lead to a similar signal and thus forge the DCC signature. While there are many physically different sources of charge-conjugate pion pairs, fortunately only few lead to strong back-to-back correlations. Particularly important is the decay $\rho(770) \to \pi^+\pi^-$ but due to the high ρ mass, at least one of the pions has a momentum above 360 MeV$/c$ which is somewhat above the upper limit of the expected effect ($k_{\max} \approx 300$ MeV$/c$). Moreover, although $\eta(550)$ and $\omega(780)$ may both contribute soft $\pi^+\pi^-$ pairs, these all arise in three-body decays and thus they are only rather weakly correlated and so they should not pose a serious problem.

In conclusion, then, we suggest that the data now being taken at RHIC be analyzed for indications of the described signature in the large-angle correlation of soft charge-conjugate pion pairs. It may also be worthwhile to scrutinize existing SPS data for this signal. If indeed identified, this signal may offer a means for probing the degree of chiral restoration achieved and the subsequent DCC dynamics.

* Condensed from nucl-th/0012020.